

UC Merced

UC Merced Electronic Theses and Dissertations

Title

Water quality and invasion ecology: Measuring delta dynamics with high spatial and temporal resolution satellite remote sensing

Permalink

<https://escholarship.org/uc/item/0k911673>

Author

Ade, Christiana

Publication Date

2022

Supplemental Material

<https://escholarship.org/uc/item/0k911673#supplemental>

Copyright Information

This work is made available under the terms of a Creative Commons Attribution-NonCommercial-ShareAlike License, available at <https://creativecommons.org/licenses/by-nc-sa/4.0/>

Peer reviewed|Thesis/dissertation

UNIVERSITY OF CALIFORNIA, MERCED

Water quality and invasion ecology: Measuring delta dynamics with
high spatial and temporal resolution satellite remote sensing

A dissertation submitted in partial satisfaction of the requirements
for the degree Doctor of Philosophy

in

Environmental Systems

by

Christiana Ade

Committee in charge:
Professor Joshua H Viers, Chair
Professor Thomas C. Harmon
Professor Erin L. Hestir
Dr. Shruti Khanna

2022

Copyright

Christiana Ade, 2022

All rights reserved

The Dissertation of Christiana Ade is approved, and it is acceptable in quality and form for
publication on microfilm and electronically:

Prof Erin L. Hestir

Prof Thomas Harmon

Dr. Shruti Khanna

Prof Joshua H. Viers

University of California, Merced

2022

Dedication

I would like to dedicate this work to my mother, Athanasia Ade, and my father, Harald Ade. Thank you so much for all your support. I could not have accomplished this without you.

Table of Contents

	List of Figures.....	vii
	List of Tables.....	ix
	Acknowledgements.....	x
	Curriculum Vitae.....	xi
	Abstract the Dissertation.....	xvii
1.	Introduction.....	18
	1.2 References.....	20
2.	Chapter 1: Assessing Fish Habitat and the Effects of an Emergency Drought Barrier on Estuarine Turbidity Using Satellite Remote Sensing*.....	23
	Abstract.....	23
	2.1 Introduction.....	24
	2.2 Study Area.....	26
	2.3 Methods.....	28
	2.3.1 Satellite Data and Image Pre-processing.....	28
	Land and vegetation masking.....	28
	2.3.2 Turbidity Data.....	30
	2.3.3 Turbidity Mapping: Model Calibration and Validation.....	30
	2.3.4 Habitat Mapping.....	31
	2.3.5 Impacts of the Emergency Saltwater Intrusion Barrier on Turbidity.....	32
	2.4 Results.....	33
	2.4.1 Turbidity Suitability for Endangered Fish.....	33
	2.4.2 Turbidity Time Series: Evaluation of Barrier Effect.....	36
	2.5 Discussion.....	40
	2.5.1 Turbidity Algorithm Calibration.....	40
	2.5.2 Habitat Maps: Frequency of Turbidity Suitability.....	42
	2.5.3 Evaluation of Emergency Saltwater Intrusion Barrier Impacts on Turbidity.....	43
	2.6 Conclusions.....	44
	2.7 Appendices.....	44
	2.7 Acknowledgements.....	46
	2.8 References.....	46
3.	Chapter 2: Genus-level mapping of invasive floating aquatic vegetation using Sentinel-2 satellite remote sensing*.....	52
	3.1 Introduction.....	53
	3.2 Materials and Methods.....	54
	3.2.1 Experimental Design.....	54
	3.2.2 Acquisition and pre-processing of Sentinel-2 imagery.....	58
	3.2.3 Imaging spectroscopy acquisitions and classification process.....	59
	3.3 Sentinel-2 Image Classification.....	60
	3.3.1 Training and validation data.....	60
	3.2.2 Sentiel-2 Random Forest Model Selection.....	61
	3.3 Results.....	62
	3.3.1 Model Accuracies.....	62
	3.3.2 S2 Random Forest Variable Importance.....	64
	3.3.3 S2 and AIS genus-level map comparison.....	65

3.4	Discussion.....	67
3.4.1	Model Accuracies	67
3.4.2	Percent coverage comparison: Differences between S2 and AIS and S2 limitations	69
3.4.3	Percent coverage of FAV classes.....	69
3.4.4	Impact of environmental conditions: tidal stage	71
3.4.5	Sentinel-2 characteristics that enable differentiation between FAV classes and the neighboring vegetation.....	72
3.5	Conclusions.....	73
3.6	Acknowledgements and funding	74
3.7	Appendix.....	74
3.8	References.....	74
4.	Chapter 3: Priority effects, niche breadth and environmental plasticity of invasive floating aquatic vegetation phenology revealed by satellite remote sensing*	80
	Abstract.....	80
4.1	Introduction.....	81
4.2	Study Site.....	82
4.3	Methods	85
4.3.1	Acquisition and pre-processing of Sentinel-2 Imagery.....	85
4.3.2	Seasonal Dynamics Maps	85
4.3.3	Vegetation regions of interest statistical analysis	87
4.4	Results.....	88
4.5	Discussion.....	93
4.5.1	Selective comparison to prior RS studies	93
4.5.2	Phenology & potential mechanisms of invasion success.....	94
4.6	Conclusion	96
4.7	Appendix.....	98
4.8	References.....	101
5.	Conclusions.....	107
5.1	Main Findings and future goals	107

List of Figures

Figure 2-1. Maps of the study area including general locations discussed in the text. (a) The SPOT-5 Take-5 (S5T5) waterways in the Sacramento–San Joaquin River Delta, Suisun, and Grizzly Bays are shaded gray. Continuous in situ turbidity stations are represented by circles (Nephelometric Turbidity Units; NTU). (b) Four subregions areas used to evaluate the potential influence of the emergency saltwater intrusion barrier, including 1. The portion of the San-Joaquin River, 2. Fisherman’s Cut, 3. Franks Tract, 4. Little Franks Tract. The barrier location is shown in red. CDEC, California Data Exchange Center.....27

Figure 2-2. Raster turbidity as calculated by Equation (1) vs. the corresponding station in situ turbidity (n = 167). (b) The calibrated raster turbidities (determined by applying a linear model fitted in a) vs. the corresponding station turbidity measurements. Stations are grouped by color relating to different geographic zones of the Delta: west (green), north (orange), central (purple), and south (pink). RMSE, root mean squared error; FNU, Formazin Nephelometric Units; %NRMSE, percent normalized RMSE.31

Figure 2-3. Using 16 acquisitions from April 16 to September 8, 2015, percent of total waterways within certain levels of percent frequency of suitable turbidity. The orange bar is the waterways percentage for the estimated map (in Figure 2-3). Gray bars show the range of waterways percentage when considering the upper and lower bound maps as determined from the RMSE of the turbidity retrievals (4.7 NTU).....34

Figure 2-4. Delta smelt habitat potential as determined by the frequency of suitable turbidity >12 NTU over the course of the time series April 6–September 8, 2015.35

Figure 2-5. Seven S5T5 images that were acquired during the 20-mm fish trawl from April to July 2015 were used to match the frequency of suitable turbidity conditions during this period to fish counts.....36

Figure 2-6. Site adjusted turbidity maps in NTU for two pairs of pre- and post-barrier installation images. The top pair has similar flood tide conditions and the bottom pair has similar ebb tide conditions. The barrier was installed on May 28, 2015 and removed November 15, 2015. The increase in masked pixels on August 9 corresponds to the increased presence of submerged vegetation patches.....38

Figure 2-7. Turbidity maps for pre and post tide pairs centered on the four substudy areas (A). Mean turbidity and standard deviation for each subregion is shown for all image dates (B). The ebb and flood pairs are highlighted in turquoise and yellow, respectively. Horizontal lines represent mean turbidity for all images before the barrier installation, and after the barrier installation separately.....40

Figure 3-1. Field photos of vegetation classes and list of species in each vegetation community type. See Ta et al. 2017 for more in-depth descriptions of targeted invasive aquatic vegetation.....56

Figure 3-2. Map of the Delta sub-study areas. RGB images were created using imaging spectroscopy acquisitions.58

Figure 3-3. Variable importance for Sentinel-2 random forest models for each match-up date. Mean Decrease Accuracy (left) and Mean Decrease Gini (right). Variables are ordered by average decrease across all three models. Spectral indices consistently rank high in importance across all three model dates.64

Figure 3-4. Ward Cut (top) and Rhode Island (bottom) comparison between Sentinel-2 and Imaging spectrometer maps. Shows good agreement at the FAV genus level between locations of larger water primrose (yellow) and water hyacinth patches (purple). Orange non-photosynthetic vegetation (NPV) patches on the edge of islands in 2019 AIS maps are patches of floating NPV which cannot be detected by S2 spatial or spectral resolution.	66
Figure 3-5. Spectral response of a riparian vegetation pixel that was misclassified as water hyacinth and a water hyacinth pixel.	70
Figure 3-6. Comparison of the impact of limited spatial resolution in S2 data using water primrose patches. Coarse pixel resolution is more likely to cause misclassification at class boundaries due to pixel mixing.	71
Figure 3-7. Tidal stage comparison for fall match-ups at Big Break. Fall 2018 Sentinel-2 acquisition occurs during a flood tide which impedes detection of full SAV extent. Fall 2019 Sentinel-2 acquisition occurs at a low tide and shows a much closer match-up between S2 and imaging spectrometer maps.	72
Figure 4-1. The three sub study areas in the Delta.	84
Figure 4-2. Sentinel-2 image dates used in time series analysis.	85
Figure 4-3. Metrics of seasonal dynamics derived from EVI time series using TIMESAT (a) Start of growing season (SoS), (b) end of growing season (EoS), (c) length of growing season, (d) Growth rate at beginning of season, (e) Senescence rate at end of growing season. Grey dots represent EVI derived from satellite time series for a single water hyacinth pixel in Rhode Island. Black line represents the fitted asymmetric gaussian curve calculated by TIMESAT. Figure adapted from (Eklundha and Jönsson, 2017).	86
Figure 4-4. Example of TIMESAT extracted start dates and end dates throughout the three-year time series for water primrose (green), water hyacinth (purple), and emergent vegetation (orange). Large dots on the left side of curves represent TIMESAT extract start dates while those on the right indicate end dates.	88
Figure 4-5. The classification map and five phenology metrics extracted for Sherman Island, Rhode Island, and Liberty Island for 2020.	90
Figure 4-6. Violin plots with encompassed box plots of seasonal dynamics across the Sherman Island, Rhode Island, and Liberty Island for water primrose, water hyacinth, and emergent vegetation from 2018 – 2020.	91
Figure 4-7. Violin plots with encompassed box plots of seasonal dynamics across the Delta for water primrose, water hyacinth, and emergent vegetation from 2018 – 2020. ...	92
Figure 4-8. Differences in phenology between two emergent vegetation genus types (EMR-Cattail and EMR-Tule) and aquatic and terrestrialized water primrose (Prim-Aqua and Prim-Terra) present in Liberty Island. Points were selected via field data and photointerpretation. Phenology curves for both types of water primrose show breadth and priority effects relative to Cattail and Tule. However, tule patches neighboring terrestrialized water primrose have later shifted phenologies compared to Cattail, which may make tule more susceptible to invasion by water primrose.	96
Figure 4-9. Differences in phenology between two sub-classes of water primrose from the outer (Prim_out) and inner patch (Prim_in) and water hyacinth in Rhode Island. Points were selected via field data and photointerpretation. Prim_out and water hyacinth phenologies demonstrate examples of niche breadth and priority effects, while Prim_in and water hyacinth suggest potential niche partition between the two invasive.	96

List of Tables

Table 2-1. Spectral Bands of the S5T5 instrument and their corresponding wavelengths in micrometers.	29
Table 2-2. Image acquisition dates, the number of in situ turbidity sensors used for site calibrated turbidity retrievals (units: NTU) and their turbidity ranges for each date. 29	29
Table 3-1. Target classes and their descriptions.	57
Table 3-2. Match-up dates and tidal ranges ¹ for corresponding imaging spectrometer acquisitions and Sentinel-2 over passes.	58
Table 3-3. Sentinel-2 band characteristics. Asterix indicates band was not used during classification.	59
Table 3-4. Vegetation and water indexes used in the Sentinel-2 classification process.	61
Table 3-5. Sentinel-2 and airborne imaging spectrometer classification performance by match-up date. Overall accuracy = OA, Producer's accuracy = PA, User's Accuracy = UA. SAV = submerged aquatic vegetation. Soil and non-photosynthetic vegetation (NPV) accuracies are not listed but were 93 – 100% and primarily confused with each other.	63
Table 3-6. Difference in percent coverage between Sentinel-2 and airborne imaging spectrometer (AIS) classification maps for 4 sub study areas and Delta wide. AIS percent coverage was subtracted from that of S2; therefore, negative values indicate S2 underestimation (blue), while positive values indicate S2 overestimation (yellow) relative to AIS maps.	66
Table 4-1. Sentinel-2 band characteristics. Asterisk indicates band was used in vegetation index calculation.	85
Table 4-2. Phenology metrics extracted from TIMESAT and corresponding definitions. 87	87

Acknowledgements

I would have not been able to complete this dissertation without the support and guidance of many people throughout my time as a graduate student. I am extremely grateful to everyone that I have worked with and befriended over this time. They have all influenced my life in immeasurable ways.

First and foremost, I would like to thank my PhD. Advisor, Erin Hestir. We have been working together since 2015 and sometimes I cannot believe it has been that long! In that time, Erin has inspired me and helped me become a better researcher. She encouraged me to pursue my research interests and personal goals. She has always supported me and believed in me even when I had doubts. I am incredibly grateful for all the conversations and experiences we have shared. I look forward to continuing to collaborate with her in the future as a colleague. Thank you for taking me with you from NCSU to UC Merced. I am so glad I came along.

I would also like to thank my supportive committee members that provided key suggestions and guidance to improve my research. I want to thank Shruti Khanna for geeking out and getting excited over Delta research with me, Joshua Viers for always being realistic, encouraging me to put on my ecology hat and providing funding during my last semester, and Thomas Harmon for encouraging me to think about my research beyond remote sensing and exposing me soldering and Arduino boards (seriously, electronics are so fun). I enjoyed collaborating with all of you.

I also want to thank my lab members for providing useful feedback and always providing an ear. I learned to become a better mentor from all of you and enjoyed working with all of you.

I want to thank my numerous funding sources who made all this research possible, including the Delta Stewardship Council, UC Merced, and NASA JPL. With a special thanks to Christine Lee.

I want to thank my friends for always being there for me and listening to me talk about my work. Thanks for adding a light heartedness to my research by joking that I “detect fish from space.” I am just going to list some of your initials here so that my dissertation does not come up on a google search of your name – JI, MD, ML, RP, ABS, BW, AFJ, BC, BLB, KR, CA, EB, BG, TJK, KJP, KS, and AR. Thank you for all the great memories.

Most importantly, I would like to thank my family – Mami, Papi, and Alexander. To both my parents, thank you for being such an inspiration and for all your brave sacrifices. Mami, thank you for supporting me in every single way that you do and providing words of wisdom. Papi, thank you for your guidance, teaching me to take things one step at a time and motivating me become a better researcher (to always “look at the data”). To Alexander, thank you for inspiring me to always try my hardest and be dedicated to my goals. I am incredibly lucky and grateful to have you as my family. I really cannot express how grateful I am for all of you. I would not have been able to complete this journey if it wasn’t for you.

Curriculum Vitae

Email: cade@ucmerced.edu

EDUCATION

University of California Merced Merced, CA 2017 - 2022
Doctor of Philosophy in Environmental Systems
Department of Environmental and Civil Engineering
Water Quality and Invasion Ecology: Measuring Delta Dynamics with High Spatial and Temporal Resolution Satellite Remote Sensing

North Carolina State University Raleigh, NC 2015 - 2017
Master of Science, Marine, Earth and Atmospheric Sciences
Effects of Resolution on Multi-Temporal Remote Sensing of Wetlands: Toward a Wetland Phenology Indicator

North Carolina State University Raleigh, NC 2014 - 2015
Geospatial Information Sciences Graduate Certificate Program

University of North Carolina at Chapel Hill Chapel Hill, NC 2010 - 2014
Bachelor of Science in Environmental Science, Minor in Geography

RESEARCH EXPERIENCE

NASA Jet Propulsion Laboratory 2020 - 2021
Volunteer Intern Co-mentors: Dr. Christine Lee and Dr. Michelle Gierach
Evaluated sample Surface Biology and Geology datasets (PRISM) and various atmospheric correction approaches across different coastal water bodies. Investigated algorithm implementation to level 3 data products and assessed product uncertainties relative to their applications use.

University of California Merced, Dept. of Civil and Environmental Engineering 2019 – 2021
Graduate Research Assistant Advisor: Dr. Erin Hestir; Project PI: Dr. Susan Ustin
Developed methodologies and well documented workflows for mapping wetland vegetation and tracking changes in composition and phenology using Sentinel-2 imagery. Supervised creation of a Google Earth Engine dashboard for evaluating wetland vegetation phenology metrics at restoration sites. Lead research efforts for three of four science objectives, organized overall project reporting and data dissemination.

University of California Merced, Dept. of Civil and Environmental Engineering 2017 – 2019
Graduate Research Assistant Advisor: Dr. Erin Hestir; Project PI: Dr. Christine Lee
Collaborated with NASA JPL Applied Sciences and Oregon State University to enhance water quality mapping in the Sacramento San Joaquin Delta with satellite and imaging spectroscopy data. Generated maps and developed workflow to enable stakeholders to process AVIRIS-NG and SPOT 5 (Take 5) imagery. Demonstrated capability of use high frequency satellite observations for evaluating impacts of an emergency drought barrier on turbidity and habitat of an endangered fish species.

University of California Merced

Summer 2019

Graduate Research Assistant Advisor: Dr. Erin Hestir; Project PI: Dr. Kerry-Anne Cawse-Nicholson
Advanced research for the HySPIRI preparatory mission and lowered the barrier for managers to use imaging spectroscopy data by translating a pipeline for mapping aquatic vegetation from a commercial coding language to open source (R).

North Carolina State University, Dept of Marine Earth and Atmospheric Sciences 2015 - 2017

Graduate Research Assistant

Advisor: Dr. Erin Hestir

Hestir

Contributed to research projects and proposals by gathering and analyzing satellite remote sensing data collected over wetland ecosystems. Researched vegetation phenology dynamics using a multi-sensor approach, including Landsat 8 and experimental Sentinel-2 data. Assessed sensor resolution requirements for mapping aquatic vegetation communities and phenology with satellite imagery.

SKILLS

- **Remote Sensing Image Analysis:** ENVI, Google Earth Engine, ArcGIS, and QGIS
- **Programming Languages:** Proficient - R. Literate - Python, IDL, Matlab, Unix Shell Scripting

HONORS, AWARDS, AND GRANTS

UC Merced Environmental Systems Summer Award (2020) – US\$ 3,400

Delta Stewardship Council. Low-cost satellite remote sensing of the Sacramento-San Joaquin Delta to enhance mapping for invasive and native aquatic vegetation. PI: Susan Ustin. (2019) – US \$ 382,421

UC Merced Environmental Systems Professional Development Award (2019) – US \$ 2,000 UC Merced

Environmental Systems Professional Development Award (2018)– US\$ 2,000

Ocean Carbon and Biogeochemistry Grant for IOCCG Summer School (2018)- US\$ 2,200

UC Merced Environmental Systems Professional Development Award (2018)– US\$ 1,000

UC Merced Environmental Systems Summer Award (2018)– US\$ 3,400

Ocean Carbon and Biogeochemistry Program Travel Grant for IOCS Meeting (2017)– US\$ 1,000

NCGIS Conference G. Herbert Stout Award (2017)

University of Washington Geohackweek Student Travel Grant Award (2016)– US\$1,050

PEER REVIEWED PUBLICATIONS

1. **C. Ade**, E.L. Hestir, C.M. Lee. (2021). Assessing Fish Habitat and the Effects of an Emergency Drought Barrier on Estuarine Turbidity Using Satellite Remote Sensing. *Journal of American Water Resources Association (JAWRA)*. 1– 19. doi:10.1111/1752-1688.12925
2. F. Muller-Karger, E.L. Hestir, **C. Ade** et al. (2018). Satellite sensor requirements for monitoring essential biodiversity variables of coastal ecosystems. *Ecological Applications* 28: 749-760 doi: 10.1002/eap.1682

3. T. Chandler, A. Drake, E. Brown, H. Julian, N. Simonsen, **C. Ade**, K. Wangyao, R.M. Kamens, and S.H. Gheewala. (2014). Comparative Life Cycle Assessment of Tropical Island Municipal Solid Waste Strategies. *Journal of Sustainable Energy and Environment*. 5: 75-84. (JSEE Journal)

PEER REVIEWED PUBLICATIONS IN PREPARATION

1. **C. Ade**, S. Khanna, M. Lay, S.H. Ustin E.L. Hestir. Genus-level mapping of invasive floating aquatic vegetation using Sentinel-2 satellite remote sensing. (submitted to Remote Sensing)
2. **C. Ade**, A. Weingram, E.L. Hestir, S. Khanna. Priority effects, niche breadth and environmental plasticity of invasive floating aquatic vegetation phenology revealed by satellite remote sensing.

BOOK REVIEWS AND BOOK CHAPTERS

1. E.A. Bolch, M.J. Santos, **C. Ade**, et al. (2019). Remote Detection of Invasive Species. In: CavenderBares, J (Ed) Remote Sensing of Plant Biodiversity: Using spectral signals of plants to understand the biology and biodiversity of plants, plant communities, ecosystems and the tree of life, Springer, New York.
2. **C. Ade** and E.L. Hestir. (2017). Review of Remote Sensing and GIS for Ecologists: Using Open Source Software. PE & RS. June Issue

CONFERENCE PROCEEDINGS

1. **C. Ade**, E.L. Hestir, S. Khanna, S.L. Ustin. (2016). High Resolution Mapping of Wetland Ecosystems: Spot-5 Take 5 for Evaluation of Sentinel-2. European Space Agency Living Planet Symposium. Prague, Czech Republic. (*Conference proceedings*)

CONFERENCE PRESENTATIONS

* denotes supervised student

1. C. Ade, E.L. Hestir, C.M. Lee. (2021). Assessing Fish Habitat Potential and the Effects of an Emergency Barrier on Turbidity in a Drought Impacted Estuary Using Satellite Remote Sensing. GEO AquaWatch Project Updates Webinar. (Oral)
2. J. Burmistrova, C. Ade, S. Khanna, M. Lay, A. Weingram*, E.L. Hestir. (2021). Using Sentinel-2 to Provide Open-Access Tools for Plant and Water Mapping in the Sacramento Bay-Delta. 11th Biennial Bay Delta Science Conference. (Oral)
3. A. Weingram*, **C. Ade**, E.L. Hestir, S. Khanna. (2020). Vegetation Index Sensitivity Analysis for Wetland Vegetation Phenology Using Sentinel-2 Data. AGU Fall Meeting 2020. (*Poster*)

4. J. Burmistrova, S. Khanna, **C. Ade**, E.L. Hestir. (2020). Satellite Remote Sensing of Functional Flows to Improve Ecological Performance Metrics for the Sacramento-San Joaquin River Delta, California. AGU Fall Meeting 2020. (*Oral*)
5. C.M. Lee, N. Tufillaro, B. Palmieri, A. Osti, S. Acuña, T. Sommer, G.H. Halverson, E.L. Hestir, **C. Ade**. (2019). Assessment of Water Flow Operations Impacts on Turbidity Using Satellite Remote Sensing. AGU Fall Meeting 2019. San Francisco, CA. (*Oral*)
6. G.H. Halverson, C.M Lee, G.C. Hulley, K.A. Cawse-Nicholson, Brendan Palmieri, Amye Osti, E.L. Hestir, **C. Ade**, S. Acuña. (2019). Smelt Habitat Suitability and Thermal Refugia in the San Francisco Bay Delta as Seen by Landsat and ECOSTRESS with Comparison to CDEC. AGU Fall Meeting 2019. San Francisco, CA. (*Oral*)
7. M. Vermillion, C.M Lee, **C. Ade**, E.L. Hestir, M.M. Gierach, D.R. Thompson. (2019). Improving Water Quality Retrievals from Imaging Spectroscopy Datasets using ISOFIT Atmospheric Correction: a Case Study in Grizzly Bay, California. AGU Fall Meeting 2019. San Francisco, CA. (*Oral*)
8. **C. Ade**, A.S Fernandez Bou, T.C. Harmon, E.L. Hestir. (2019). Boogie Flux: Incorporating Low-cost, Rapidly Deployable CO₂ Chambers into Multi-scale Aquatic Flux Studies. AGU Fall Meeting 2019. San Francisco, CA. (*Poster*)
9. Q. Xu, A.L. Westerling, C. Wiedinmyer, M.D. Hurteau, **C. Ade**. (2018). Estimating Wildfire Emissions in California. AGU Fall Meeting 2018. Washington, DC. (*Poster*)
10. E.L. Hestir and **C. Ade**. (2018). Advances in terrestrial and aquatic ecology enabled by four decades of imaging spectroscopy and the future of observing surface biology from space. AGU Fall Meeting 2018. Washington, DC. (*Oral*)
11. E.L. Hestir, **C. Ade**, C.M Lee, S. Khanna, M. Santos, J.A. Greenberg, A.C. Planes, S. Ustin. (2018). Fish versus tomatoes and other tales of using remote sensing to meet California's co-equal goals of providing water supplies and protecting ecosystems. AGU Fall Meeting 2018. Washington, DC. (*Oral*)
12. **C. Ade**, E.L. Hestir, C.M. Lee. (2018). Improvements in Water Quality Mapping using Hyperspectral Remote Sensing. 10th Biennial Bay-Delta Science Conference. Sacramento, California. (*Poster*)
13. **C. Ade**, E.L. Hestir, S. Khanna, C.M. Lee, S.L. Ustin. (2018). Aquatic Weed Detection to Support Fish and Water Resources Management An Imaging Spectroscopy Story to guide future SBG Aquatic Applications. 2018 HypIRI Science and Applications Workshop. Washington, DC. (*Poster*)
14. **C. Ade** and E.L. Hestir. (2017). Effects of Resolution on Multi-Temporal Remote Sensing of Wetlands: Towards a Wetland Vegetation Phenology Indicator. 9th Biennial Bay-Delta Science Conference. Sacramento, California. (*Poster*)
15. **C. Ade**, E.L. Hestir, S. Khanna, S.L. Ustin. (2017). Exploring Sensor Resolution Requirements for Mapping Wetland Vegetation Phenology. Society of Wetland Scientists meeting 2017 Annual Meeting. San Juan, Puerto Rico. (*Oral*)

16. **C. Ade** and E.L. Hestir. (2017). The Benefit of Increased Temporal Resolution on Monitoring Inland Water Quality. International Ocean Colour Science Spring Meeting 2017. Lisbon, Portugal. (*Poster*)
17. **C. Ade** and E.L. Hestir. (2017). Exploring the Benefit of Increased Temporal Resolution on Monitoring Inland Water Quality Using a Sentinel-2 Proxy. ASLO Winter Meeting 2017. Honolulu, Hawaii. (*Poster*)
18. **C. Ade**, E.L. Hestir, S. Khanna, S.L. Ustin. (2016). Comparison of Sensor Resolution Trade-offs Between Landsat 8 and a Sentinel-2 Proxy for Mapping Wetland Vegetation Phenology. AGU Fall Meeting 2016. San Francisco, CA. (*Oral*)
19. M. Amanatides, **C. Ade**, and E.L. Hestir. (2016). Determining the Optimal View Angle for Hyperspectral Based Estimates of Wetland Plant Biomass. 6th Annual HypSIRI Data Product Symposium and Aquatic Forum. Greenbelt, MD. (*Poster*)
20. **C. Ade**, E.L. Hestir, I. Dornova, C. Fichot, M. Gierach, B. Bergamaschi, L. Windham-Myers, K. Byrd, S. Khanna, S.L. Ustin. (2016). DEWSS: Dual Ecosystem and Water Supply Sustainability for the Sacramento- San Joaquin River Delta. European Space Agency Living Planet Symposium. Prague, Czech Republic. (*Poster*)
21. E.L. Hestir, **C. Ade**, and M. Amanatides. (2015). Earth Observations and Remote Sensing for Biodiversity, Water Quality and Security. North Carolina State University Global Change Symposium. Raleigh, NC. (*Poster*)

TEACHING EXPERIENCE

- **University of California Merced Valle De Exploracion**
Guest Lecturer Spr. 2020
& 2021
Remote Sensing Using Google Earth Engine
- **University of California Merced - University Extension**
Primary Instructor Spr. 2019
2-Day Workshop - Remote Sensing Using Google Earth Engine.
- **University of California Merced, Environmental Systems**
Laboratory Teaching Assistant Fall 2018
ES/ENVE 152/252: Remote Sensing and Global Environmental Change with Dr. Erin Hestir
- **University of California Merced, Environmental Systems**
Co-developer Spr. 2018
ES 295: Advanced Remote Sensing with Dr. Erin Hestir
- **University of California Merced, Environmental Systems**
Guest Lecturer April 2018
Remote Sensing Applications with R (ES 207: Environmental Data Analysis)
- **North Carolina State University, Dept. of Marine, Earth and Atmospheric Sciences**
Guest Lecturer Jan. 2017
Image Processing and Analysis (MEA 593: Remote Sensing and Global Environmental Change)
- **North Carolina State University, Dept. of Marine, Earth and Atmospheric Sciences**
Guest Lecturer Sep. 2016
Raster Data Processing and Analysis (MEA 493: Remote Sensing and Global Environmental Change)
- **North Carolina State University, Dept. of Marine, Earth and Atmospheric Sciences**
Laboratory Teaching Assistant 2015 - 2017
MEA 110: Online and in-class Geology I Laboratory with Dr. David McConnell
MEA 100: Earth System Science: Exploring the Connections

OUTREACH AND MENTORING

- **Valle De Exploracion** Spring 2020, 2021
Graduate Student Panelist
- **Environmental Systems Department Seminar Lead** Spring 2020
Organized graduate student lunches with speakers, managed website with seminar abstracts and presenter biographies, coordinated speaker schedules.

Abstract the Dissertation

Water quality and invasion ecology: Measuring delta dynamics with high spatial and temporal resolution satellite remote sensing

By

Christiana Ade

Doctor of Philosophy, Environmental Systems Program
University of California, Merced, 2022
Dr. Erin Hestir, Graduate Advisor

Globally, terrestrial aquatic interfaces, like deltas, face a large number of ecosystem stressors. Monitoring and characterizing mechanisms of change in these areas is relevant to supporting human populations while maintaining ecological integrity. This requires high spatial and temporal resolution satellite-based observations, which have only recently become available to observe rapid changes in these dynamic systems. Sentinel-2, launched in 2016, provides a 5-day temporal resolution and 10 m spatial resolution which allows for detecting fine-scale changes in both water quality and aquatic vegetation. This dissertation is motivated by two primary interacting themes: 1) using remote sensing to study water quality, vegetation composition and phenology across aquatic ecosystems, and 2) providing knowledge and insight to support ecosystem management and informed decision making. Using the high spatial and temporal resolution capabilities of Sentinel-2, this dissertation addresses three main research objectives that correspond to three manuscripts (Chapters 1 – 3). The study site for all works is the California Sacramento San Joaquin Delta. Chapter 1 evaluates the impacts of an emergency drought barrier on turbidity and endangered fish habitat suitability. This manuscript is already published in the Journal of American Water Resource Association. The results demonstrate how high spatial, high temporal resolution satellite data enhances field observations by providing additional spatial context. Chapter 2 provides a framework for mapping aquatic vegetation, specifically distinguishing between two types of invasive floating aquatic vegetation at the genus level – water primrose and water hyacinth. Classification accuracy assessments and comparisons to maps derived from higher resolution airborne imaging spectroscopy data demonstrate that Sentinel-2 can be used to fill in inter-annual gaps in aquatic vegetation maps from summer to fall. Chapter 3 builds off Chapter 2 and reveals the phenology of water primrose may be a key component of its recent invasion success. Water primrose patches show examples of niche breadth, priority effects, and environmental plasticity relative to water hyacinth and emergent vegetation. Our findings highlight the need for spatially resolved phenology metrics. Overall, this dissertation provides insights into water quality and aquatic vegetation invasion ecology and provides improved methods for ecosystem managers to continue to investigate ecosystem stressors.

1. Introduction

Terrestrial aquatic interfaces (TAI), such as freshwater tidal estuaries and wetlands, are some of the most biologically and geochemically diverse ecosystems on Earth (DOE, 2017). Although these areas only represent a small portion of the Earth's surface, they provide a large array of ecosystem services, including food, water, habitat, flood protection, sediment and carbon storage (Ward et al., 2020). However, these systems are under threat due to natural and anthropogenic climate change, as well as changes in land use resulting from increasing populations and urban expansion (Gardner et al., 2015). These areas are also some of the most anthropogenically modified ecosystems on earth, and the demand for water and energy by a rapidly growing global population negatively impacts biodiversity and ecosystem functions (Carpenter et al., 2011; Newton et al., 2020). Characterizing mechanisms of change in these areas is relevant to understanding the Earth's system as a whole and sustainably managing TAI systems.

The spatio-temporal variability of TAIs makes studying these areas challenging. Traditional field measurements can be difficult to collect, labor intensive and costly, limiting their temporal frequency and areal coverage. As a result, coastal habitats and wetlands, comprise some of the most understudied ecosystems globally. Characterizing these ecosystems to meet conservation, socioeconomic, or scientific goals requires sensitive measurements at a sufficient temporal frequency and over an area that ideally covers the full area of interest. Additionally, such measurements should also be cost effective.

Developing satellite-based remote sensing (RS) capabilities has been the systematic technological response of the environmental community to fill the gaps of field work and has transformed our knowledge and understanding of ecosystem function and change (Cohen and Goward, 2004, Wulder et al., 2012). RS observations have been used to track changes in wetland vegetation and surface waters (Chen et al., 2014; Henderson and Lewis, 2008; Huang et al., 2018; McCombs et al., 2016), and offer relevant information for improved management practices and policy (Kachelriess et al., 2014; Richardson and Ledrew, 2006). While several of previous and current satellite missions do not provide the measurement resolutions needed to fully resolve properties and processes in TAIs, the ability of more recent missions to detect changes in water quality, biodiversity and ecosystem function is still extremely valuable and remains understudied (Hestir et al., 2015; Muller-Karger et al., 2018).

The overall goal of my dissertation is to utilize high frequency, high spatial resolution satellite remote sensing for resolving key water quality parameters, aquatic vegetation composition and phenology interannually and annually and how this relates to species invasion and management objectives. Consequently, my work focuses on exploiting Sentinel-2 satellite capabilities, which provides several documented improvements over other commonly used sensors, like MODIS and Landsat, for studying complex ecosystems with high spatio-temporal variation, such as wetlands and estuaries (Hedley et al., 2012; Lefebvre et al., 2019; Sánchez-Espinosa and Schröder, 2019; Villa et al., 2018). In addition to supporting our ability to answer questions related to ecosystem function, my methods

and research outcomes can provide support for management and monitoring these areas by focusing on the Sacramento San Joaquin Delta (the Delta), one of the most heavily altered and invaded estuaries globally (Cohen and Carlton, 1998; Nichols et al., 1986).

This dissertation is motivated by two primary interacting themes: 1) using remote sensing to study water quality, vegetation composition and phenology across aquatic ecosystems, and 2) providing knowledge and insight to support ecosystem management and informed decision making. Since the main chapters of my thesis are organized as self-contained, standalone manuscripts with the intent and complete commitment to get them all published in the peer-reviewed literature, main findings are only summarized here and the reader is referred to these chapter for more details.

Chapter 1 focuses on mapping turbidity in the Delta during the 2015 drought using Spot5Take5 an experimental Sentinel-2 dataset. Using this dataset, a high-frequency and high-resolution timeseries of turbidity was generated and used to examine two management relevant case studies concerning endangered fish habit and the installation of an emergency saltwater intrusion barrier. Turbidity derived habitat frequency maps indicated areas of potential refuge for endangered Delta Smelt with limited connectivity. Maps also indicated a potential increase in turbidity as a result of barriers in two locations, thereby enhancing previous findings with spatial context. This work is relevant to management decisions in the Delta because it highlights the use of high-resolution satellite imagery to compliment field campaigns with systematic snapshots providing context and the ability to supplement areas with limited in situ data. (Ade et al., 2021)

Chapter 2 investigates the ability of Sentinel-2 to distinguish between invasive floating aquatic vegetation (FAV) at the genus level while also identifying emergent and submerged aquatic vegetation at the community level. FAV target classes are water primrose and water hyacinth. Previous studies rely on airborne imaging spectroscopy (AIS) to separate these different covers, but due to cost imagery is acquired only once a year. In order to determine if Sentinel-2 could be used to fill in AIS temporal gaps with acceptable detection of two FAV covers, classification model accuracies and maps between the two datasets were compared visually and by difference percent class coverage. Maps matched well visually and by area, with some caveats related to pixel size, spectral resolution, and image timing.

Chapter 3 builds off Chapter 2, by investigating the phenology of floating and emergent vegetation in the context of invasion. It is generally acknowledged that phenology may play an important role in the success of invasive aquatic vegetation species, the mechanism of which can be categorized into four ecological theories: vacant niche, priority effects, niche breadth, and environmental plasticity. In order to understand the general link between growth cycles and invasions in aquatic ecosystems and the presence of any or all of these four theories, we analyzed Sentinel-2 derived phenology metrics of competing invasive floating vegetation, water primrose (*Ludwigia* spp) and water hyacinth (*Eichhornia crassipes*) and emergent macrophytes at the community level in the Sacramento San Joaquin Delta. We were specifically interested in why water primrose has become such an effective invader. Results show that water primrose has the earliest start of the growing seasons, higher rates of increase and decrease, longer growing seasons and later end dates than water hyacinth or emergent vegetation, thereby, suggesting that priority effects, niche

breadth and environmental plasticity all play a role in the invasion success of water primrose. We also noted several spatial patterns and within-class variability, which highlights the need for spatially resolved phenology dynamics, especially in spatio-temporally complex areas like wetlands. Overall, these findings show mechanisms of invasion and may be able to support management by providing spatial context of phenology supporting decision and monitoring of herbicide treatments.

1.2 References

- Ade, C., Hestir, E.L., Lee, C.M., 2021. Assessing Fish Habitat and the Effects of an Emergency Drought Barrier on Estuarine Turbidity Using Satellite Remote Sensing. *J. Am. Water Resour. Assoc.* 57, 752–770. <https://doi.org/10.1111/1752-1688.12925/FORMAT/PDF>
- Bailey, V., Rowland, J., Megonigal, J.P., Troxler, T., DeForest, J., Stover, D., 2017. Research Priorities to Incorporate Terrestrial-Aquatic Interfaces in Earth System Models. Workshop Report, September 7-9, 2016. <https://doi.org/10.2172/1471229>
- Carpenter, S.R., Stanley, E.H., Vander Zanden, M.J., 2011. State of the World's Freshwater Ecosystems: Physical, Chemical, and Biological Changes. <https://doi.org/10.1146/annurev-environ-021810-094524> 36, 75–99. <https://doi.org/10.1146/ANNUREV-ENVIRON-021810-094524>
- Chen, L., Jin, Z., Michishita, R., Cai, J., Yue, T., Chen, B., Xu, B., 2014. Dynamic monitoring of wetland cover changes using time-series remote sensing imagery. *Ecol. Inform.* 24, 17–26. <https://doi.org/10.1016/J.ECOINF.2014.06.007>
- Cohen, A.N., Carlton, J.T., 1998. Accelerating Invasion Rate in a Highly Invaded Estuary. *Science* (80-.). 279, 555–558. <https://doi.org/10.1126/science.279.5350.555>
- Gardner, R., Barchiesi, S., Beltrame, C., Finlayson, C., 2015. State of the world's wetlands and their services to people: a compilation of recent analyses.
- Hedley, J., Roelfsema, C., Koetz, B., Phinn, S., 2012. Capability of the Sentinel 2 mission for tropical coral reef mapping and coral bleaching detection. *Remote Sens. Environ.* 120, 145–155. <https://doi.org/10.1016/J.RSE.2011.06.028>
- Henderson, F.M., Lewis, A.J., 2008. Radar detection of wetland ecosystems: a review. <http://dx.doi.org/10.1080/01431160801958405> 29, 5809–5835. <https://doi.org/10.1080/01431160801958405>
- Hestir, E.L., Brando, V.E., Bresciani, M., Giardino, C., Matta, E., Villa, P., Dekker, A.G., 2015. Measuring freshwater aquatic ecosystems: The need for a hyperspectral global mapping satellite mission. *Remote Sens. Environ.* 167, 181–195. <https://doi.org/https://doi.org/10.1016/j.rse.2015.05.023>
- Huang, C., Chen, Y., Zhang, S., Wu, J., 2018. Detecting, Extracting, and Monitoring Surface Water From Space Using Optical Sensors: A Review. *Rev. Geophys.* 56,

333–360. <https://doi.org/10.1029/2018RG000598>

- Kachelriess, D., Wegmann, M., Gollock, M., Pettorelli, N., 2014. The application of remote sensing for marine protected area management. *Ecol. Indic.* 36, 169–177. <https://doi.org/10.1016/J.ECOLIND.2013.07.003>
- Lefebvre, G., Davranche, A., Willm, L., Campagna, J., Redmond, L., Merle, C., Guelmami, A., Poulin, B., 2019. Introducing WIW for Detecting the Presence of Water in Wetlands with Landsat and Sentinel Satellites. *Remote Sens.* 2019, Vol. 11, Page 2210 11, 2210. <https://doi.org/10.3390/RS11192210>
- Liang, Q., Zhang, Yuchao, Ma, R., Loiselle, S., Li, J., Hu, M., Zhang, Yunlin, Giardino, C., Li, L., Mishra, D.R., Gloaguen, R., Thenkabail, P.S., 2017. A MODIS-Based Novel Method to Distinguish Surface Cyanobacterial Scums and Aquatic Macrophytes in Lake Taihu. *Remote Sens.* 2017, Vol. 9, Page 133 9, 133. <https://doi.org/10.3390/RS9020133>
- Mccombs, J.W., Herold, N.D., Burkhalter, S.G., Robinson, C.J., 2016. Accuracy assessment of NOAA coastal change analysis program 2006-2010 land cover and land cover change data. ingentaconnect.com. <https://doi.org/10.14358/PERS.82.9.711>
- Muller-Karger, F.E., Hestir, E., Ade, C., Turpie, K., Roberts, D.A., Siegel, D., Miller, R.J., Humm, D., Izenberg, N., Keller, M., Morgan, F., Frouin, R., Dekker, A.G., Gardner, R., Goodman, J., Schaeffer, B., Franz, B.A., Pahlevan, N., Mannino, A.G., Concha, J.A., Ackleson, S.G., Cavanaugh, K.C., Romanou, A., Tzortziou, M., Boss, E.S., Pavlick, R., Freeman, A., Rousseaux, C.S., Dunne, J., Long, M.C., Klein, E., McKinley, G.A., Goes, J., Letelier, R., Kavanaugh, M., Roffer, M., Bracher, A., Arrigo, K.R., Dierssen, H., Zhang, X., Davis, F.W., Best, B., Guralnick, R., Moisan, J., Sosik, H.M., Kudela, R., Mouw, C.B., Barnard, A.H., Palacios, S., Roesler, C., Drakou, E.G., Appeltans, W., Jetz, W., 2018. Satellite sensor requirements for monitoring essential biodiversity variables of coastal ecosystems. *Ecol. Appl.* 28, 749–760. <https://doi.org/10.1002/EAP.1682>
- Newton, A., Icely, J., Cristina, S., Perillo, G.M.E., Turner, R.E., Ashan, D., Cragg, S., Luo, Y., Tu, C., Li, Y., Zhang, H., Ramesh, R., Forbes, D.L., Solidoro, C., Béjaoui, B., Gao, S., Pastres, R., Kelsey, H., Taillie, D., Nhan, N., Brito, A.C., de Lima, R., Kuenzer, C., 2020. Anthropogenic, Direct Pressures on Coastal Wetlands. *Front. Ecol. Evol.* 8, 144. <https://doi.org/10.3389/FEVO.2020.00144/BIBTEX>
- Nichols, F.H., Cloern, J.E., Luoma, S.N., Peterson, D.H., 1986. The Modification of an Estuary. *Science* (80-.). 231, 567–573. <https://doi.org/10.1126/SCIENCE.231.4738.567>
- Richardson, L.L., Ledrew, E.F., 2006. Remote Sensing of Aquatic Coastal Ecosystem Processes Science and Management Applications.
- Sánchez-Espinosa, A., Schröder, C., 2019. Land use and land cover mapping in wetlands one step closer to the ground: Sentinel-2 versus landsat 8. *J. Environ. Manage.* 247,

484–498. <https://doi.org/10.1016/J.JENVMAN.2019.06.084>

Villa, P., Pinardi, M., Bolpagni, R., Gillier, J.-M., Zinke, P., Nedelcut, F., Bresciani, M., 2018. Assessing macrophyte seasonal dynamics using dense time series of medium resolution satellite data. *bioRxiv* 216, 230–244. <https://doi.org/10.1101/279448>

Ward, N.D., Megonigal, J.P., Bond-Lamberty, B., Bailey, V.L., Butman, D., Canuel, E.A., Diefenderfer, H., Ganju, N.K., Goñi, M.A., Graham, E.B., Hopkinson, C.S., Khangaonkar, T., Langley, J.A., McDowell, N.G., Myers-Pigg, A.N., Neumann, R.B., Osburn, C.L., Price, R.M., Rowland, J., Sengupta, A., Simard, M., Thornton, P.E., Tzortziou, M., Vargas, R., Weisenhorn, P.B., Windham-Myers, L., 2020. Representing the function and sensitivity of coastal interfaces in Earth system models. *Nat. Commun.* 11, 2458. <https://doi.org/10.1038/s41467-020-16236-2>

2. Chapter 1: Assessing Fish Habitat and the Effects of an Emergency Drought Barrier on Estuarine Turbidity Using Satellite Remote Sensing*

Christiana Ade, Erin L. Hestir, Christine M. Lee

¹ School of Engineering, University of California Merced, 5200 N. Lake Road, Merced, California, 95340 USA (Ade, Hestir), NASA Jet Propulsion Laboratory, California Institute of Technology, Pasadena, CA, United States (Lee) (Correspondence to Ade: cade@ucmerced.edu)

*This chapter is published in the Journal of American Water Resources Association. Ade, C., Hestir, E.L., Lee, C.M., 2021. Assessing Fish Habitat and the Effects of an Emergency Drought Barrier on Estuarine Turbidity Using Satellite Remote Sensing. *J. Am. Water Resour. Assoc.* 57, 752–770. doi/full/10.1111/1752-1688.12925

Abstract

Estuaries worldwide are experiencing stress due to increased droughts, which often prompt intervention by environmental managers and government agencies. Effective management of water resources in estuarine systems can be enhanced by new technologies and methodologies to support decision-making processes. Here, we evaluate the use of high frequency, high resolution satellite remote sensing within two management-relevant case studies in the San Francisco Estuary and the Sacramento-San Joaquin River Delta. We used a remote sensing-derived time series of turbidity maps to 1) identify favorable turbidity conditions for the endangered fish species, delta smelt (*Hypomesus transpacificus*), during the height of the great California drought in the dry season of 2015, and 2) evaluate changes in turbidity following the installation of an emergency saltwater intrusion barrier. The mapping results indicate several persistent areas of turbidity refugia throughout the summer in the north and west Delta; however, there was infrequent connectivity. A comparison of images captured during ebb tides before and after barrier installation showed a mean increase of 6.6 Nephelometric Turbidity Units (NTU) in the San Joaquin River and 4 NTU in Fisherman's Cut. Our assessment of the barrier supports previous findings, which used field samples to conclude barrier installation may have resulted in increased turbidity near the barrier and enhances these findings by providing spatial context.

Keywords: remote sensing; turbidity; drought; spot-5 take-5; delta smelt; hypomesus transpacificus; sacramento-san joaquin delta; san francisco estuary)

2.1 Introduction

While estuaries provide important ecosystem services to humans, they are also one of the most endangered and modified habitats on earth (Barbier et al. 2011). Droughts can further exacerbate estuarine habitat degradation by diminishing water flow and connectivity between fresh and saltwater sources, thereby impacting water speed, clarity and salinity of estuaries worldwide (Wetz and Yoskowitz 2013). As climate change continues to affect the amount and timing of precipitation and increases the frequency and severity of low flow in certain regions, estuarine water quality and ecology will likely be degraded (Wetz and Yoskowitz 2013, IPCC 2007). To mitigate negative drought impacts, such as increased salinity on water resources, water resource managers often modify water flows. However, these alterations may inadvertently alter water quality in ways that negatively impact ecosystem function and habitat quality. Consequently, there is a need to monitor water quality changes due to drought and management interventions in order to track potential competing impacts on the ecosystem and management for threatened and endangered species.

The 2012-2016 California drought was one of the longest and warmest droughts on record caused by an anomalously persistent ridge of high pressure in the Pacific Ocean (Swain et al. 2017). Low inflows to the Sacramento-San Joaquin River Delta, the hub of California's water system, resulted in a precipitous drop in Delta exports to Southern California and San Francisco Bay area cities, from 6.5 million acre feet in 2011 before the drought to 1.8 million acre feet in 2015 (Lund et al. 2018). The low inflows and follow-on effects on exports and environmental flows prompted a response by state agencies tasked with managing the balance between a healthy ecosystem and sustainable water supply. In May 2015, the California Department of Water Resources (CDWR) erected an emergency rock wall barrier to reduce salinity intrusion into the Central Sacramento- San Joaquin Delta. The objective was to prevent saltwater contamination of drinking water supplies and conserve water in upstream reservoirs that would otherwise have to be released to maintain flows during the peak of the drought (Lund et al. 2018, CDWR 2016). This barrier impacted tidal current speed of the San Joaquin River (Kimmerer et al. 2019), which could have influenced the spatial distribution of turbidity. Large shifts in turbidity are of particular concern because native species, like the endangered delta smelt (*Hypomesus transpacificus*), thrive within a specific turbidity window (12 – 80 Nephelometric Turbidity Units; NTU) (Hasenbein et al. 2016), and the State is obligated to manage pumping operations based on this water quality parameter (CDWR 2012). Potential changes as a result of the barrier were previously studied and reported conflicting conclusions regarding impacts on turbidity (Kimmerer et al. 2019, ICF 2015). However, these conclusions were drawn mainly from point-based data from continuous monitoring stations and discrete sampling. Available satellite data presents an opportunity to evaluate changes in turbidity across larger areas of interest and with spatial continuity.

Satellite remote sensing offers 'wall-to-wall' spatial coverage with a systematic repeated sampling interval, enabling evaluation of spatial dynamics that are unobservable using in situ sampling alone (Lymburner et al. 2016, Giardino et al. 2019, Vanhellemont and Ruddick 2014). Turbidity is a water quality parameter that represents the amount of light absorption and scattering with a water column and is highly amenable for assessment via optical remote sensing methods. While there is no dedicated satellite sensor for

monitoring inland water quality, turbidity can be mapped from two classes of satellite remote sensing instruments: land imaging systems and ocean color sensors. Ocean color sensors, such as VIIRS, MODIS, MERIS, Sentinel-3 OCI, and SeaWiFs are characterized by a high repeat period (1-2 days) necessary to capture the dynamic changes in water conditions but have too coarse of a spatial resolution for many inland water bodies (typically 300 m – 1 km). Land imaging systems such as Landsat, Sentinel-2 and SPOT have the spatial resolution necessary for mapping inland waters (~ 10 – 60 m), but this comes with a trade of a decreased swath width and thus a longer revisit interval (~10-16 days), reduced signal to noise, and use of spectral information optimized for evaluating terrestrial features.

Turbidity is most commonly mapped from remote sensing imagery using empirical or semi-analytical spectral inversion methods that calculate turbidity from water-leaving reflectance values. Empirical algorithms relate a spectral band or combination of spectral bands to in situ turbidity measurements. This method has been used to accurately retrieve turbidity in several inland and coastal water bodies (Bustamante et al. 2009, Petus et al. 2010, Kabbara et al. 2008). However, empirical algorithms often result in poor retrievals when used in waters with different optical, biogeochemical, or hydrographic conditions than those used in initial algorithm development and are specific to a given sensor's spectral bands. Semi-analytical inversion algorithms are developed using underwater light transfer properties and radiative transfer models to estimate the optical conditions of the water quality (i.e., absorbance, attenuation and backscattering) and related optical water quality parameters (e.g., chlorophyll-a, suspended matter, colored dissolved organic matter) (Nechad et al. 2010, Brando et al. 2012). These parameters are then related to in situ turbidity measurements and have also been successfully applied in optically complex water bodies around the world (Dogliotti et al. 2016, Kuhn et al. 2019). These methods can be used for any optical sensor that has a spectral range encompassing the green to near-infrared regions of the spectrum (500-900 nm) (Dogliotti et al. 2015). While these methods are generalizable across a range of different sensors, they still often require regional calibration with empirically derived coefficients (Odermatt et al. 2012, Dogliotti et al. 2015).

In this study, we used an experimental satellite dataset created by the French Space Agency, CNES, SPOT-5 Take-5 (S5T5), to map turbidity in a drought-impacted estuary, and used the maps to 1) assess the habitat extent of an endangered fish during the peak of the drought, and 2) assess the impact of the emergency saltwater intrusion barrier on turbidity. The S5T5 dataset was acquired over the upper San Francisco Estuary and its delta, the Sacramento-San Joaquin during the height of the great California drought, from April-September 2015. The dataset was created by maneuvering the SPOT-5 satellite sensor into a 5-day repeat orbit, thus capturing multispectral images at 10 m pixel resolution. The S5T5 experiment provides the only high temporal and spatial resolution satellite dataset that covers the time period around the barrier installation. As a result of our analysis, we present the first delta smelt turbidity refugia map derived using remote sensing data.

2.2 Study Area

The Sacramento-San Joaquin River Delta in California (henceforth “The Delta”) provides fresh water to 27 million urban users and supports California’s \$50 billion agricultural industry (CDFA 2018). Additionally, the Delta is considered a biodiversity hotspot, providing critical habitat to several threatened and endangered fish, bird, and mammalian species (IUCN 2014). The Delta is a heavily managed and highly altered system where anthropogenic modifications such as scheduled dam releases, cross-channel gates, and pumping stations constrain hydrodynamic variability (Delta Stewardship Council 2013). To meet California’s legislated co-equal goal of providing a reliable water supply while protecting, restoring and enhancing Delta ecosystems, water management decisions are often informed by water quality characteristics – including turbidity - that correspond with suitable habitat for native fish species.

The delta smelt (*Hypomesus transpacificus*) is a pelagic fish endemic to the San Francisco Estuary and Suisun Bay. It is listed as threatened under the Federal Endangered Species Act and endangered under the California Endangered Species Act. Turbidity is an important component of the habitat occupied by the delta smelt along with temperature and salinity (Brown et al. 2013, Sommer et al. 2011, Feyrer et al. 2011, Feyrer et al. 2007). The fish are most likely to survive at turbidities greater than 12 NTU, a threshold that influences current water management practices in the Delta, including the quantity and timing of exports (Hasenbein et al. 2016). However, maintaining favorable fish habitats has been challenged by long droughts and a decrease in sediment supply from the Sacramento River (Cloern and Jassby 2012). The number of delta smelt sightings has decreased over time and the drought pushed delta smelt counts to a record low level in 2014-2015 and adult fish have not been observed during the Fall Midwater Trawl since 2018 (Moyle et al. 2016, Lund et al. 2018) (<https://www.dfg.ca.gov/delta/data/fmwt/indices.asp>). Their habitats are strongly associated with turbidity in the Spring – Fall period and environmental managers are concerned that spatial changes in the distribution and extent of high turbidity areas could draw the fish closer to the water pumps in the south Delta (Grimaldo et al. 2009). The State of California is required to shut off water pumps when specific in situ stations in the Central Delta measure turbidity greater than 12 NTU and the flow of the Sacramento River Freeport station is less than 80,000 cubic feet per second (CDWR 2012).

The year of 2015 was the fourth year in one of California’s most severe droughts and the possibility of saltwater intrusion into the Central Delta prompted the California Department of Water Resources (CDWR) to install a temporary rock wall barrier (hereafter, the “barrier”) as a preventative measure. The barrier spanned across False River in the Central Delta (**Figure 2-1**) to prevent saltwater intrusion into Franks Tract by reducing tidal dispersion across False River. The channel was officially closed on May 28th, 2015 and the barrier was fully removed by November 15th, 2015. A retrospective analysis of the impacts caused by the barrier were evaluated by Kimmerer et al. (2019) through hydrodynamic modeling (UnTrim) and in situ measurements. They determined that the barrier succeeded in decreasing the tidal prism into False River and Franks Tract, but that it increased the prism in Fisherman’s Cut and potentially the Sacramento San Joaquin River. However, they were unable to conclude if these tidal prism changes impacted turbidity. The impacts of the barrier were also studied throughout the barrier installation and removal by ICF International in collaboration with CDWR (ICF 2015), in

which they determined the barrier increased turbidity at two locations through additional discrete samples.

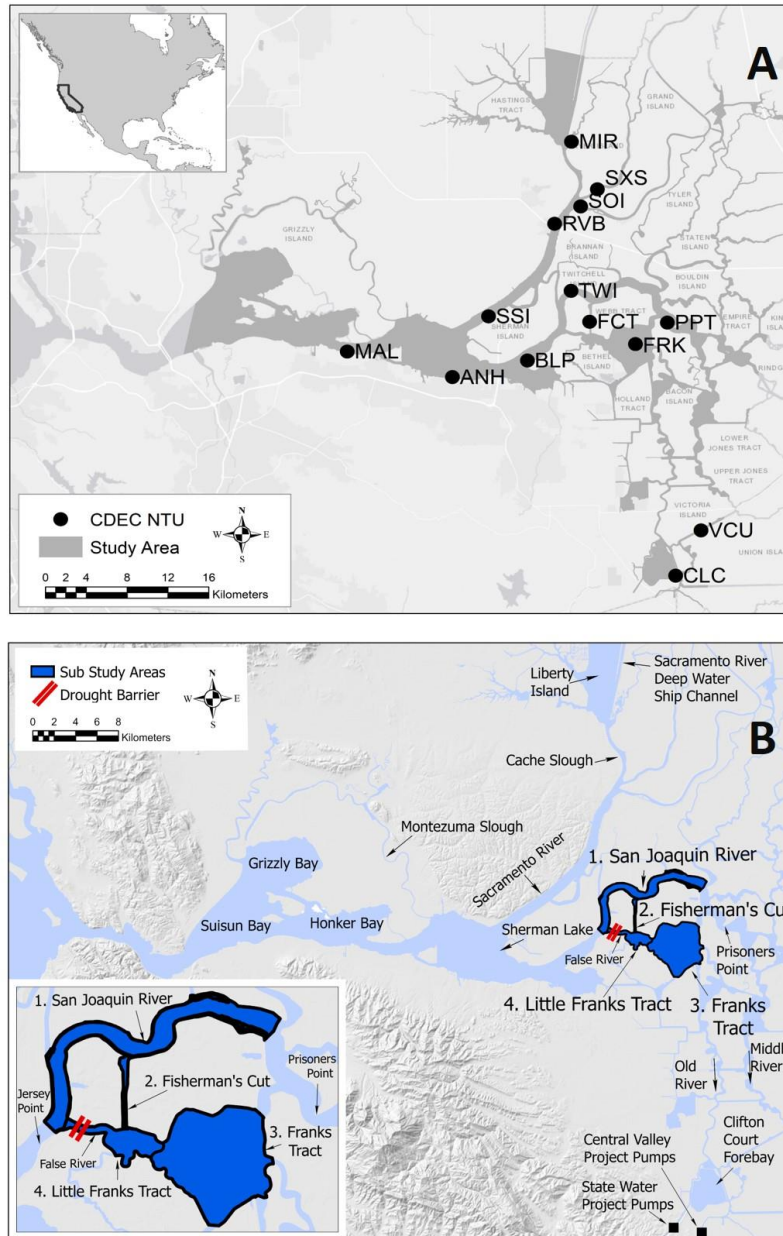


Figure 2-1. Maps of the study area including general locations discussed in the text. (a) The SPOT-5 Take-5 (S5T5) waterways in the Sacramento–San Joaquin River Delta, Suisun, and Grizzly Bays are shaded gray. Continuous in situ turbidity stations are represented by circles (Nephelometric Turbidity Units; NTU). (b) Four subregions areas used to evaluate the potential influence of the emergency saltwater intrusion barrier, including 1. The portion of the San-Joaquin River, 2. Fisherman’s Cut, 3. Franks Tract, 4. Little Frfnks Tract. The barrier location is shown in red. CDEC, California Data Exchange Center.

2.3 Methods

We used the time series of SPOT5-Take5 (S5T5) satellite imagery to derive turbidity maps that were calibrated with in situ turbidity measurements collected in NTU at fixed near continuous monitoring stations (every 15 minutes). The error of the maps was quantified using a jackknife approach. The resulting maps were then used to create a map of delta smelt potential habitat based on the 12 NTU management threshold for delta smelt to assess the effects of the drought on their habitat and the potential impacts the barrier had on turbidity.

2.3.1 Satellite Data and Image Pre-processing

The S5T5 experiment was designed by the ESA (European Space Agency) and CNES (Centre National d'Etudes Spatiales) to mimic Sentinel-2 A & B satellite data prior to their launch in June 2015 (A) and March 2017 (B). The SPOT-5 satellite orbit was modified allowing the sensor to acquire multispectral data over 150 targets across the globe every five days at a 10-m pixel resolution from April 16th to September 8th, 2015. The Delta was one of two sites in the United States selected for the experiment. The instrument collects information in four spectral bands (**Table 2-1**) and has been used for decades to map turbidity in various coastal and inland water bodies (Dekker et al. Peters 2001, Gernez et al. 2015, Doxaran et al. 2006).

Although both Sentinel satellites successfully launched, there was approximately a 3-month commissioning phase before each satellite sensor was shifted into routine operations, and global coverage at a 5-day repeat interval was not available until late 2017. Thus, the S5T5 experiment is the only existing high spatial, high temporal resolution publicly available satellite dataset we are aware of that can be used to study the effects of the installation of the barrier on dry season turbidity and delta smelt habitat availability in the Delta.

Level 2A surface reflectance products and accompanying masks were downloaded through the S5T5 client (www.theia-land.fr, Accessed February 2021). Level 2A products are created using the atmospheric correction algorithm MACCS (Multi-sensor Atmospheric Correction and Cloud Screening) (Hagolle et al. 2015). Images were converted from bit signed integer to reflectance values using a scale factor of 1,000. Clouds and cloud shadows were screened using the provided cloud masks at the most stringent thresholds. Ten scenes were excluded from analysis if there was greater than 5% cloud cover within the Delta boundary or excluded after visual inspection if the cloud mask was unsuccessful (e.g., large patches of haze and fog were missed by the mask). A total of 16 scenes from the S5T5 experiment (April 16 - September 8, 2015) were used to construct the turbidity time series (**Table 2-2**). The image boundary of each S5T5 scene did not directly overlap, so they were all cropped to the area visible in every swath (**Figure 2-1 A**, waterway labeled in grey).

Land and vegetation masking

A land/vegetation mask was created using a high resolution vegetation map from Ustin et al. (2016) and the California Aquatic Resource Inventory (CARI) Version 0.1 (SFEI 2015). The CARI dataset was used here to delineate waterways from wetlands west of the confluence of the Sacramento and San Joaquin Rivers. The Ustin et al. (2016) dataset is

based on airborne hyperspectral vegetation surveys and captures detailed vegetation coverage for wetlands east of the river confluence. Areas mapped by Ustin et al. (2016) as soil, riparian, emergent, non-photosynthetic and floating vegetation were masked in all S5T5 scenes. On an image by image basis, pixels not suitable for mapping water quality (e.g., those with sun-glint or mats of aquatic macrophytes and algae) were also removed by thresholding the SWIR band > 0.068 (Vanhellemont and Ruddick 2016) and calculated Normalized Difference Vegetation Index (NDVI) > 0.23 (based on NDVI values where submerged aquatic vegetation was present).

Table 2-1. Spectral Bands of the S5T5 instrument and their corresponding wavelengths in micrometers.

Band Name	Wavelength (μm)
Green	0.500 – 0.590
Red	0.610 – 0.680
Near Infrared (NIR)	0.781 – 0.890
Shortwave infrared (SWIR)	1.580 – 1.750

Table 2-2. Image acquisition dates, the number of in situ turbidity sensors used for site calibrated turbidity retrievals (units: NTU) and their turbidity ranges for each date.

Image date	Number of in situ NTU sensors used for calibration	Measured in situ turbidity range (NTU)
2015-04-16	6	10.6 – 38.6
2015-05-01	8	2.6 – 22.7
2015-05-06	6	3.4 – 29.0
2015-05-16	8	4.1 – 24.5
2015-06-15	9	0.6 – 20.6
2015-06-25	12	2.9 – 19.8
2015-07-05	12	3.6 – 20.8
2015-07-15	12	4.2 – 27.1
2015-07-25	10	3.9 – 12.3
2015-07-30	12	1.9 – 14.4
2015-08-09	10	3.9 – 34.2
2015-08-14	12	3.3 – 22.3
2015-08-19	13	0.9 – 18.3
2015-08-24	12	1.2 – 14.1
2015-09-03	12	2.4 – 16.4
2015-09-08	13	3.1 – 19.3

2.3.2 Turbidity Data

Turbidity measurements in NTU were retrieved from California Data Exchange Center (CDEC: <https://cdec.water.ca.gov/>, Accessed September, 2019), which provides data from water quality sensors at 15-min intervals. NTU measurements are acquired by measuring scattering using a white light at a 90-degree angle. Fourteen NTU stations were used for algorithm calibration because we wanted to achieve the best possible calibration model related to management decisions which are made relative to the threshold units of NTU.

For each image date, the in situ measurement acquired closest to satellite acquisition time (approx. 10:50 am) was selected. Station dates with NA or a negative value were removed, as were those with a rapid change greater than 15 NTU that was not sustained for more than 1 or 2 readings. Removed NTU readings include the station SOI on 2015-07-30. Additionally, three stations in the western Delta (GZL, RYC, and HON) were excluded because they were installed halfway through the timeseries and provided only a few data points after masking. Although this eliminated some high turbidity calibration points (>100 NTU), this was not of concern for the focus of this study, which requires accurate calibration for low to medium turbidity conditions that center around the management threshold of 12 NTU for the delta smelt.

2.3.3 Turbidity Mapping: Model Calibration and Validation

Turbidity Calculation.

A widely used semi-analytical algorithm developed by Nechad et al. (2010) to retrieve surface turbidity from remote sensing reflectance of a single band was applied using the S5T5 red band (0.610 – 0.680 μm) (Eq. 1)

$$\text{Turbidity (FNU)} = \frac{A^\lambda \rho_\omega(\lambda)}{1 - \frac{\rho_\omega(\lambda)}{C^\lambda}} \quad \text{Eq 1.}$$

where $\rho_\omega(\lambda)$ is the water reflectance at a specific wavelength, A and C are band specific calibration coefficients. This model was developed for Formazin Nephelometric Units (FNU); however, for the Delta FNU and NTU have been considered as interchangeable (Morgan-King and Schoellhamer 2013). Here we used $A = 253.51$, $C = 0.1641$ which are related to a band center of 645 μm as determined in Nechad et al. (2010). To ensure accurate mapping near the 12 NTU standard, we selected a single red band algorithm over NIR/SWIR band-switching algorithms (e.g., Dogliotti et al. 2015) because high correlation has been demonstrated between in situ turbidity and the reflectance in the red band for low-moderate turbidity values (1.5-45 NTU) (Goodin et al. 1996, Maltese et al. 2013, Bustamante et al. 2009).

Turbidity Calibration

Resulting turbidity maps from Eq. 1 were further tuned for local conditions by calibrating them with in situ turbidity measurements (NTU) (**Figure 2-2**). Turbidity values from Eq. 1 were extracted from all pixels within a 30-m buffer of each station location using ArcMap 10.5.1 (ESRI 2016) and R 3.6.1 (R Foundation for Statistical Computing, Vienna, Austria). Stations with less than 10 pixels were excluded from further analysis because this indicated too much of the channel was occupied by vegetation or other

unsuitable pixels. The calibration model was determined by calculating the ordinary least-squares regression for the mean turbidity of pixels within the buffer regressed against the value recorded by the station (**Figure 2-2 A**). Model stability was evaluated using a jackknifing procedure in which each station reading was removed once, and correlation coefficients and root mean squared error (RMSE) were recomputed (Efron 1981). The recomputed values and their associated standard error related to the jackknife approach were slope of 0.63 ± 0.07 , y-intercept of -0.34 ± 1.21 and RMSE 8.29 ± 0.36 . The final calibration model using all station data was:

$$\text{StationNTU} = 0.634 * \text{SatelliteNTU} - 0.336 \quad \text{Eq 2.}$$

Applying the calibration model Eq. 2 to all turbidity maps from Eq. 1 resulted in a final RMSE of 4.7 NTU and percent normalized RMSE (%NRMSE) of 12.4 % (**Figure 2-2B**).

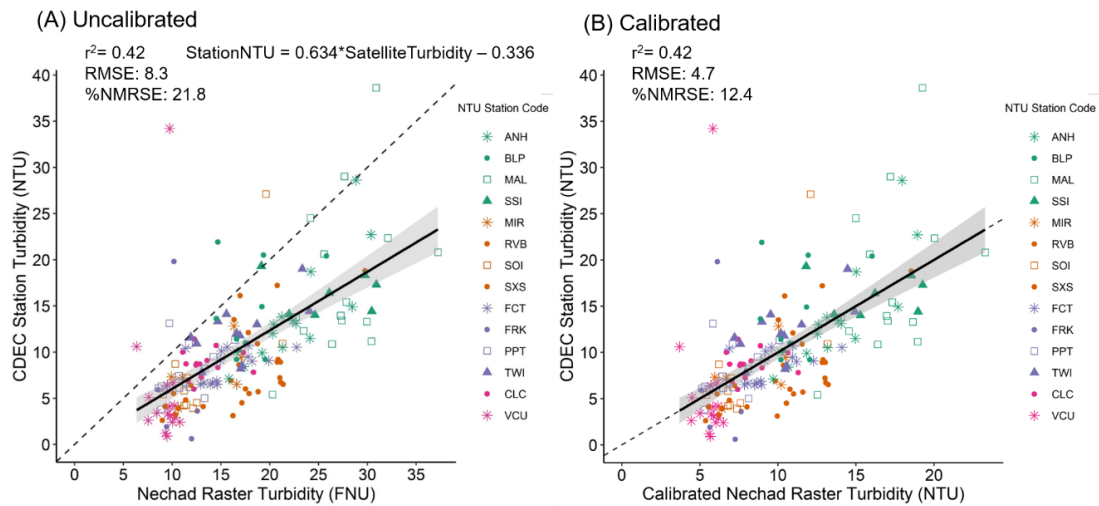


Figure 2-2. Raster turbidity as calculated by Equation (1) vs. the corresponding station in situ turbidity (n = 167). (b) The calibrated raster turbidities (determined by applying a linear model fitted in a) vs. the corresponding station turbidity measurements. Stations are grouped by color relating to different geographic zones of the Delta: west (green), north (orange), central (purple), and south (pink). RMSE, root mean squared error; FNU, Formazin Nephelometric Units; %NRMSE, percent normalized RMSE.

2.3.4 Habitat Mapping

Water Quality Suitability Maps

A turbidity suitability map was created for delta smelt by thresholding the calibrated turbidity time series for 12 NTU and above. A binary raster for each image was created where all pixels greater than 12 NTU received a value of 1 (suitable turbidity) and all below received a value of 0 (unsuitable turbidity). The frequency of occurrence of suitable turbidity was then calculated as the number of times a pixel was above 12 NTU divided by the number of images in the time series (16 images) and converted to a percent. The upper and lower bound estimates of percent frequency of suitable turbidity was calculated by

subtracting or adding the calibrated RMSE (4.7 NTU) to each turbidity map and applying a threshold at 12 NTU to each resulting map. The three maps (estimate, upper and lower bounds) were then categorized by the percent of time a pixel was suitable for delta smelt throughout the time series. The six categories are 0%, 6 - 20%, 20 - 40%, 40 - 60%, 60 - 80%, 80 - 100%. The estimate map was evaluated to identify areas of frequently suitable turbidity conditions that may be acting as turbidity refugia for delta smelt and were assessed for connectivity of frequently suitable turbidity conditions. While the upper and lower bound maps were used to determine the range of percent waterways within each frequency category.

Fish Trawl Habitat Evaluation

We compared the number of fish caught during the 2015 20-mm trawl survey to the habitat frequency map produced using the first 7 binary rasters created above (image dates: 2015-04-16 – 2015-07-05), which correspond to the dates over which the trawl survey occurred. The California Department of Wildlife surveys 67 stations every two weeks between March – July to record sub-juvenile and juvenile delta smelt abundance (<https://wildlife.ca.gov/Conservation/Delta/20mm-Survey>; Accessed May 2020). All fish counts taken between April 13th and July 7th (7 field campaigns) were totaled by station. Spatial similarity was visually compared between suitable turbidity frequency hotspots and fish capture locations.

2.3.5 Impacts of the Emergency Saltwater Intrusion Barrier on Turbidity

Potential impacts of the barrier on turbidity were assessed for a focal area around the barrier and were divided into four sub-regions based on previous findings by Kimmerer et al. (2019) and MacWilliams et al. (2016): the lower portion of the San Joaquin River, Fisherman’s Cut, Franks Tract, and Little Franks Tract & False River to the east of the barrier (henceforth referred to as Little Franks Tract) (**Figure 2-1B**). This portion of the San Joaquin River was observed by Kimmerer et al. (2019) to have an increase in tidal speed and particle transport due to the barrier, therefore, we anticipated higher turbidity post-installation. Turbidity was anticipated to increase or remain the same in Fisherman’s Cut due to the increased tidal speed in the San Joaquin River. Turbidity was hypothesized to decrease in Frank’s Tract because the barrier would disrupt the flow of water entering the Tract through False River, commonly described as the “nozzle” (Kimmerer et al. 2019). A similar decrease was expected for Little Frank’s Tract; however, any decreases might be negated if there is a large enough increase in Fisherman’s Cut which connects directly to Little Frank’s Tract.

The potential impacts of the barrier were assessed by comparing pairs of pre-and post-installation turbidity maps with similar stage height and tidal conditions. Pairs were selected using CDEC river stage sensors (ANH and FAL) and NOAA tide cycle information (Antioch and Rio Vista). One map pair with similar tidal flood conditions was identified for April 16th and August 9th and one with similar tidal ebb conditions was identified for May 6th and July 7th. It is impossible to have a directly comparable day for before and after barrier installation because of the complexities of this system and the nature of remote sensing measurements, but these two image pairs were the closest in terms of tidal cycle. There is no supporting evidence based on CDEC turbidity sensor time series

that turbidity would be consistently different between April/May and August/July, thus we assumed that detectable changes would be due to barrier influence and not seasonal turbidity trends. For both map pairs, turbidity patterns were visually interpreted, and mean turbidity for each of the four sub-regions described above was calculated.

2.4 Results

2.4.1 Turbidity Suitability for Endangered Fish

Turbidity Suitability Maps

Figure 2-3 shows the turbidity suitability estimate map for delta smelt derived from the NTU calibration. **Figure 2-4** shows percent of waterways within each frequency percentage bin of suitable turbidity including the lower and upper bound estimates. The upper and lower bound maps are provided in **Appendix 2-7**. The estimate map indicated that only 5.6% of waterways were suitable delta smelt habitat for more > 60% of the study period (**Figure 2-4**). These areas of persistent turbidity suitability are indicative of potential turbidity refugia and are located in the upper portion of Grizzly Bay, where adult delta smelt are known to live and Liberty Island, a recognized spawning area (Moyle et al. 2016) (**Figure 2-3**). The 40 – 60% frequency bin comprised 10% of waterways and included portions of the Cache-Lindsey Slough complex (base of Liberty island), Montezuma Slough and Honker Bay, which are documented common habitat for the delta smelt (Murphy and Hamilton 2013, Sommer et al. 2011). There was little connectivity between areas of persistent turbidity suitability: 30% of waterways were labeled as never suitable and 50% of waterways including the Sacramento River were labeled between 6 – 20% frequency of suitability. The Sacramento River is the primary corridor between the North Delta and Suisun Bay and is important for the migration of some delta smelt (Hobbs et al. 2019), which may have been possible at least once or more often during the summer drought season based on turbidity conditions. Additionally, there was little to no connectivity to the Southern Delta and the Clifton Court Forebay, an area of concern for managers because it is the entry way to water pumps where the fish would become entrained (Grimaldo et al. 2009, Sommer et al. 2011).

The maps of lower and upper bounds displayed large differences in suitability frequency and connectivity between the potential refugia identified above (**Figure 2-4 & Appendix 2-7**). The map of turbidity suitability resulting from the upper bound estimates of turbidity indicates that as much as ~100% of waterways were suitable for delta smelt at some point during the time series, while the lower bound map labelled 75% of waterways as never suitable. Despite this difference in percent frequency, all three maps consistently indicated that portions of Grizzly Bay and Liberty Island had suitable turbidity conditions > 20%. However, the lower bound map only identifies 40% of Liberty Island as habitable (northeastern portion) while the estimate and upper bound maps identified 90 -100% of the region to be habitable at some point. The upper bound map also labels portions of Montezuma Bay, Cache Slough, the Sacramento Deep Water Channel, and the San Joaquin River as highly suitable. It is also the only map to identify the Sacramento River as a persistently suitable area that is connected to the central and south Delta at least > 40% of the time series. While Sherman Lake, located at the confluence of the Sacramento and San Joaquin Rivers, is also labeled as suitable at least some of the time in all maps, it is unlikely this is another potential zone for turbidity refugia. The turbidity retrieval results in Sherman

Lake may be highly influenced by the presence of mud banks and deep submerged aquatic vegetation that was not masked. The reflectance signal from the bottom could have increased retrieved turbidity values, and areas infested with submerged vegetation are not considered to be favorable for Delta Smelt (Sommer and Mejia 2013).

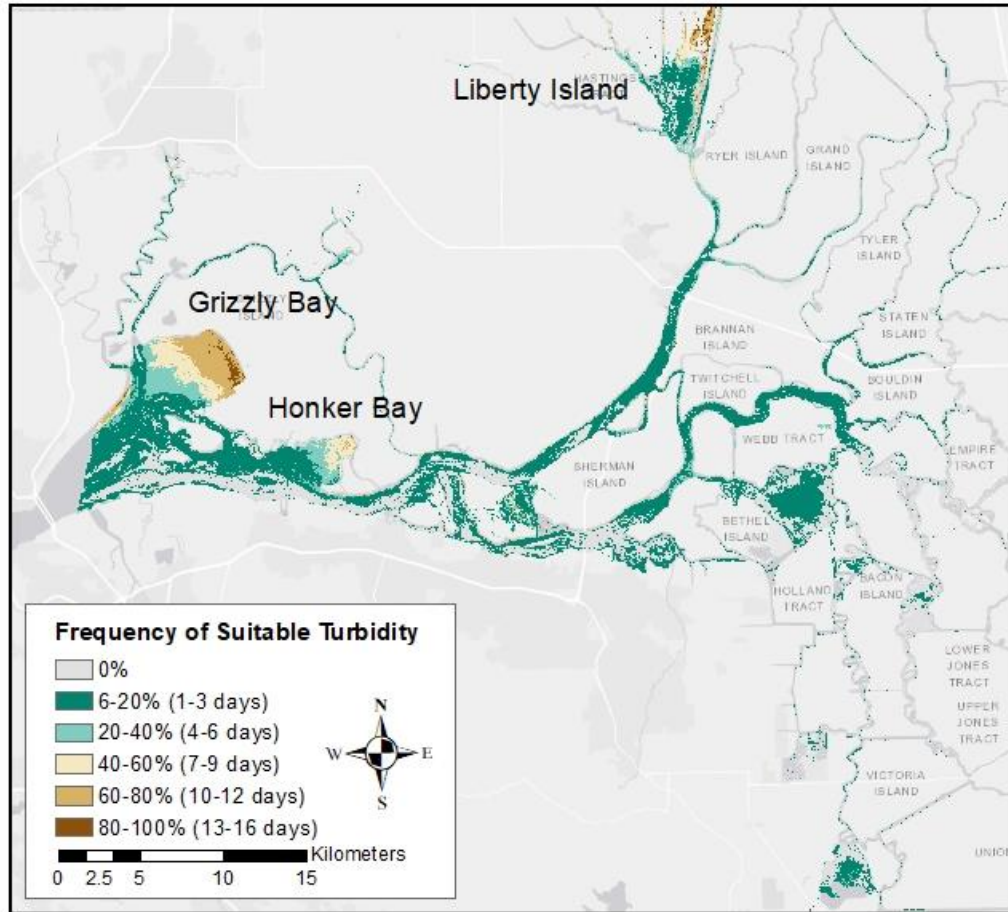


Figure 2-3. Using 16 acquisitions from April 16 to September 8, 2015, percent of total waterways within certain levels of percent frequency of suitable turbidity. The orange bar is the waterways percentage for the estimated map (in **Figure 2-3**). Gray bars show the range of waterways percentage when considering the upper and lower bound maps as determined from the RMSE of the turbidity retrievals (4.7 NTU).

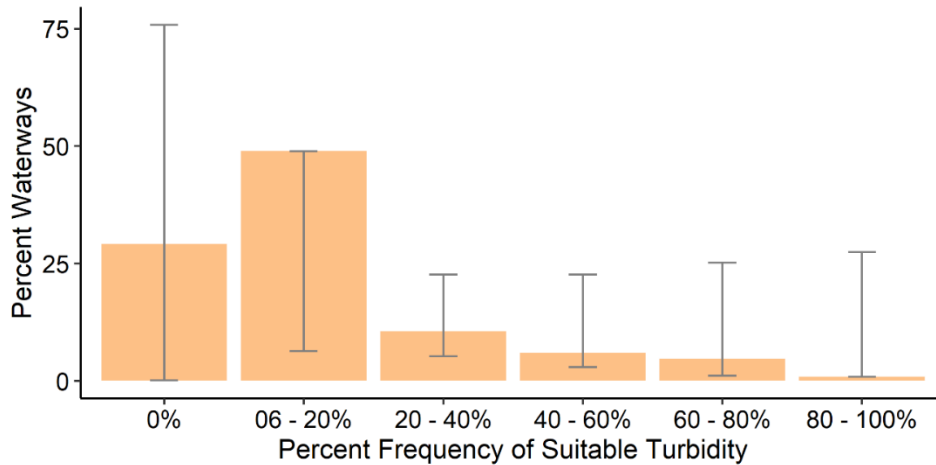


Figure 2-4. Delta smelt habitat potential as determined by the frequency of suitable turbidity >12 NTU over the course of the time series April 6–September 8, 2015.

Fish Trawl Habitat Evaluation

Our suitable turbidity frequency map (April – July) matched eight of nine fish trawl stations, including Montezuma Slough, portions of the Sacramento River, the San Joaquin River, Liberty Island, and the Sacramento Deep Water Channel (**Figure 2-5**). The highest fish count was 76 fish in the Sacramento Deep Water Channel which corresponded to an area of > 50% suitable turbidity frequency (4-7 days). In the southern Delta, one fish was counted in an area characterized as unsuitable and there was little to no connectivity between this southern station and the persistent refugia.

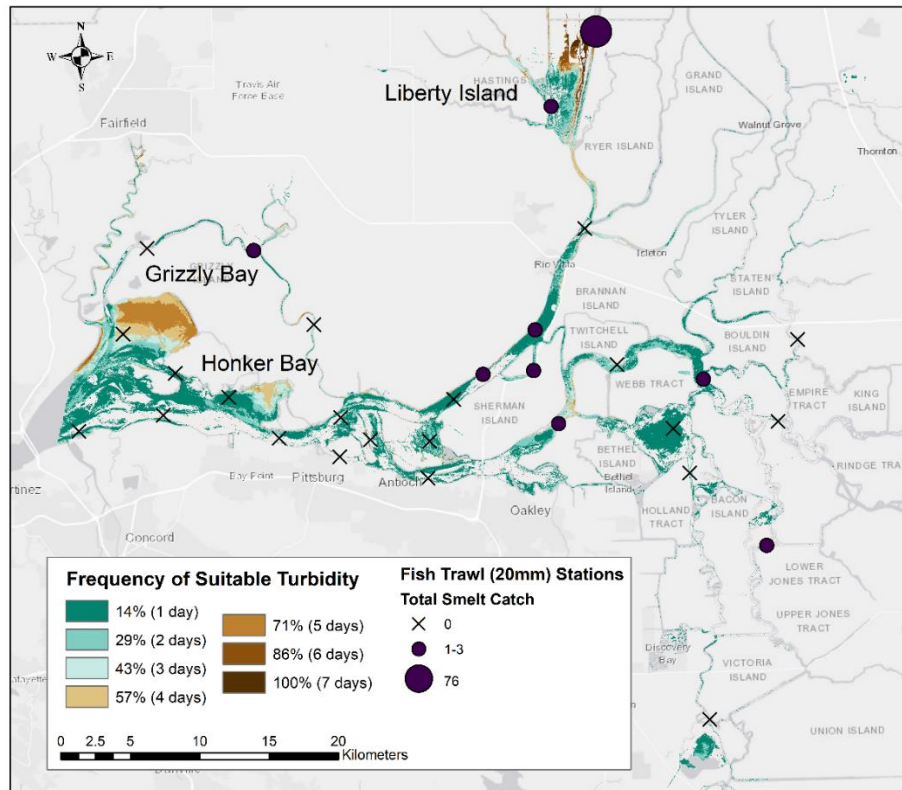


Figure 2-5. Seven S5T5 images that were acquired during the 20-mm fish trawl from April to July 2015 were used to match the frequency of suitable turbidity conditions during this period to fish counts.

2.4.2 Turbidity Time Series: Evaluation of Barrier Effect

One of the largest drivers of changes in turbidity in this system is tidal influences, where tidal stage has variable impacts in sub-regions in terms of water level and turbidity (Wright and Schoellhamer 2005). To account for tidally driven changes, images were grouped using tidal stage and river height. As a result, this study was able to map differences in turbidity during flood and ebb tidal stages and under pre- and post-barrier status (**Figure 2-6**) for all waterways visible in S5T5. The mean turbidity in each sub-region was evaluated for all pre- and post-barrier installation images throughout the time series with special attention to the flood and ebb pairs (**Figure 2-7**). When considering all image dates pre- and post-barrier installation, three of the four subregions had lower average turbidity after barrier installation (marked by black horizontal lines), except for the San Joaquin River. For Franks and Little Franks Tract, this matched our hypothesis that decreases in turbidity levels associated with the installation of the barrier may be due to reduction in flow; however, the differences were small and within the range of turbidity retrieval error, ranging from a difference of 0.4 – 2.1 NTU in mean turbidity. In the tidal pair comparisons, the ebb pairs showed greater changes in turbidity (0.4 – 6.6 NTU) than flood pairs (0.1 – 1.7 NTU).

San Joaquin River. The reach of the San Joaquin River that was evaluated in this study showed the greatest difference in the ebb pair; there was a 6.6 NTU increase in mean turbidity for the sub-region after barrier installation. When considering the standard deviation of the region, there is still a detectable increase of approximately 3 NTU (pre: 7.3 ± 1.9 NTU; post: 13.9 ± 1.7 NTU). However, this is less than the turbidity retrieval error estimate (4.7 NTU). Overall, this finding matched our hypothesis that the increased tidal speed reported by Kimmerer et al. (2019) would result in increased particle transport and thus higher turbidity values for the post-barrier image. This was not reflected in the flood pair – the difference was less than 0.5 NTU, thus providing evidence against our hypothesis that an increase in turbidity would be sustained after the installation of the barrier.

Fisherman’s Cut. Fisherman’s Cut was the only other area to show a large difference in an ebb pair. There was a 4 NTU increase in mean turbidity of the sub region after the barrier (pre: $11.3 \text{ NTU} \pm 2.1$; post: $15.3 \text{ NTU} \pm 2.9$). In the July 7th map (post ebb), this increase appears to be a result of increased turbidity in the San Joaquin River (**Figure 2-7**). This matches our hypothesis that there would be increased turbidity in the region due to the increased tidal flows in the San Joaquin River resulting from the barrier. However, the increase in NTU is smaller than the difference in standard deviation and turbidity retrieval error estimate indicating that there is no detectable change in this region. Unsuitable pixel masking in the pre-barrier flood image removed much of the channel, making it impossible to draw a definitive conclusion for the flood pair. In the post flood image, there is a higher turbidity value within Fisherman’s Cut channel than in the San Joaquin River, indicating that some changes in turbidity could be related to sediment resuspension rather than barrier installation.

Franks Tract. Both tidal pairs showed little change in turbidity, of the two the flood pair had a higher difference with a $1.8 \text{ NTU} \pm 1.4$ decrease in mean turbidity. When considering the standard deviation there was no detectable change which contrasted our hypothesis that the barrier would reduce flow into the region and result in a lower turbidity. The pre-barrier flood image matches the previously described “nozzle” effect because it shows higher turbidity flowing into the bottom portion of the Tract via False River. This pattern is not present in the post-image, but most of the area of Franks Tract is masked out due to large patches of submerged vegetation (Kimmerer et al. 2019), making it difficult to resolve any spatial patterns. Increased abundance in submerged vegetation from July – September which corresponds to increased masking of unsuitable pixels may be the cause of lower turbidity values in several post barrier images rather than the barrier itself. The post barrier ebb image does not include a ‘nozzle’ effect and areas of higher turbidity within Franks Tract appear to be originating from the San-Joaquin River (**Figure 2-7**). The additional flow and consequently an additional turbidity input from the San Joaquin River into the top of Franks Tract explains the minimal difference in turbidity between the pre and post ebb images.

Little Franks Tract. Turbidity in Little Franks Tract decreased for both tidal pairs; the flood pair had a higher difference of $1.4 \text{ NTU} \pm 1.4$. Although this supported our hypothesis that reduced flows through False River would result in a turbidity decrease in Little Franks Tract, the overlap in standard deviation makes results inconclusive. The ebb post image shows an apparent inflow of turbidity from Fisherman’s Cut, which may be minimizing

the difference between the pre and post turbidity values. Similar to Franks Tract, spatial patterns are difficult to discern in the post-barrier flood image due to vegetation and ‘unsuitable’ water pixel masking.

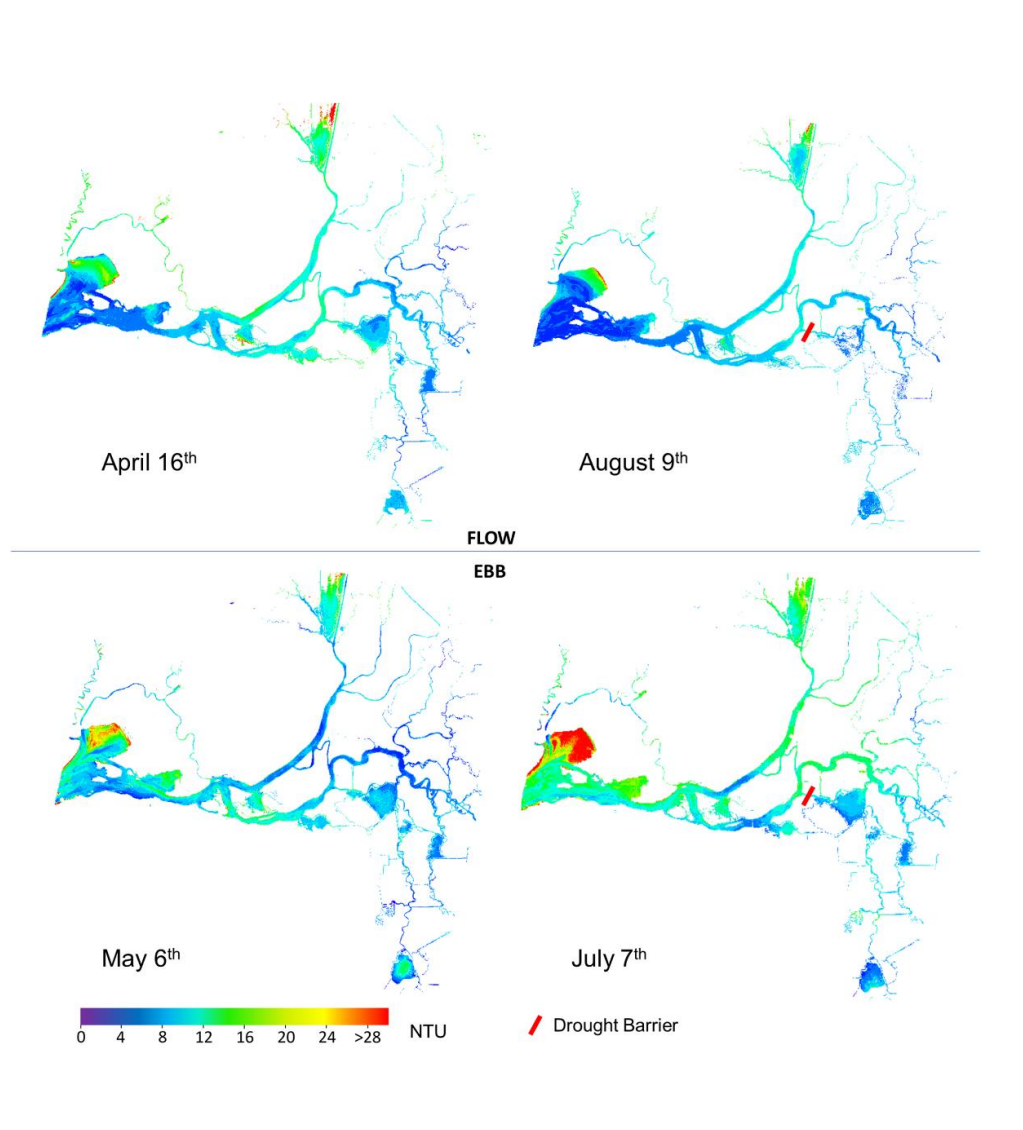
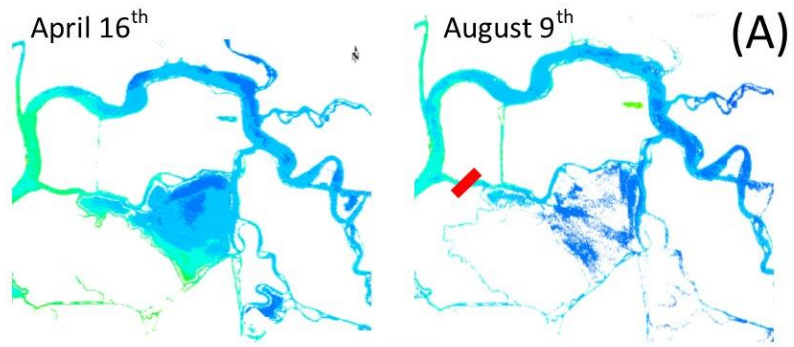
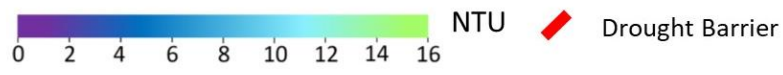
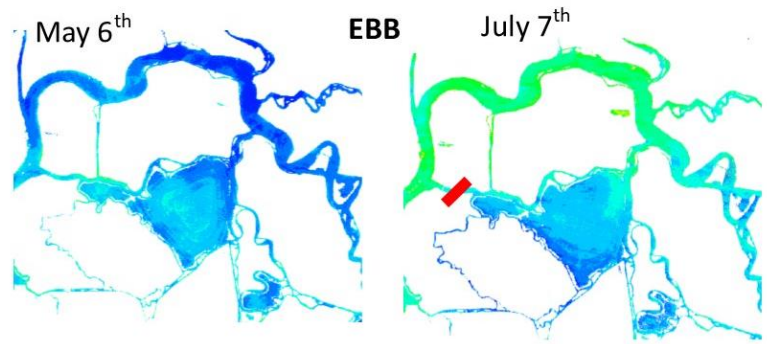


Figure 2-6. Site adjusted turbidity maps in NTU for two pairs of pre- and post-barrier installation images. The top pair has similar flood tide conditions and the bottom pair has similar ebb tide conditions. The barrier was installed on May 28, 2015 and removed November 15, 2015. The increase in masked pixels on August 9 corresponds to the increased presence of submerged vegetation patches.



FLOOD



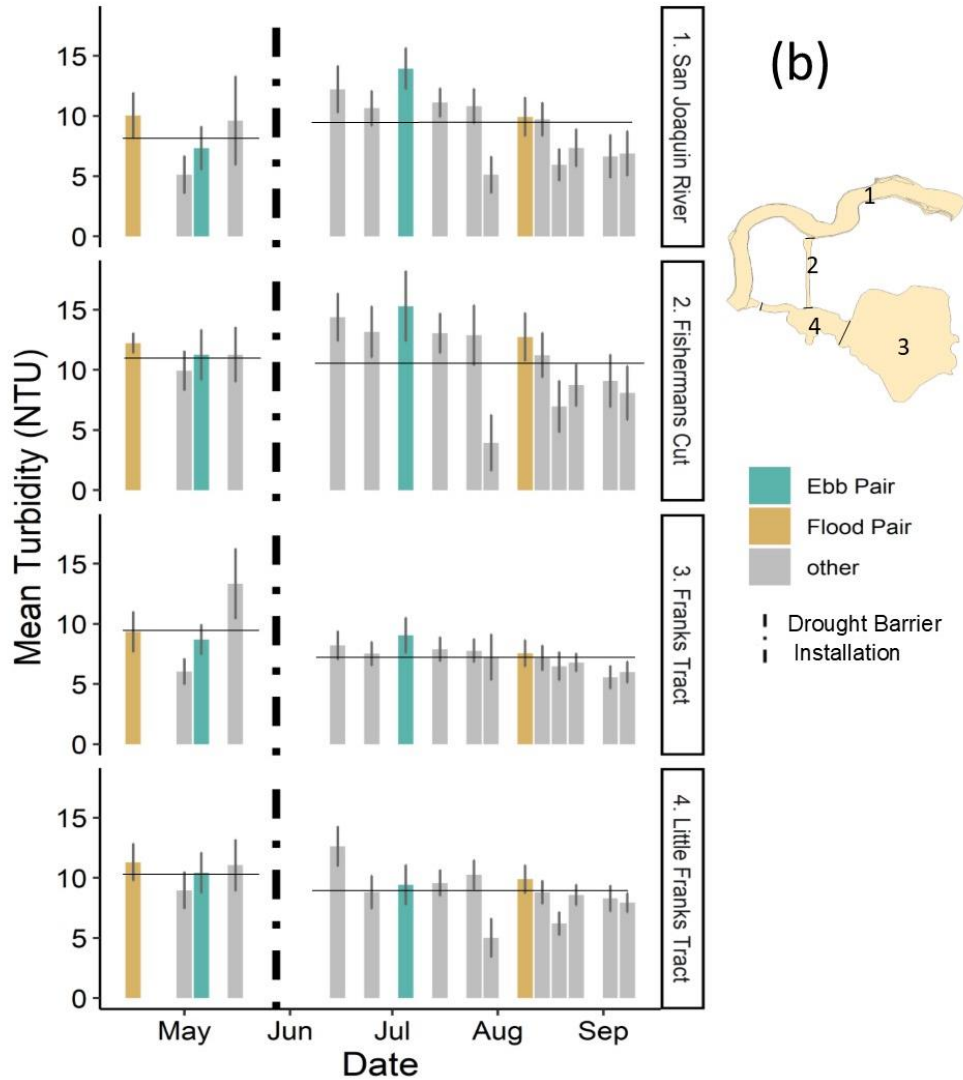


Figure 2-7. Turbidity maps for pre and post tide pairs centered on the four substudy areas (A). Mean turbidity and standard deviation for each subregion is shown for all image dates (B). The ebb and flood pairs are highlighted in turquoise and yellow, respectively. Horizontal lines represent mean turbidity for all images before the barrier installation, and after the barrier installation separately.

2.5 Discussion

2.5.1 Turbidity Algorithm Calibration

Image calibration resulted in a RMSE of 4.7 NTU and an r^2 of 0.44 (compared to an RMSE of 8.3 NTU uncalibrated) and was within the range of acceptable values reported during calibration/validation of turbidity products in other optically complex waters

(Dogliotti et al. 2015, Vanhellemont 2019). Other studies may report lower RMSE and higher r^2 values because the algorithms are applied to a single date rather than a time series or across a larger range of values. Here, sources of error include a mismatch between the satellite turbidity products and in situ NTU measurements due to vertical turbidity gradients. CDEC stations are located about one meter below the water surface while optical remote sensing instruments are making an integrated measurement of the surface water through approximately the photic zone (Bukata et al. 1995). Thus, any areas of high lateral variability or vertical turbidity gradients could result in a mismatch between turbidity retrieved from satellites and in situ measurements used during calibration. Additionally, there is a spatial mismatch between the two measurements, the in situ stations are point measurements whereas the corresponding satellite derived turbidities are the average of a 3 by 3-pixel window (900 m²). Although, this method is a common noise-reducing procedure and is based on the assumption that turbidity conditions are similar up to ~1km based on averaged particle size settling velocities (Hestir et al. 2016), it is possible that there is a larger turbidity variability near certain station locations (ICF 2015). Other sources of potential error are related to the algorithm application; the Nechad et al. 2010 algorithm outputs values in FNU rather than NTU. Both measure light scattered at a 90-degree angle, but NTU measurements are made with a white light whereas FNU are measured with an 860 nm (NIR) light. This difference in units might account for some error; however, the two measurements have been considered as interchangeable in the Delta (Morgan-King and Schoellhamer 2013). Also, site specific A and C coefficients may further improve algorithm accuracy, as these coefficients were derived for the ocean color sensors using reflectance spectra collected in the North Sea and they may not be applicable in certain optically complex waters (Nechad et al. 2010). We were unable to include site specific coefficients because the required measurements were not collected during the 2015 overpasses; however, we recommend that future studies consider parameterizing A and C coefficients to their system.

This study did not consider high turbidity conditions, which require different handling of atmospheric correction and turbidity algorithms with more sensitive NIR and SWIR bands than those available on SPOT 5 (Giardino et al. 2019, Vanhellemont 2019, Pahlevan et al. 2017). In fact, atmospheric correction is the biggest source of uncertainty between remote sensing turbidity products and in situ measurements (Salama and Stein 2009). The atmosphere accounts for up to 90% of the signal over water and thus accurate remote sensing retrievals over water require more accurate atmospheric correction models than terrestrial remote sensing applications. The atmospheric correction method, MACCS, used to produce S5T5 to surface reflectance products was created for terrestrial applications and although we were able to get reasonable turbidity retrievals, future users of satellite data should use improved methods designed for water. We were unable to apply more sophisticated atmospheric correction over water in this study due to the limitations of the SPOT sensor's spectral band configuration. However, Sentinel-2, the satellite that S5T5 was created to mimic, is now fully operational and has more spectral information in the blue and SWIR regions, and higher signal to noise over water. Further, there are specific atmospheric correction algorithms designed for retrieving water quality parameters with Sentinel-2, which might result in improved match-up with in situ measurements (Vanhellemont 2019).

2.5.2 Habitat Maps: Frequency of Turbidity Suitability

Several areas of potential delta smelt refugia were identified from turbidity suitability maps, despite differences in suitability frequency and levels of connectivity between the estimate, upper and lower bound maps. The largest and most consistent areas of turbidity were Grizzly Bay and Honker Bay in the west, and Liberty Island in the north, which are locations of adult delta smelt habitat and spawning ground (Moyle et al. 2016). The estimate and upper bound maps also indicated additional turbidity refugia in Montezuma Slough, the lower portion of San Joaquin, the Cache Slough Complex, and the Sacramento River and the Sacramento Deep Water Channel. These areas are similar to historical and present refugia described in Merz et al. (2011), Moyle et al. (2016) and Sommer et al. (2011). The higher frequency and persistently turbid areas mapped in this study also match hotspots mapped in Polansky et al. (2018) and high density areas mapped in Murphy and Hamilton (2013). Our maps differed from Polansky et al. (2018) and Murphy and Hamilton (2013) in two ways - we identified a specific hotspot in the northeast of Liberty Island and the suitable area in the San Joaquin River extends further upstream. This extended area may reflect potential effects of the barrier on turbidity and subsequently delta smelt habitat because we detected increased turbidity in this portion of the San Joaquin River and Kimmerer et al. (2019) concluded this area experienced an increased tidal speed post barrier.

Suitable turbidity maps indicate that there may have been limited connectivity between delta smelt refugia during the dry season of the peak of the 2012 – 2016 drought (April – September 2015). The spatial patterns of refugia and connectivity of suitable turbidity conditions may have different implications for the three distinct life-history phenotypes of delta smelt – freshwater resident, brackish-water resident, and semi-anadromous (Hobbs et al. 2019). The Sacramento River had a low frequency of turbidity suitability over from April-September 2015, which may have been problematic for the semi-anadromous fish because this waterway serves as a main corridor between their northern spawning ground and adult habitat in the west Delta. The areas of persistent turbidity suitability in Liberty Island and the Sacramento Deep Water Channel correspond with previous research that indicated a small portion of the fish population live year-round in freshwater or brackish water, commonly in these regions (Sommer et al. 2011, Sommer and Mejia 2013, Hobbs et al. 2019). These resident fish would be unaffected by the lack of connectivity in the lower Sacramento River, but they might have been forced into very specific areas of their historical habitat because of limited turbidity. The correspondence of 20-mm trawl fish catches with areas mapped as frequently suitable further supports these findings (**Figure 2-5**). Our maps show limited connectivity between the Southern Delta and persistent smelt refugia, which may indicate why delta smelt are rarely present in this area during summer months (Moyle et al. 2016) and indicates that despite concerns, fish may not have migrated close to the water pumping stations. However, the potential extended area of suitable habitat in the San Joaquin may be of concern because fish that travel downriver could get trapped in reverse flows and become entrained at the water pumping facility (Grimaldo et al. 2009).

The variation between the turbidity suitability estimate map and its upper and lower bounds make it difficult to reach a definite conclusion about the frequency of connectivity patterns. However, the observed “hotspot” of 76 fish in the Sacramento Deep Water

Channel is consistent with our observation of this area as being a persistent refuge. While significant numbers of fish were not recovered in other refuges, we also did not observe hotspot counts of fish in areas that were not refuges or only infrequently refuges. Improved/additional accounting of delta smelt habitat characteristics would support a more robust detection of habitat refugia and connectivity. Here we focused on the 12 NTU standard because of its importance to management decisions, but delta smelt thrive best between 12-80 NTU, thus we recommend future suitability maps also incorporate the upper bound of favorable turbidity for Smelt (Hasenbein et al. 2016). Including the whole turbidity window was not possible with this dataset because it would require improved characterization of highly turbid regions like the Western Delta. This will be achievable in future maps that are derived from more sophisticated satellites with improved atmospheric correction for turbid waters and additional calibration stations in high turbidity areas. Here we identified refugia based on turbidity suitability; however, turbidity is only one aspect of delta habitat and definitive refugia should be identified through habitat suitability maps which by adding other known habitat variables requirements and their windows, such as salinity and temperature, which may also be derived from remote sensing products (Varunan and Shanmugam 2018, Schaeffer et al. 2018).

2.5.3 Evaluation of Emergency Saltwater Intrusion Barrier Impacts on Turbidity

There is some evidence the barrier had an impact on turbidity in Fisherman's Cut and a portion of the San Joaquin River during an ebb tide, but not a flood tide. This aligns with findings by the ICF International (2015), which determined turbidity increased in Fisherman's Cut and Old River mouth (connected to the San Joaquin River near Franks Tract) as a result of the barrier. Through additional field sampling, they reported the largest difference occurred at the end of flood and ebb tides because of sustained higher velocities. This may support why we were only able to detect substantial changes in turbidity for the ebb pair; during satellite overpass the tide was near the end for the ebb pair, but near the middle of the flood tide. For both regions, the standard deviation and/or turbidity retrieval error estimate were greater than the observed change; however, this was only true for the San Joaquin River when considering both the standard deviation and retrieval error simultaneously. Therefore, there is likely still a detectable change between the pre-and post-barrier ebb images for the San Joaquin River because the retrieval error estimate had regional differences in performance with the Central Delta potentially having smaller errors than the global RMSE (Figure 2-2B). This sub-region shifted to >12 NTU post-barrier which may have negative implications for delta smelt as it might encourage travel further upstream closer to water pumps. Despite visual differences between pre-and post-barrier turbidity maps, potential changes in Franks Tract and Little Franks Tract were small or difficult to detect because of unsuitable pixel masking – largely due to increased patches of vegetation in late summer through Fall (Kimmerer et al. 2019). However, it does appear as though there was a slight decrease in turbidity for both areas because of the reduced tidal speed entering False River.

Although we calculated the mean turbidity condition by sub-region for our pre-and post-barrier comparison, the addition of spatially contiguous turbidity data is still useful for environmental assessments because it offers visual support of differences detected in and between the study areas. Turbidity products also allow users to 'sample' any sub-

region, rather than being limited by a priori determined station locations or the cost/time for additional discrete sampling campaigns. For example, the increased turbidity observed in Fisherman's Cut during the ebb tide is likely due to increased turbidity from the San Joaquin River and not to local resuspension near the in situ turbidity sensor because the turbidity increased across both locations simultaneously. Additionally, the maps show the difference between the pre and post ebb pair in Franks Tract may have been minimized by the additional turbidity inputs at the north end of Franks Tract from the increased turbidity in San Joaquin River. This allows us to update the Kimmerer et al. (2019) conclusion, in which they detected decreased water clarity near Prisoners Point in San Joaquin River but could not confidently conclude it was due to the barrier. Our maps show increased turbidity throughout the San Joaquin River which leads us to conclude that the barrier potentially affected turbidity. Future studies may consider a multi-sensor approach to enable greater data density and longer time series.

2.6 Conclusions

We used high spatial resolution satellite imagery to demonstrate the potential of remote sensing for aiding management decisions by evaluating two case studies related to turbidity during a drought. Turbidity refugia for the delta smelt were mapped based on the percent frequency that a pixel met turbidity thresholds important to management decisions in the Sacramento-San Joaquin Delta. To our knowledge, this is the first suitable turbidity frequency map created for the delta smelt derived with remote sensing imagery and the only time series map created from high frequency repeat data collected during the peak of the California drought. It is also the first evaluation of potential impacts the 2015 emergency saltwater intrusion barrier had on turbidity using remote sensing data. Our results are consistent with findings determined by the state using discrete field samples and supplement these with spatially continuous data. The addition of remote sensing derived water quality maps could facilitate or enhance future management decisions by 1) complementing extensive field campaigns with synoptic, systematic regular snapshots of a larger region for spatial context and scaling, 2) allowing users to 'sample' any area rather than relying on point measurements and 3) providing measurements in areas with limited in situ data. Although suitability mapping was demonstrated with delta smelt, a similar procedure could be conducted for any estuarine species including vegetation that require certain turbidity windows or thresholds for survival.

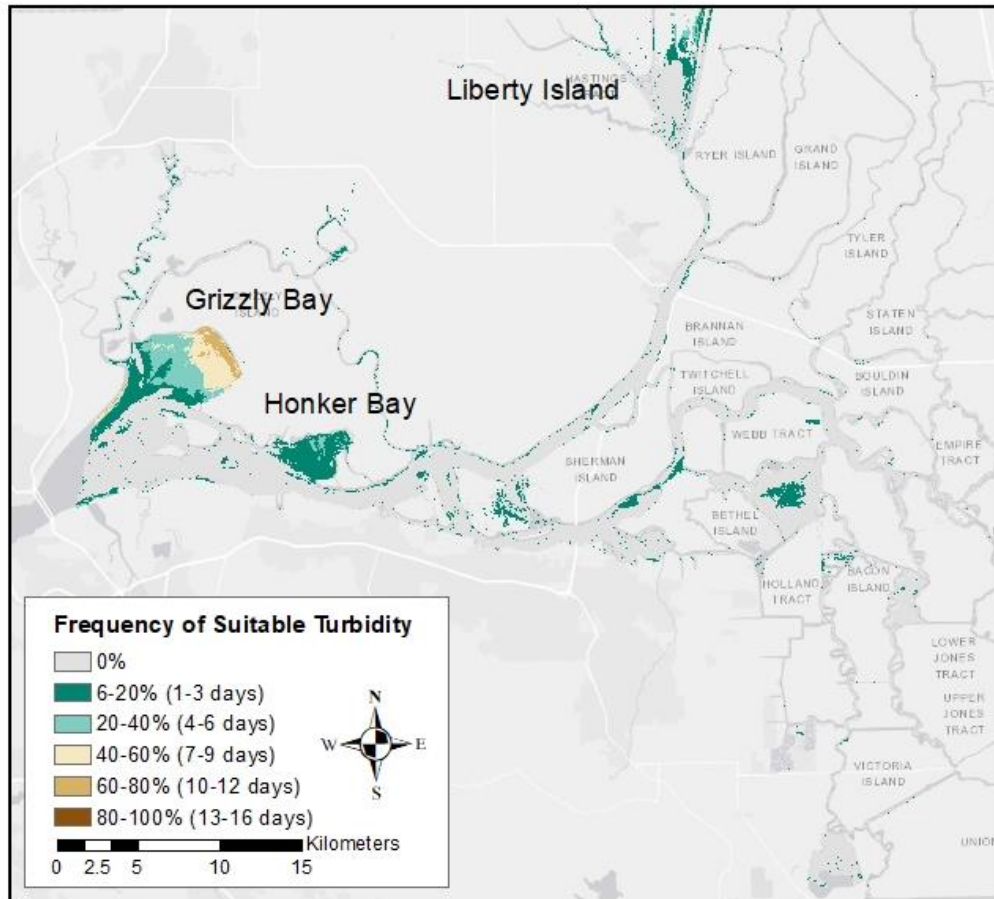
The recent launch of Sentinel-2A & B by the European Space Agency, provides 10 to 20 m spatial resolution at a 5-day repeat period and has been proved useful for mapping inland waters. As the temporal and spatial resolution of satellites improves, methodology should be developed to evaluate the effectiveness and impacts of conservation and mitigation strategies in response to a drought and extend turbidity products further, so they can be used for supporting improved management decision making.

2.7 Appendices

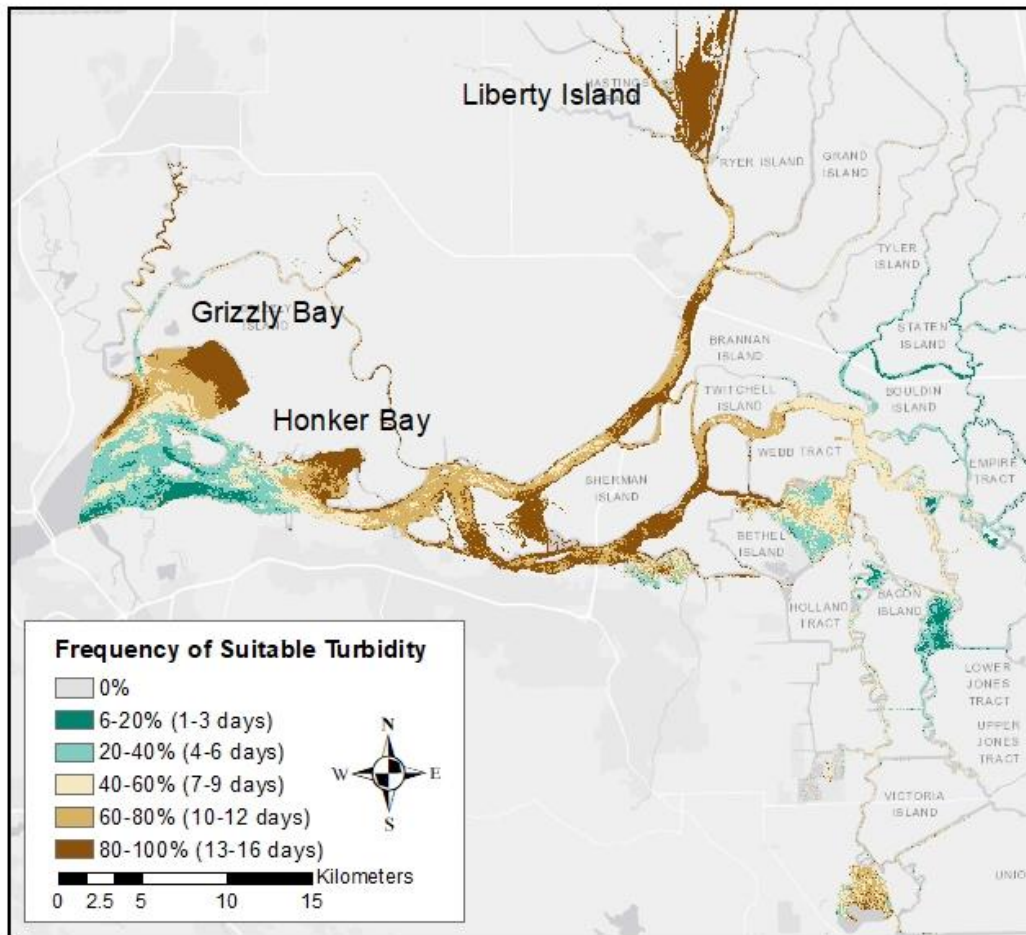
Lower and Upper Bound Turbidity Suitability Maps

This appendix displays the upper and lower bound maps of suitable turbidity conditions. The upper and lower bound estimates of percent frequency of suitable turbidity was calculated by subtracting or adding the calibrated RMSE (4.7 NTU) to each turbidity

map and applying a threshold at 12 NTU to each resulting map. The maps were binned into six categories by the percent of time a pixel was suitable for delta smelt throughout the time series.



3A-1. Lower bound delta smelt habitat potential as determined by the frequency of suitable turbidity >12 NTU for calibrated turbidity images minus the 4.7 NTU RMSE over the course of the time series April 6–September 8, 2015.



3A-2. Upper bound delta smelt habitat potential as determined by the frequency of suitable turbidity >12 NTU for calibrated turbidity images minus the 4.7 NTU RMSE over the course of the time series April 6–September 8, 2015.

2.7 Acknowledgements

The authors would like to thank CESBIO, CNES and ESA for the SPOT5 (Take5) experiment and D. Gomez for editing maps. Funding for this work was provided by NASA agreement NNH16ZDA001N, and the University of California Merced School of Engineering.

2.8 References

Barbier, E.B., S.D. Hacker, C. Kennedy, E.W. Koch, A.C. Stier, and B.R. Silliman. 2011. "The value of estuarine and coastal ecosystem services." *Ecological Monographs* 81 (2):169-193. <https://doi.org/10.1890/10-1510.1>

Brando, V.E., A.G. Dekker, Y.J. Park, and T. Schroeder. 2012. "Adaptive semianalytical inversion of ocean color radiometry in optically complex waters." *Applied Optics* 51 (15):2808-2833. <https://doi.org/10.1364/AO.51.002808>

Brown, L.R., W.A. Bennett, R.W. Wagner, T. Morgan-King, N. Knowles, F. Feyrer, D.H. Schoellhamer, M. T. Stacey, and M. Dettinger. 2013. "Implications for Future Survival of Delta Smelt from Four Climate Change Scenarios for the Sacramento–San Joaquin Delta, California." *Estuaries and Coasts* 36 (4):754-774. <https://doi.org/10.1007/s12237-013-9585-4>

Bukata, R.P, J.H. Jerome, A.S. Kondratyev, and D.V. Pozdnyakov. 1995. *Optical properties and remote sensing of inland and coastal waters*: CRC press.

Bustamante, J., F. Pacios, R. Díaz-Delgado, and D. Aragonés. 2009. "Predictive models of turbidity and water depth in the Doñana marshes using Landsat TM and ETM+ images." *Journal of Environmental Management* 90 (7):2219-2225. <https://doi.org/10.1016/j.jenvman.2007.08.021>.

CDFA (California Department of Food and Agriculture). 2018. "California Agricultural Statistics Review, 2017–2018." https://www.nass.usda.gov/Statistics_by_State/California/Publications/Annual_Statistical_Reviews/2019/2018cas-all.pdf

CDWR (California Department of Water Resources). 2012. "Delta Smelt Turbidity Monitoring Project - 2008 Memorandum Report".

CDWR (California Department of Water Resources). 2016. "2015 Emergency Drought Barrier Project". https://www.waterboards.ca.gov/waterrights/water_issues/programs/water_quality_cert/westfalse/docs/edb_pd.pdf

Cloern, J.E., and A.D. Jassby. 2012. "Drivers of change in estuarine-coastal ecosystems: Discoveries from four decades of study in San Francisco Bay." *Reviews of Geophysics* 50 (4).

Dekker, A.G., R J. Vos, and S.W. M. Peters. 2001. "Comparison of remote sensing data, model results and in situ data for total suspended matter (TSM) in the southern Frisian lakes." *Science of The Total Environment* 268 (1):197-214. [https://doi.org/10.1016/S0048-9697\(00\)00679-3](https://doi.org/10.1016/S0048-9697(00)00679-3).

Delta Stewardship Council. 2013. "The Delta Plan 2013 Ensuring a reliable water supply for California, a healthy Delta ecosystem, and place of enduring value".

Dogliotti, A.I., K.G. Ruddick, B. Nechad, D. Doxaran, and E. Knaeps. 2015. "A single algorithm to retrieve turbidity from remotely-sensed data in all coastal and estuarine waters." *Remote Sensing of Environment* 156:157-168. <https://doi.org/10.1016/j.rse.2014.09.020>.

Dogliotti, A.I., K. Ruddick, and R. Guerrero. 2016. "Seasonal and inter-annual turbidity variability in the Río de la Plata from 15 years of MODIS: El Niño dilution effect." *Estuarine, Coastal and Shelf Science* 182:27-39. <https://doi.org/10.1016/j.ecss.2016.09.013>.

Doxaran, D., P. Castaing, and S.J. Lavender. 2006. "Monitoring the maximum turbidity zone and detecting fine-scale turbidity features in the Gironde estuary using high spatial resolution satellite sensor (SPOT HRV, Landsat ETM+) data." *International*

Journal of Remote Sensing 27 (11):2303-2321.

<https://doi.org/10.1080/01431160500396865>

Efron, B. 1981. "Nonparametric estimates of standard error: The jackknife, the bootstrap and other methods." *Biometrika* 68 (3):589-599.

<https://doi.org/10.1007/s12237-010-9343-9>

ESRI (Environmental Systems Research Institute). 2017. ArcGIS 10.5.1. Redlands, California.

Feyrer, F., K. Newman, M. Nobriga, and T. Sommer. 2011. "Modeling the effects of future outflow on the abiotic habitat of an imperiled estuarine fish." *Estuaries and Coasts* 34 (1):120-128. <https://doi.org/10.1007/s12237-010-9343-9>

Feyrer, F., M.L. Nobriga, and T.R. Sommer. 2007. "Multidecadal trends for three declining fish species: habitat patterns and mechanisms in the San Francisco Estuary, California, USA." *Canadian Journal of Fisheries and Aquatic Sciences* 64 (4):723-734. <https://doi.org/10.1139/f07-048>

Gernez, P., V. Lafon, A. Lerouxel, C. Curti, B. Lubac, S. Cerisier, and L. Barillé. 2015. "Toward Sentinel-2 high resolution remote sensing of suspended particulate matter in very turbid waters: SPOT4 (Take5) Experiment in the Loire and Gironde Estuaries." *Remote sensing* 7 (8):9507-9528. <https://doi.org/10.3390/rs70809507>

Giardino, C., V.E. Brando, P. Gege, N. Pinnel, E. Hochberg, E. Knaeps, I. Reusen, R. Doerffer, M. Bresciani, F. Braga, S. Foerster, N. Champollion, and A. Dekker. 2019. "Imaging Spectrometry of Inland and Coastal Waters: State of the Art, Achievements and Perspectives." *Surveys in Geophysics* 40 (3):401-429. <https://doi.org/10.1007/s10712-018-9476-0>

Goodin, D.G., J.A. Harrington Jr., M.D. Nellis, and D.C. Rundquist. 1996. "Mapping Reservoir Turbidity Patterns Using SPOT-HRV Data." *Geocarto International*. 11:71-78. <https://doi.org/10.1080/10106049609354563>

Grimaldo, L.F., T. Sommer, N. Van Ark, G. Jones, E. Holland, P.B. Moyle, B. Herbold, and P. Smith. 2009. "Factors Affecting Fish Entrainment into Massive Water Diversions in a Tidal Freshwater Estuary: Can Fish Losses be Managed?" *North American Journal of Fisheries Management* 29 (5):1253-1270. <https://doi.org/10.1577/M08-062.1>

Hagolle, O., S. Sylvander, M. Huc, M. Claverie, D. Clesse, C. Dechoz, V. Lonjou, and V. Poulain. 2015. "SPOT-4 (Take 5): Simulation of Sentinel-2 time series on 45 large sites." *Remote sensing* 7 (9):12242-12264. <https://doi.org/10.3390/rs70912242>

Hasenbein, M., N.A. Fangue, J. Geist, L.M. Komoroske, J. Truong, R. McPherson, and R.E. Connon. 2016. "Assessments at multiple levels of biological organization allow for an integrative determination of physiological tolerances to turbidity in an endangered fish species." *Conservation Physiology* 4 (1). <https://doi.org/10.1093/conphys/cow004>.

Hestir, E L., D.H. Schoellhamer, J. Greenberg, T. Morgan-King, and S.L. Ustin. 2016. "The Effect of Submerged Aquatic Vegetation Expansion on a Declining Turbidity Trend in the Sacramento-San Joaquin River Delta." *Estuaries and Coasts* 39 (4):1100-1112. <https://doi.org/10.1007/s12237-015-0055-z>

Hobbs, J.A., L.S. Lewis, M. Willmes, C. Denney, and E. Bush. 2019. "Complex life histories discovered in a critically endangered fish." *Scientific Reports* 9 (1):16772. <https://doi.org/10.1038/s41598-019-52273-8>

ICF International. 2015. "Biological Assessment of Potential Effects on Listed Fishes from the West False River Emergency Drought Barrier Project". (ICF 00208.14.) Sacramento, CA.

Prepared for AECOM, Sacramento, CA.

IPCC, Climate Change. 2007. "The physical science basis. Contribution of working group I to the fourth assessment report of the Intergovernmental Panel on Climate Change." Cambridge University Press, Cambridge, United Kingdom and New York, NY, USA 996:2007.

IUCN. 2014. "Biodiversity Hotspots." <http://www.biodiversity-z.org/content/biodiversity-hotspots>.

Kabbara, N., J. Benkhelil, M. Awad, and V. Barale. 2008. "Monitoring water quality in the coastal area of Tripoli (Lebanon) using high-resolution satellite data." *ISPRS Journal of Photogrammetry and Remote Sensing* 63 (5):488-495. <https://doi.org/10.1016/j.isprsjprs.2008.01.004>.

Kimmerer, W., F. Wilkerson, B. Downing, R. Dugdale, E. Gross, K. Kayfetz, S. Khanna, A. Parker, and J. Thompson. 2019. "Effects of Drought and the Emergency Drought Barrier on the Ecosystem of the California Delta." *San Francisco Estuary and Watershed Science* 17. <https://doi.org/10.15447/sfews.2019v17iss3art2>

Kuhn, C., A. de Matos Valerio, N. Ward, L. Loken, H.O. Sawakuchi, M. Kampel, J. Richey, P. Stadler, J. Crawford, R. Striegl, E. Vermote, N. Pahlevan, and D. Butman. 2019. "Performance of Landsat-8 and Sentinel-2 surface reflectance products for river remote sensing retrievals of chlorophyll-a and turbidity." *Remote Sensing of Environment* 224:104-118. <https://doi.org/10.1016/j.rse.2019.01.023>.

Lund, J., J. Medellin-Azuara, J. Durand, and K. Stone. 2018. "Lessons from California's 2012–2016 Drought." *Journal of Water Resources Planning and Management* 144 (10). [https://doi.org/10.1061/\(ASCE\)WR.1943-5452.0000984](https://doi.org/10.1061/(ASCE)WR.1943-5452.0000984).

Lymburner, L., E. Botha, E. Hestir, J. Anstee, S. Sagar, A. Dekker, and T. Malthus. 2016. "Landsat 8: Providing continuity and increased precision for measuring multi-decadal time series of total suspended matter." *Remote Sensing of Environment* 185:108-118. <https://doi.org/10.1016/j.rse.2016.04.011>.

MacWilliams, M. L., E.S. Ateljevich, S.G. Monismith, and C. Enright. 2016. "An Overview of Multi-Dimensional Models of the Sacramento–San Joaquin Delta." *San Francisco Estuary and Watershed Science* 14 (4). <https://doi.org/10.15447/sfews.2016v14iss4art2>

Maltese, A., F. Capodici, G. Ciraolo, and G. La Loggia. 2013. "Coastal zone water quality: Calibration of a water-turbidity equation for MODIS data." *European Journal of Remote Sensing* 46 (1):333-347. <https://doi.org/10.5721/EuJRS20134619>

Merz, J.E., S. Hamilton, P.S. Bergman, and B. Cavallo. 2011. "Spatial perspective for delta smelt: a summary of contemporary survey data." *California Fish and Game* 97:164-189.

Morgan-King, T. L., and D. H. Schoellhamer. 2013. "Suspended-Sediment Flux and Retention in a Backwater Tidal Slough Complex near the Landward Boundary of an Estuary." *Estuaries and Coasts* 36 (2):300-318. <https://doi.org/10.1007/s12237-012-9574-z>.

- Moyle, P.B., L.R. Brown, J.R. Durand, and J.A. Hobbs. 2016. "Delta smelt: life history and decline of a once-abundant species in the San Francisco Estuary." *San Francisco Estuary and Watershed Science* 14 (2).
<https://doi.org/10.15447/sfew.s.2016v14iss2art6>
- Murphy, D.D., and S.A. Hamilton. 2013. "Eastward migration or marshward dispersal: Understanding seasonal movements by delta smelt." *San Francisco Estuary and Watershed Science* 11. <https://doi.org/10.15447/sfew.s.2013v11iss3art12>
- Nechad, B., K.G. Ruddick, and Y. Park. 2010. "Calibration and validation of a generic multisensor algorithm for mapping of total suspended matter in turbid waters." *Remote Sensing of Environment* 114 (4):854-866.
<https://doi.org/10.1016/j.rse.2009.11.022>
- Odermatt, D., A. Gitelson, V.E. Brando, and M. Schaepman. 2012. "Review of constituent retrieval in optically deep and complex waters from satellite imagery." *Remote Sensing of Environment* 118:116-126. <https://doi.org/10.1016/j.rse.2011.11.013>
- Pahlevan, N., J.C. Roger, and Z. Ahmad. 2017. "Revisiting short-wave-infrared (SWIR) bands for atmospheric correction in coastal waters." *Optics express* 25 (6):6015-6035. <https://doi.org/10.1364/OE.25.006015>
- Petus, C., G. Chust, F. Gohin, D. Doxaran, J.-M. Froidefond, and Y. Sagarmínaga. 2010. "Estimating turbidity and total suspended matter in the Adour River plume (South Bay of Biscay) using MODIS 250-m imagery." *Continental Shelf Research* 30 (5):379-392. <https://doi.org/10.1016/j.csr.2009.12.007>
- Polansky, L., K.B. Newman, M.L. Nobriga, and L. Mitchell. 2018. "Spatiotemporal Models of an Estuarine Fish Species to Identify Patterns and Factors Impacting Their Distribution and Abundance." *Estuaries and Coasts* 41 (2):572-581.
<https://doi.org/10.1007/s12237-017-0277-3>
- Salama, M.S., and A. Stein. 2009. "Error decomposition and estimation of inherent optical properties." *Applied Optics* 48 (26):4947-4962.
<https://doi.org/10.1364/AO.48.004947>
- Schaeffer, B.A., J. Iames, J. Dwyer, E. Urquhart, W. Salls, J. Rover, and B. Seegers. 2018. "An initial validation of Landsat 5 and 7 derived surface water temperature for U.S. lakes, reservoirs, and estuaries." *International Journal of Remote Sensing* 39 (22):7789-7805. <https://doi.org/10.1080/01431161.2018.1471545>
- SFEI, San Francisco Estuary Institute. 2015. *California Aquatic Resource Inventory (CARI) version 0.1*. edited by San Francisco Estuary Institute (SFEI).
- Sommer, T., and F. Mejia. 2013. "A Place to Call Home: A Synthesis of Delta Smelt Habitat in the Upper San Francisco Estuary." *San Francisco Estuary and Watershed Science* 11. <https://doi.org/10.15447/sfew.s.2013v11iss2art4>
- Sommer, T., F.H. Mejia, M.L. Nobriga, F. Feyrer, and L. Grimaldo. 2011. "The spawning migration of delta smelt in the upper San Francisco Estuary." *San Francisco Estuary and Watershed Science* 9 (2). <http://dx.doi.org/10.15447/sfew.s.2014v9iss2art2>
- Swain, D.L., D. Singh, D.E. Horton, J.S. Mankin, T.C. Ballard, and N.S. Duffenbaugh. 2017. "Remote Linkages to Anomalous Winter Atmospheric Ridging Over the Northeastern Pacific." *Journal of Geophysical Research Atmospheres*. 122, 12,112-194,209. <https://doi.org/10.1002/2017JD026575>

Ustin, S., S. Khanna, J. Bellvert, J.D. Boyer, and K. Shapiro. 2016. "Impact of Drought on Submerged Aquatic Vegetation (SAV) and Floating Aquatic Vegetation (FAV) Using AVIRIS-NG Airborne Imagery." Sacramento (CA): Calif. Dept. of Fish and Wildlife

Vanhellemont, Q. 2019. "Adaptation of the dark spectrum fitting atmospheric correction for aquatic applications of the Landsat and Sentinel-2 archives." *Remote Sensing of Environment* 225:175-192. <https://doi.org/10.1016/j.rse.2019.03.010>.

Vanhellemont, Q., and K. Ruddick. 2014. "Turbid wakes associated with offshore wind turbines observed with Landsat 8." *Remote Sensing of Environment* 145:105-115. <https://doi.org/10.1016/j.rse.2014.01.009>.

Vanhellemont, Q., and K. Ruddick. 2016. "ACOLITE processing for Sentinel-2 and Landsat-8: atmospheric correction and aquatic applications." *Proc. Ocean Optics Conference*.

Varunan, T., and P. Shanmugam. 2018. "Use of Landsat 8 data for characterizing dynamic changes in physical and acoustical properties of coastal lagoon and estuarine waters." *Advances in Space Research* 62 (9):2393-2417. <https://doi.org/10.1016/j.asr.2018.07.002>.

Wetz, M.S., and D.W. Yoskowitz. 2013. "An 'extreme' future for estuaries? Effects of extreme climatic events on estuarine water quality and ecology." *Marine Pollution Bulletin* 69 (1):7-18. <https://doi.org/10.1016/j.marpolbul.2013.01.020>.

Wright, S.A., and D.H. Schoellhamer. 2005. "Estimating sediment budgets at the interface between rivers and estuaries with application to the Sacramento-San Joaquin River Delta." *Water Resources Research* 41 (9). <https://doi.org/10.1029/2004wr003753>.

3. Chapter 2: Genus-level mapping of invasive floating aquatic vegetation using Sentinel-2 satellite remote sensing*

Christiana Ade¹, Shruti Khanna², Mui Lay³, Susan L. Ustin³, and Erin L. Hestir¹

¹ School of Engineering, University of California Merced, Merced, California, USA

² California Department of Fish and Wildlife, 2109 Arch-Airport Road, Stockton, California, 95206 USA

³ Center for Spatial Technologies and Remote Sensing, Department of Land Air and Water Resources, University of California, One Shields Avenue, Davis, CA 95616, USA

Correspondence: cade@ucmerced.com

*This chapter was submitted for review to *Remote Sensing* on May 03, 2022

Abstract

Invasive floating aquatic vegetation negatively impacts wetland ecosystems and mapping this vegetation through space and time can aid in designing and assessing effective control strategies. Current remote sensing methods for mapping floating aquatic vegetation at the genus-level relies on airborne imaging spectroscopy, resulting in temporal gaps because routine hyperspectral satellite coverage is not yet available. Here we achieved genus level and species level discrimination between two invasive aquatic vegetation species using Sentinel 2 multi-spectral satellite data and machine-learning classifiers in summer and fall. The species of concern were water hyacinth (*Eichornia crassipes*) and water primrose (*Ludwigia* spp). Our classifiers also identified submerged and emergent aquatic vegetation at the community level. Random forest models using Sentinel-2 data achieved an average overall accuracy of 90%, and class accuracies of 79-91% and 85-95% for water hyacinth and water primrose, respectively. To our knowledge, this is the first study that has mapped water primrose to the genus level using satellite remote sensing. Sentinel-2 derived maps compared well to those derived from airborne imaging spectroscopy and we also identified misclassifications that can be attributed to the coarser Sentinel-2 spectral and spatial resolutions. Our results demonstrate that the intra-annual temporal gaps between airborne imaging spectroscopy observations can be supplemented with Sentinel-2 satellite data and thus, rapidly growing/expanding vegetation can be tracked in real time. Such improvements have potential management benefits by improving understanding of the phenology, spread, competitive advantages, and vulnerabilities of these aquatic plants.

3.1 Introduction

Invasive floating aquatic vegetation (FAV) species are a global concern due to their negative impacts on fragile wetland ecosystem processes such as nutrient cycling, hydrology, and energy budgets (Gordon 1998, Scheffer et al. 2003, Dukes and Mooney 2004, O’Farrell et al. 2009, Pejchar and Mooney 2009). Their introduction threatens ecosystem biodiversity and function, and often results in economic impact to fisheries, hydropower generation and transportation services (Ongore et al., 2018; Pimentel et al., 2005; Thouvenot et al., 2013a). Understanding invasion pathways, processes, impacts and triggers of change is an essential step in effective wetland management and is dependent on accurate mapping of vegetation and species prevalence though time (Thamaga and Dube, 2018a).

Satellite remote sensing is a favored tool for monitoring invasive vegetation due to its synoptic views and repeat coverage; however, discrimination of multiple aquatic species in areas of high spatio-temporal complexity is often difficult due to spectral similarity between species and high spectral variation within a class (Adam et al., 2010; Gallant, 2015; Guo et al., 2017). Imaging spectroscopy has historically been the favored tool for mapping vegetation at the species or genus level because it offers the high spectral resolution capable of discriminating between multiple aquatic species within the same functional type (Everitt et al., 2011; Hestir et al., 2008; Khanna et al., 2011; Santos et al., 2012; Schmidt and Skidmore, 2003). Airborne imaging spectroscopy (AIS) also commonly has a high spatial resolution, which is important for mapping multiple FAV species that often co-occur within the same patch (Bolch et al., 2021; Hestir et al., 2008; Khanna et al., 2012). However, spaceborne imaging spectrometers with systematic, repeat sampling capabilities are currently rare and commercial AIS campaigns to collect such data are expensive – often resulting in annual and intra-annual data gaps. Such gaps hinder the ability to relate invasive species distribution to environmental and anthropogenic drivers of change during the growing season (Kleinschroth et al., 2021). Newer multispectral satellites such as Sentinel-2A & B (S2) have a repeat period of 5 days at improved spectral and spatial resolutions compared to older multispectral satellites often used in wetland studies like Landsat or MODIS. This makes S2 an attractive contender for mapping FAV species that are mobile and rapidly expand throughout the growing season.

The S2 sensors provide the opportunity to discriminate between multiple FAV at the species and genus level throughout the growing season because of their high revisit frequency and high spatial resolution along with additional bands (relative to Landsat) that are intrinsically linked to vegetation traits (Drusch et al., 2012). S2 has been used to distinguish between multiple emergent aquatic vegetation species (e.g. *Spartina alterniflora*, *Phragmites australis*) but the potential to spectrally discriminate between different types of FAV has yet to be determined (Dong et al., 2020; Gong et al., 2021). Although S2 has previously been used to map invasive FAV, such as water hyacinth, most study sites in the literature focus on relatively homogenous environments and community types, or target only one invasive species (Dersseh et al., 2020; Singh et al., 2020; Thamaga and Dube, 2018b). These prior studies also do not demonstrate the extent of S2’s utility

across a range of environments, nor do they differentiate floating vegetation at the genus or species-level.

The Sacramento-San Joaquin Delta (henceforth the Delta) is an extensively modified wetland system comprised of multiple tidally influenced habitat types including open lake-like and channelized riverine environments. The spatial heterogeneity and range of wetland environments in the Delta make it a unique setting for testing the potential of S2 to distinguish FAV at the species or genus-level, while simultaneously mapping submerged and emergent aquatic vegetation at the community level to provide holistic wetland maps that can inform and assess management actions. Currently, aquatic vegetation in the Delta is mapped to the species, genus, and community level using annual AIS acquisitions (Khanna et al., 2022, 2011). However, the imagery is costly and thus only consists of one annual snapshot per year, which does not allow for intra-annual tracking of aquatic vegetation composition and coverage. At times, lack of funding has resulted annual data gaps as well, further increasing the temporal gaps.

Here, we demonstrate for the first time that separation between invasive FAV at the genus and species level is possible using Sentinel-2. We compared our Sentinel-2 maps to those derived from AIS, the current near-operational method employed for aquatic mapping in the Delta. Our classifiers distinguish between invasive FAV water hyacinth (*Pontederia crassipes*; formerly *Eichornia crassipes*) and water primrose (*Ludwigia* spp.) and identify submerged and emergent aquatic vegetation at the community level for both summer and fall imagery, demonstrating that the intra-annual temporal gap can be closed, and rapidly expanding vegetation can be tracked throughout the growing season. Such improvements have multiple possible management benefits. For example, the State of California spends millions of dollars each year to control IAV in the Delta and costs are likely to continue to rise (Jetter et al., 2018). Gaining a better understanding of invasive FAV distribution and spread within the year can lead to more informed and effective control strategies.

3.2 Materials and Methods

3.2.1 Experimental Design

Two floating aquatic macrophytes, water hyacinth (*Pontederia crassipes*) and water primrose (*Ludwigia* spp.), were targeted in this study. Water primrose, although nominally rooted, develops adventitious roots that can draw nutrients directly from the water. This allows water primrose to form floating canopies that extend several meters into the channel from the shore (Rejmánková, 1992). In contrast, water hyacinth is truly free-floating aquatic macrophyte – often anchoring itself to nearby emergent vegetation (Penfound and Earle, 1948). Both are among some of the most invasive aquatic macrophytes globally and are frequently referred to as ‘ecosystem engineers’ because of their ability to alter physical, biological and chemical processes to their benefit (Grewell et al., 2019; Malik, 2007; Thouvenot et al., 2013b). For these reasons, we focused our extension of mapping capabilities on these two FAV aquatic macrophytes. Overall, our classification scheme is comprised of 8 classes - water hyacinth, water primrose, emergent aquatic vegetation (EAV), submerged aquatic vegetation (SAV), riparian vegetation, open water, non-photosynthetic vegetation (NPV), and soil (**Figure 3-1**).

This study was conducted for the Delta, which is the hub of California’s water system spanning approximately 2220 km² in Northern and Central California. It is a heavily engineered system comprised of a diverse network of channels and freshwater tidal marshes at the confluence of the Sacramento and the San Joaquin rivers (**Figure 3-2**) The Delta is also recognized as one of the most invaded estuaries in the world (Cohen and Carlton, 1998). In the past few decades, water primrose and water hyacinth have negatively impacted water quality, water pumping, and native species, and there are ongoing efforts to control persistence and spread (DBW, 2019; Jetter et al., 2018; Khanna et al., 2019).

As part of the control and monitoring programs, AIS efforts to map these invasive floating species have been led by the Center of Spatial Technologies and Remote Sensing (CSTARS) at UC Davis from 2004-2008 and 2014-2021 (Hestir et al., 2012, 2008; Khanna et al., 2011, (Khanna et al., 2022; Ustin et al., 2021). An imaging spectrometer is flown on a low-altitude aircraft collecting high spatial resolution (~1.7-3 m pixels) and high spectral quality data. These data are used to prepare maps for California State Agencies and for assessing annual invasive species spread and community dynamics.

To evaluate the potential of S2 for filling intra-annual data gaps, we compared the performance of a machine learning classifier using Sentinel-2 data to the current state of the art approach for FAV mapping in the Delta derived from AIS (Ustin et al. 2021). To compare the two products, we identified the closest S2 overpass to AIS acquisition with low cloud cover, we refer to these date pairs as “match up dates” that include fall 2018, fall 2019, and summer 2020 (**Table 3-2**). We label our mapping efforts FAV genus-level because multiple *Ludwigia* species are present in the Delta, but the exact number is unknown; they are difficult to visually distinguish in the field let alone from space.

While we mapped the entire Delta and made Delta-wide comparisons, for visualization and demonstration, map results are presented for four smaller sub-regions representative of the range of different habitat types in the Delta (**Figure 3-2**). Big Break is a brackish, shallow flooded island located downstream of the confluence of the Sacramento and San Joaquin Rivers. Liberty Island, an abandoned, flooded island, is a freshwater site influenced by the Sacramento River. Rhode Island and Ward Cut are islands along the San Joaquin River, that include a diverse mix of upland riparian and freshwater marsh habitats with large areas of deep open water bound by levees.

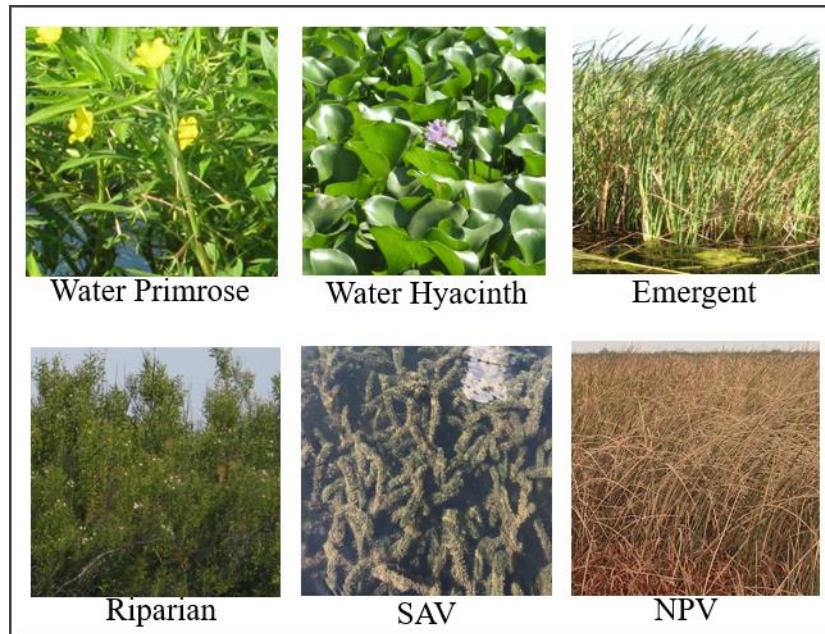


Figure 3-1. Field photos of vegetation classes and list of species in each vegetation community type. See Ta et al. 2017 for more in-depth descriptions of targeted invasive aquatic vegetation.

Table 3-1. Target classes and their descriptions.

Map Class	Description
Water Hyacinth	<i>Pontederia crassipes</i>
Water Primrose	<i>Ludwigia</i> spp.
Emergent Vegetation (EAV)	Cattail (<i>Typha</i> spp.) Common reed (<i>Phragmites australis</i>) Tule (<i>Schoenoplectus</i> spp.)
Riparian	For example: Willow species (<i>Salix</i> spp.), Oak species (<i>Quercus</i> spp), and Cottonwood (<i>Populus</i> spp.)
Submerged Aquatic Vegetation (SAV)	Algae mats Brazillian waterweed (<i>Egeria densa</i>) Coontail (<i>Ceratophyllum demersum</i>) Curly leaf pondweed (<i>Pomatogedon crispus</i>) Fanwort (<i>Cabomba caroliniana</i>) Sago pondweed (<i>Stuckenia pectinata</i>) Watermilfoil (<i>Myriophyllum spicatum</i>) Waterweed (<i>Elodea canadensis</i>)
Non-Photosynthetic Vegetation (NPV)	Senescent or dead vegetation
Soil	Soil
Water	Water

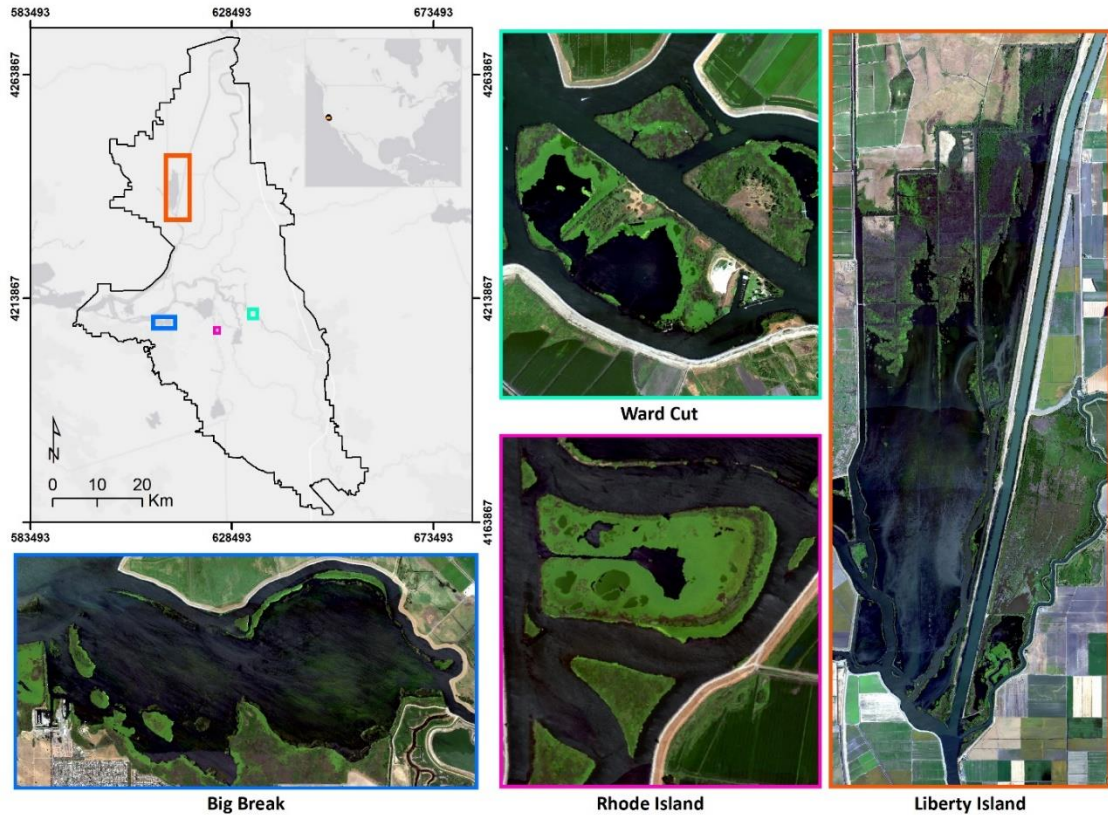


Figure 3-2. Map of the Delta sub-study areas. RGB images were created using imaging spectroscopy acquisitions.

Table 3-2. Match-up dates and tidal ranges¹ for corresponding imaging spectrometer acquisitions and Sentinel-2 over passes.

Match up date	Imaging Spectrometer Acquisition Date	Closest Sentinel-2 Image Date	Imaging Spectrometer	Sentinel-2 Sensor	Tidal range AIS ¹ (m)	Tidal Range S2 (m)
Fall 2018	2018-10-06 – 2018-10-09	2018-10-07	HyMap	S2B	0.01-0.25	0.49 - 0.64
Fall 2019	2019-09-23 – 2019-09-27	2019-10-02	HyMap	S2B	0.01 -1.02	0.28 – 0.39
Summer 2020	2020-07-15 – 2020-07-18	2020-07-18	Fenix 1K	S2B	0.01-0.37	0.17-0.30

¹ Tidal ranges were downloaded from NOAA for the sensors at Antioch and Rio Vista (Station ID: 9415064 and 9415316, respectively). The ranges include measurements from stations.

3.2.2 Acquisition and pre-processing of Sentinel-2 imagery

Level-1C (L1C) top of atmosphere (TOA) reflectance products for Sentinel-2 tiles capturing the legal Delta boundary (10SFH, 10SFG and 10SEH) were downloaded from the Copernicus Open Access Hub for each of the three match-up dates listed in **Table 2**. Products were atmospherically corrected to Level-2A (L2A) bottom of atmosphere

reflectance (BOA) using Sen2Cor version 2.8.0. Sentinel-2A and 2B collect information in 13 spectral bands at 10, 20, and 60 m resolutions (**Table 3**). The Sen2r 1.4.0 R package was used to resample 20 – 60m bands to a 10 m spatial resolution, mosaic tiles, and convert products from their native SAFE file format to ENVI files (Ranghetti et al., 2020).

Table 3-3. Sentinel-2 band characteristics. Asterix indicates band was not used during classification.

<i>Sentinel-2 Bands</i>	<i>Wavelengths (μm)</i>	<i>Spatial Resolution (m)</i>
<i>Band 1 – Coastal Aerosol</i>	0.430 – 0.457	60
<i>Band 2 – Blue</i>	0.440 – 0.538	10
<i>Band 3 – Green</i>	0.537 – 0.582	10
<i>Band 4 – Red</i>	0.646 – 0.684	10
<i>Band 5 – Vegetation Red Edge</i>	0.694 – 0.713	20
<i>Band 6 – Vegetation Red Edge</i>	0.731 – 0.749	20
<i>Band 7 – Vegetation Red Edge</i>	0.769 – 0.797	20
<i>Band 8 – NIR</i>	0.785 – 0.900	10
<i>Band 8A – Narrow NIR*</i>	0.849 – 0.881	20
<i>Band 9 – Water Vapor*</i>	0.932 – 0.958	60
<i>Band 10 – Cirrus*</i>	1.337 – 1.412	60
<i>Band 11 – SWIR 1</i>	1.539 – 1.682	20
<i>Band 12 – SWIR 2</i>	2.078 – 2.320	20

3.2.3 Imaging spectroscopy acquisitions and classification process

In fall 2018 and 2019, HyMap imaging spectroscopy data were collected over the Delta at a 1.7x1.7m ground resolution in 126 bands (400 – 2,500 nm, bandwidth ~15nm) with a 20% overlap in flightlines by HyVista Corporation (Sydney, Australia). HyVista performed atmospheric calibration and delivered the data to CSTARS at UC Davis with geo-location files (GLT) for further processing. In July of 2020, SpecTIR LLC (Reno, Nevada, USA), flew their Fenix 1K hyperspectral imager over the Delta. The Fenix sensor measures 323 spectral bands across the visible to shortwave infrared spectrum (397nm - 2450nm) at a nominal spatial resolution of 2x2m. SpecTIR also provided data to CSTARS after atmospheric calibration and included geographic lookup table files to associate each pixel with a geographic location. All airborne spectroscopy campaigns were conducted during low tide and flown to minimize sunglint.

Locations of aquatic vegetation species, riparian vegetation, and water are collected within a two-week window of image acquisition (~800–2000 points per campaign) using handheld high precision (sub-meter accuracy) GeoXT and GeoXH Trimble DGPS units (Trimble Navigation Limited, Sunnyvale, California) with Wide Area Augmentation System (WAAS) differential correction. Each location marks a dominant species, along with information on patch size, percent cover of each species present, and vegetation condition. Patch width and length are labeled as small (3-5 m), medium (5-10 m), large (10-15 m), and extra-large (>15 m). Classification training and validation polygons are

then created through photointerpretation using field collected points and ground reference photos as a reference, in ArcMap (ArcGIS 10, Redlands, California) (Ustin et al. 2021).

CSTARS classifies the spectroscopy data using a random forest algorithm trained and validated with the field collected reference data. A separate random forest model is developed for each campaign. Input data include a suite of spectral indexes, spectral angle mapper rule images, linear spectral unmixing fractional cover, and continuum removal of absorption features (Khanna et al., 2018). The polygons are randomly split into 50/50 training and validation data. Class accuracies are evaluated using confusion matrices that report an overall accuracy, user's and producer's accuracies, and the Kappa statistic (Rosenfield and Fitzpatrick-Lins, 1986; Story and Congalton, 1986). The overall accuracy indicates the probability that the label of a pixel in the classified image agrees with validation data at the location. The user's accuracy indicates the probability that an image pixel labeled as a certain class is that class at the field location. producer's accuracy measures omission error – the probability that a predicted class matches the labeled reference data. The Kappa statistic (K) also indicates the level of overall agreement between the field data and the classification map, but it accounts for the probability of random agreement between the two datasets (Rosenfield and Fitzpatrick-Lins, 1986). Kappa values range from 0 to 1 with values greater than 0.5 indicating good agreement and values greater than 0.8 indicating exceptional agreement between the classification map and the validation dataset.

We used these previously generated maps, associated accuracy assessments, and training and validation polygons to conduct a visual and percent coverage comparison between AIS and S2 aquatic vegetation maps. AIS maps range from nine to sixteen classes depending on the year and we adjusted the classes to match ours. Tule/cattail and phragmites were grouped together into EAV. *Arundo donax* (giant cane) was grouped with riparian vegetation because it is generally found on higher ground and levees adjoining channels. Floating vegetation such as *Azolla*, duckweed and pennywort were excluded from comparisons because they occupy less than 0.5% of mapped waterways. Non-photosynthetic floating vegetation was grouped with NPV. The summer 2020 classification map identifies areas of water primrose encroachment into emergent marsh as a separate class “emergent primrose” (Ustin et al., 2021), which we did not re-assign as either water primrose or EAV.

3.3 Sentinel-2 Image Classification

3.3.1 Training and validation data

Training and validation pixels were primarily selected from the same GPS points collected for AIS classification. Point locations of field observations were adjusted to match the courser resolution of Sentinel-2 by eliminating points in patches that were heavily mixed or too small to be detected at a 10 m spatial resolution. Since the boats used for data collection often record GPS locations at the edge of a patch due to potential propeller entanglement, observation points labeled extra-large or large (>10-15m) were spatially nudged to the nearest vegetation or water patch center visible in Sentinel-2

imagery. Water, soil and NPV locations were randomly sampled from training and validation polygons created for the AIS classifications. Additional points were added via photo interpretation from careful examination of Google Earth Imagery and 2017 LiDAR digital surface models. A separate adjustment was made for each of the three match-up images listed in **Table 3-2**, which resulted in a total of ~2,400 points available for selection during the classification experiments. Each class ranged from 80-120 points per date depending on class and not all points were marked as suitable for each match-up date. The water hyacinth class had the least amount of points across all dates because it occurs in small patches and occupies the least area of our target classes during the period of study.

3.2.2 *Sentinel-2 Random Forest Model Selection*

Following the AIS classifications process, we also used random forest to create our classifications. Random forest (RF) models are commonly used for remote sensing image classification across sites and sensors (Berhane et al., 2018; Magidi et al., 2021; Mahdianpari et al., 2017; Singh et al., 2020). Such models have been successful for aquatic vegetation mapping in the Delta using AIS data collected from both UAV and manned aircraft (Khanna et al. 2018, Bolch et al. 2021). Random forest is an automated algorithm that builds hundreds of classification tree models and then selects the most frequent solution (Breiman 2001). Although RF models often result in improved classification accuracies over other traditional image classification methods, they are sensitive to training data selection (Liaw and Wiener, 2002). To account for this issue and select the optimal RF model, different sets of labeled training and testing data were examined using a bootstrapped approach. For each match-up date, 100 RF models were built by randomly dividing points into 50% training and 50% independent test data. The ‘best’ performing RF model was selected based by first selecting ranking the models on overall accuracy, and then selecting a high overall accuracy model that also had high class-specific accuracies of target FAV classes. The ‘best’ performing model was then applied to the Sentinel-2 image. We chose to construct a separate model for each match-up date to align our classification process with the AIS classification process, ensuring a fair comparison.

The models were constructed and evaluated using the caret (Kuhn, 2008) and randomForest (Liaw and Wiener, 2002) R packages. The model was built with default number of trees (ntrees = 500) (R Foundation for Statistical Computing, Vienna, Austria). The random forest model inputs included Sentinel-2 reflectance bands (**Table 2**) and nine spectral indices (**Table 4**). We selected these indices due to their correlation with plant biophysical properties and previously documented success in other aquatic vegetation classification models (Bolch et al., 2021; Hestir et al., 2008; S Khanna et al., 2018; Thamaga and Dube, 2018a). Similar to the AIS process, overall accuracy, user’s and producer’s accuracy and a **K** statistic were calculated for each date. The K was calculated to compare the two datasets, but was not used as a metric for best model selection due to its similar functionality to overall accuracy (Foody, 2020).

Table 3-4. Vegetation and water indexes used in the Sentinel-2 classification process.

Index	Formula	Source
NDVI	$\frac{\rho_{NIR} - \rho_{RED}}{\rho_{NIR} + \rho_{RED}}$	(Rouse et al., 1974)
NDAVI	$\frac{\rho_{NIR} - \rho_{BLUE}}{\rho_{NIR} + \rho_{BLUE}}$	(Villa et al., 2013)
WAVI	$(1 + L) \frac{\rho_{NIR} - \rho_{BLUE}}{\rho_{NIR} + \rho_{BLUE} + L}$ *Here, L = 0.5	(Villa et al., 2014)
SAVI	$(1 + L) \frac{\rho_{NIR} - \rho_{RED}}{\rho_{NIR} + \rho_{RED} + L}$ *Here, L = 0.5	(Huete, 1988)
NDVIRE2	$\frac{\rho_{NIR} - \rho_{VR2}}{\rho_{NIR} + \rho_{VR2}}$	(Gitelson and Merzlyak, 1994)
NDVIRE3	$\frac{\rho_{NIR} - \rho_{VR3}}{\rho_{NIR} + \rho_{VR3}}$	(Fernández-Manso et al., 2016)
NDWI	$\frac{\rho_{Green} - \rho_{NIR}}{\rho_{Green} + \rho_{NIR}}$	(McFeeters, 1996)
NDMI	$\frac{\rho_{NIR} - \rho_{SWIR}}{\rho_{NIR} + \rho_{SWIR}}$	(Gao, 1996)
MNDWI	$\frac{\rho_{Green} - \rho_{SWIR}}{\rho_{Green} + \rho_{SWIR}}$	(Xu, 2006)

3.3 Results

3.3.1 Model Accuracies

The Sentinel-2 and AIS performance by match-up date is summarized in **Table 3-5**. S2 FAV genus-level RF models yielded overall accuracies of 87-90%. Water primrose had the highest producer's accuracy from 91-96%, while water hyacinth had the second highest user's accuracy ranging from 85-94%. Producer's and user's accuracies for SAV and water were above 90% for fall 2019 and summer 2020 and were slightly lower for fall 2018, the S2 date with the highest tide (**Table 3-2**). Riparian vegetation had the lowest producer's accuracy followed by water hyacinth. Riparian and emergent vegetation had the lowest user's accuracies (74-85%). Although not listed in the tables below, Soil and NPV user's and producer's accuracies were between 93-100 %. These classes were mostly confused with each other or NPV was confused with vegetation pixels labeled as partially dry in the GPS field data. The primary source of confusion was between class pairs with similar spectral signatures: water primrose and water hyacinth, emergent and riparian vegetation, and water and SAV. Qualitative examination of imagery revealed that

misclassification commonly occurred at class boundaries and in smaller vegetation patches where pixels are more likely to be mixed.

S2 overall accuracy results (87-90%) are just slightly below the overall accuracy reported for AIS maps (90-91%) (**Table 3-5**). S2 producer's accuracies for water primrose 91-96% were comparable with AIS producer's accuracies of 91-94%, while user's accuracies were lower 80-92% (S2) vs 89-95% (AIS). S2 water hyacinth had higher user's accuracy than AIS in Fall 2018 and summer 2020. The EAV class had relatively lower producer's and user's accuracies for both S2 and AIS data at 77-68% and 61-88%, respectively. EAV has the lowest class accuracies for AIS, indicating that in some locations this class is difficult to detect even with high spatial and spectral resolution data. The riparian class had the greatest differences in accuracy between the two sets of imagery and S2 was always lower. SAV and water class accuracies were comparable between the two datasets. S2 had higher SAV and water accuracy in fall 2019, potentially because some AIS flightlines were acquired at higher tidal stages than S2 (**Table 3-2**).

Table 3-5. Sentinel-2 and airborne imaging spectrometer classification performance by match-up date. Overall accuracy = OA, Producer's accuracy = PA, User's Accuracy = UA. SAV = submerged aquatic vegetation. Soil and non-photosynthetic vegetation (NPV) accuracies are not listed but were 93 – 100% and primarily confused with each other.

Class	Type of Accuracy	2018F		2019F		2020S	
		S2	AIS	S2	AIS	S2	AIS
	OA (%)	87	91	89	90	90	90
	Kappa	0.85	0.9	0.88	0.89	0.89	0.89
Water	PA (%)	79	86	78	94	80	88
Hyacinth	UA (%)	94	89	85	89	93	92
Water	PA (%)	91	94	94	95	96	91
Primrose	UA (%)	83	92	92	95	80	89
Emergent	PA (%)	82	83 ^a 73 ^b	81	83 ^a 84 ^b	86	85 ^a 61 ^b
	UA (%)	77	87 ^a 83 ^b	79	87 ^a 88 ^b	86	81 ^a 76 ^b
Riparian	PA (%)	74	97	78	90	78	92
	UA (%)	80	94	75	90	85	84
SAV	PA (%)	86	91	90	79	96	91
	UA (%)	84	83	92	82	91	97
Water	PA (%)	88	91	92	84	90	99
	UA (%)	90	92	90	83	96	91

^a Tule/cattail class in AIS maps

^b Phragmites class in AIS maps

3.3.2 S2 Random Forest Variable Importance

Figure 3-3 shows the random forest variable importance for S2 models: variables are ordered by the mean decrease accuracy considering all models. Spectral indexes were consistently ranked with high importance, along with the green spectral reflectance band followed by SWIR and NIR spectral reflectance bands (**Figure 3-3**). High importance of spectral indexes has been previously identified in other aquatic vegetation classification studies targeting floating vegetation (Bolch et al., 2021; Thamaga and Dube, 2018c). The NIR band contributes to separation of different FAV covers and emergent vegetation while the SWIR bands are critical to differentiating emergent and FAV from water (Khanna et al., 2011). Although ranked lower than most other spectral bands in our models, the red edge bands have reasonably high mean average decrease values indicating they were valuable to model performance. The two red edge indexes, NDVIre2 and NDVIre3, were the least important in all models.

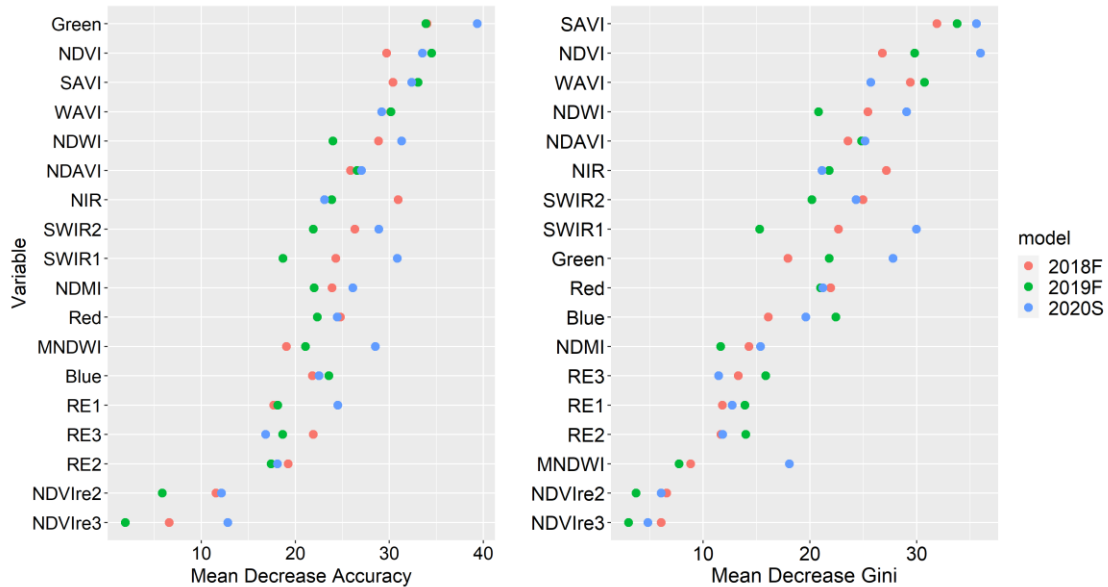


Figure 3-3. Variable importance for Sentinel-2 random forest models for each match-up date. Mean Decrease Accuracy (left) and Mean Decrease Gini (right). Variables are ordered by average decrease across all three models. Spectral indices consistently rank high in importance across all three model dates.

3.3.3 S2 and AIS genus-level map comparison

Visual comparison in two sites

Classification results between the two sensors were visually similar for all three dates throughout much of the Delta, here we show this by comparing 2019 Fall Sentinel-2 and AIS maps of Ward Cut and Rhode Island in **Figure 4**. We chose to display these two sites because they contain all study classes and exhibit a range of different vegetation patch sizes and shapes. Generally good agreement between maps is observed at the FAV genus level between locations of larger water primrose (yellow) and water hyacinth patches (purple); however, there are some thinner water hyacinth patches present in AIS maps that are undetected at the coarser S2 resolution (**Figure 4A**). The largest differences between the two maps result from EAV and riparian confusion and the detected SAV coverage relative to tidal stage during image acquisition (**Table 2**).

Percent coverage comparison

To characterize over- or underestimation of classes in S2 maps relative to AIS maps, we calculated the percent area each class occupied in both maps and subtracted AIS percent area from that of S2 in 4 key study sites and the Delta as a whole (**Table 3-6**). Thus, negative values in **Table 3-6** indicate S2 underestimation while positive values indicate S2 overestimation. Actual percent coverages are reported in **Appendix 6 A1**. We compared percent coverage rather than individual pixel agreement because the AIS maps have their own classification errors and reports to state agencies characterizing AIS mapping results primarily focus on percent coverage comparison across years. Similar to class accuracy, we only compare the five vegetation classes and open water.

Water hyacinth percent coverage was overestimated compared to AIS for all comparisons except Ward Cut in fall 2018 and 2019 and Delta wide in fall 2019; however, the difference for all these sites was quite small (0.1-0.2 %). The largest differences in water hyacinth percent coverage were in Rhode Island (0.4 -1.8 %) and across the Delta in summer 2020 (0.4 %). Rhode Island fall 2019 maps are displayed in **Figure 3-4** and show good matchup between medium and large patch locations and extent, despite having the largest percent coverage difference compared to AIS.

Water primrose was underestimated relative to AIS in all locations except Big Break in fall 2019 (no difference), and Big Break and Liberty Island in summer 2020. Water primrose percent differences in summer 2020 are impacted by the additional emergent primrose class in AIS maps which was included to characterize areas of water primrose encroachment on emergent habitat (Khanna et al., 2018). Potential explanations for difference in water hyacinth and water primrose percent coverage are provided in the discussion.

Emergent and riparian vegetation have relatively high percent coverage differences between datasets and exhibit a less distinct pattern of over- or under-estimation across years unlike the two FAV classes, although they appear to be inversely related, likely due to their class confusion. The largest difference between maps is S2 SAV underestimation and

consequently water overestimation in fall 2018 for Big Break (**Table 3-6**), which may be due to tidal height (**Table 3-2**).

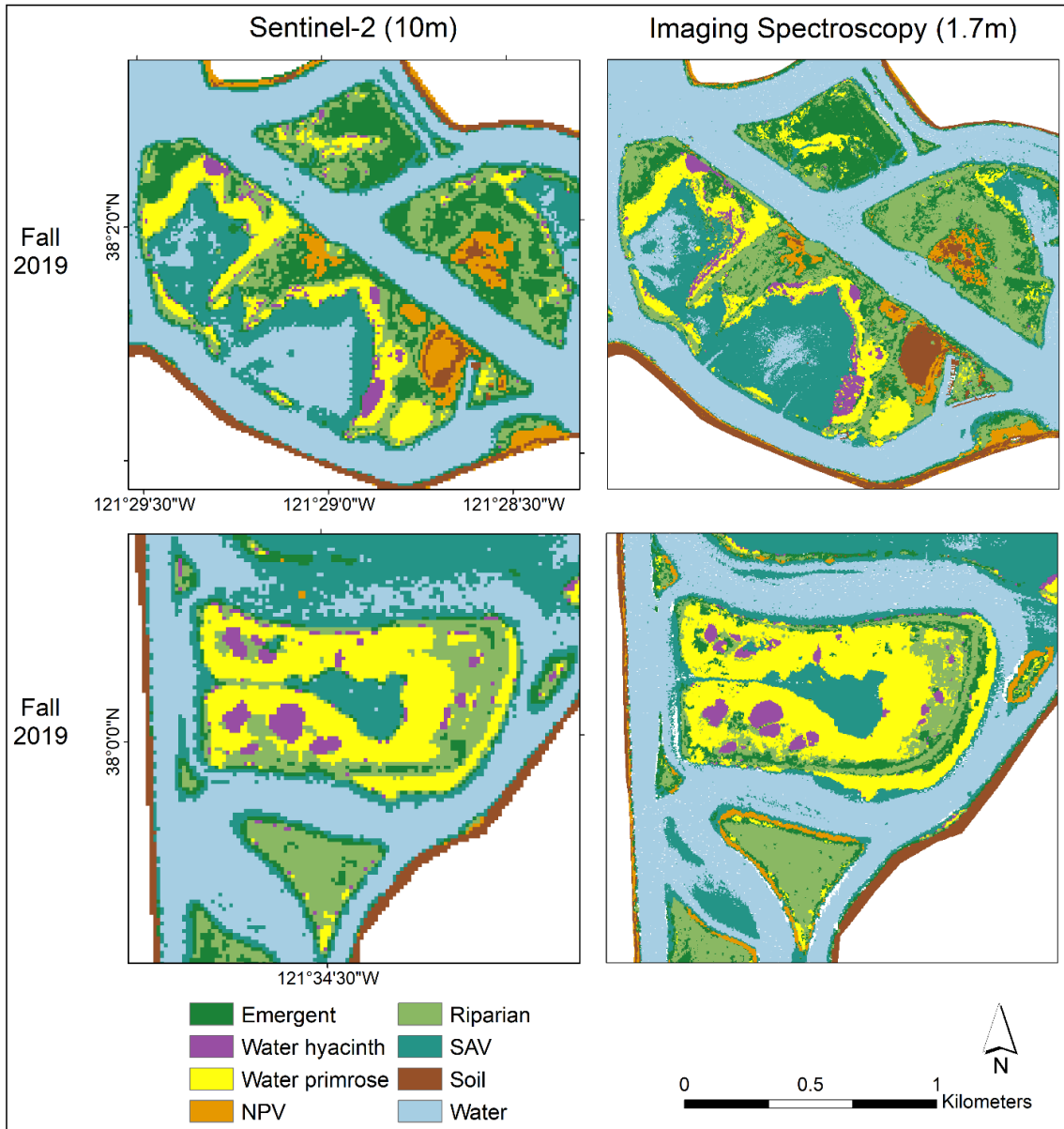


Figure 3-4. Ward Cut (top) and Rhode Island (bottom) comparison between Sentinel-2 and Imaging spectrometer maps. Shows good agreement at the FAV genus level between locations of larger water primrose (yellow) and water hyacinth patches (purple). Orange non-photosynthetic vegetation (NPV) patches on the edge of islands in 2019 AIS maps are patches of floating NPV which cannot be detected by S2 spatial or spectral resolution.

Table 3-6. Difference in percent coverage between Sentinel-2 and airborne imaging spectrometer (AIS) classification maps for 4 sub study areas and Delta wide. AIS percent coverage

was subtracted from that of S2; therefore, negative values indicate S2 underestimation (blue), while positive values indicate S2 overestimation (yellow) relative to AIS maps.

Date		Water Hyacinth	Water Primrose	EAV	Riparian	SAV	Water
2018	Ward Cut	-0.2	-0.3	-2.9	2.8	0.7	-2.1
	Rhode	0.4	-6.5	-1.3	10.4	1.9	-5.2
	Big Break	0.2	-0.8	-2.2	1.8	-31.5	32.1
	Liberty	0	-0.5	-1.3	2.6	-2.2	2.7
	Delta	0.2	-0.6	-2.7	2	-5.8	-0.5
2019	Ward Cut	-0.2	-0.2	2.3	-2.6	-0.4	-0.1
	Rhode	1.8	-1.9	-2.2	5.4	0.8	-2.1
	Big Break	0.3	0	0.1	-1.1	6.7	-6.2
	Liberty	0.2	-0.7	6.3	-6.8	7	-4.5
	Delta	-0.1	-0.3	4.1	-4.6	-2.4	0.1
2020	Ward Cut	0.4	-1.9*	2.5*	1.2*	-2.7	-1
	Rhode	1.1	-3.7*	1.1*	7.7*	7.4	-12.7
	Big Break	0.3	0.6*	-0.5*	-0.4*	-8	9.3
	Liberty	0	1.1*	5.7*	-3.1*	7.8	-8.3
	Delta	0.4	-0.4*	5.3*	-3.3*	-0.4	-6.3

* AIS emergent primrose class was not re-grouped as either primrose or emergent in S2 maps

3.4 Discussion

RS classification of multiple FAV classes is sparse in the published literature, especially in complex aquatic systems such as the Delta. Most previous works target only a single floating invasive species or classify at the community level and are conducted in areas with low spatial variability and large contiguous patches making it easier to separate FAV species from other neighboring aquatic vegetation (Dogliotti et al., 2016; Thamaga and Dube, 2019; Villa et al., 2015). Previous studies in the Delta rely on airborne imaging spectroscopy (AIS) to separate different FAV covers (Bolch et al., 2021; Khanna et al., 2011; Shruti Khanna et al., 2018). In order to determine if Sentinel-2 could be used to fill in AIS temporal gaps with acceptable detection of FAV at the genus level, we compare classification model accuracies (**Table 3-5**) and maps between the two datasets visually (e.g. **Figure 3-4**) and by difference percent class coverage (**Table 3-6**) and discuss dependence on patch size and within class variability relative to sensor spatial and spectral resolution and the influence of external factors such as tidal stage. We further compare differences for both summer and fall imagery to determine if S2 maps could be created for multiple dates throughout the growing season thereby enabling tracking of patch expansion and movement of these motile aquatic species.

3.4.1 Model Accuracies

Following a similar procedure to the near-operational AIS mapping in the Delta, we were able to achieve similar overall accuracies (OA) of 89-91% with S2 compared to 90-92% of AIS while mapping the same classes – water hyacinth (species level), water

primrose (genus level), SAV, EAV, and riparian vegetation at the community level, and open water, soil and non-photosynthetic vegetation. Our overall S2 accuracies are also comparable to other multispectral RS studies which target 4 macrophyte classes and open water 90% (Villa et al., 2015; Wang et al., 2012) (although neither target multiple FAV classes).

The average S2 class accuracy statistics for our target FAV classes – water hyacinth (PA: 79%, UA: 91%) and water primrose (PA: 95%, UA: 85%) are lower or comparable with AIS water hyacinth (PA: 89%, UA: 90%) and water primrose (PA: 93%, UA: 93%). Our performance is also better than, or in line with, other Sentinel-2 studies targeting water hyacinth, which achieved user's accuracies of 75-89 % and producer's accuracies 61-94% using random forest models (Thamaga and Dube, 2018a, 2019). To our knowledge, this is the first study to demonstrate water primrose mapping using multispectral satellite remote sensing; therefore, we are unable to compare class specific accuracies to other sites, but generally our accuracies were quite high.

The spatial resolution of the data relative to target patch size influences the detection capability of the classifiers, and subsequent differences in percent coverage calculated from Sentinel 2. Generally, larger pixel sizes lead to poorer accuracy statistics, though the relationship is not linear; the effect of pixel size on accuracy is dependent on the heterogeneity of the landscape and the design and geolocational precision and accuracy of field data (Frazier, 2015; Knight and Lunetta, 2003). Spatial resampling S2 bands of varying spatial resolution to 10 m may have further impacted the ability to detect small scale features. Nearest neighbor resampling is recommended to be both computationally efficient while best preserving pixel spectral information (Roy et al., 2016) and has been shown to be suitable S2 land cover classification (Zheng et al., 2017). More specialized downscaling algorithms could be explored in future research, although the effects of downscaling on classification accuracy are highly variable (Morrison et al., 2019; Vanderbilt et al., 2007). The pixel size influence on accuracy was minimized in this study through the field data collection and curation process, which paid special attention to patch size relative to the spatial resolution of the two RS datasets. Unfortunately, this same data design process may have possibly introduced lower quality training data into the models resulting in confusion between water hyacinth and water primrose and EAV and riparian vegetation. AIS observations indicate that water hyacinth patches are commonly interspersed with or surrounded by water primrose; therefore, patches labeled as majority water hyacinth in the field data may contain enough water primrose coverage to influence the spectral signature at the S2 pixel size. EAV commonly forms narrow patches which are difficult to photo-interpret and observe in the field due to logistical challenges associated with access and plant density and height obscuring field observations. This poses an issue particularly for S2 discrimination because at coarser spatial resolutions it becomes even more difficult to separate emergent vegetation from the riparian vegetation located directly behind it. It is recommended that future field data collection focus on building training datasets of large and heterogenous aquatic vegetation patches and better characterization of fractional cover and patch sizes relative to S2 pixel size.

3.4.2 Percent coverage comparison: Differences between S2 and AIS and S2 limitations

The primary differences between visual and percent coverage difference between S2 and AIS (**Table 6**) are likely caused by mixed pixels at class boundaries, AIS ability to resolve additional classes and flexible acquisition timing to control for environmental factors such as tidal stage. For example, as pixel size increases, the likelihood of a mixed pixel containing several different target classes also increases. This has several variable effects on the final mapping products. Mean patch size has been shown to increase as pixel size increases (Saura 2002). Sparse and rare classes and smaller patches decrease in abundance, or are not detected at all, while abundant classes tend to become more abundant and overestimated (Morrison et al. 2019, Bolch et al. 2021). Overall, each pixel will be assigned to the majority class, which can cause identified areas to be larger or smaller in the Sentinel-2 imagery due to pixel size rather classifier performance.

3.4.3 Percent coverage of FAV classes

Our S2 maps matched well with AIS maps visually (**Figure 3-4**), but our areal comparison analysis indicated that S2 classifiers generally overestimated water hyacinth and underestimated water primrose area relative to AIS (**Table 3-6**). Infrequent classes with small patches, such as water hyacinth, are actually expected to be underestimated since small patches are likely to be undetected at coarser spatial resolutions – this was exhibited for certain patches, for example the long and thin patch in Ward Cut is missed by S2 (**Figure 3-4**). However, under-detection of small and narrow water hyacinth patches is outweighed in percent coverage estimates because of S2 pixel size, confusion with riparian vegetation due to similar spectral signatures in multispectral space (**Figure 3-5**), and ‘sporadic’ misclassification likely due to other mixed pixels or within class spectral variability not accounted for in the training dataset. This confusion could be reduced with higher spectral resolution data, as it enables spectral unmixing of spectrally complex and similar classes (Hestir et al., 2008; Khanna et al., 2012). However, even previous AIS studies in the Delta found some confusion between these classes (Khanna et al. 2012). These studies reduced misidentification of riparian vegetation as water hyacinth by creating a riparian mask based on spatial information regarding wetland and channel configuration derived from ancillary GIS layers and LiDAR data, which we recommend for future studies (Khanna et al., 2012).

Water primrose coverage was likely underestimated due to S2 mixed pixels at class boundaries exemplified in **Figure 3-6**, which shows patch edges that are more likely to be mixed with water or SAV are classified as emergent or riparian vegetation in S2 imagery. Such effects are more pronounced for water primrose patches than water hyacinth because water primrose shares a larger interface with other classes due to its dominance in the system. In recent years, water primrose has rapidly increased in abundance and distribution in the Delta, and several regions across the Delta have experienced marsh encroachment of water primrose, where water primrose has been “terrestrializing” and creeping up on top

of emergent reeds (Khanna et al. 2018). The AIS summer 2020 maps label this as a separate class (“emergent primrose”), but S2 does not have the spectral or spatial resolution required to do so. Instead, S2 identifies the dominant class representing whichever vegetation is on top of the heterogeneous 3D structure, thereby resulting in percent coverage differences that are not directly related to misclassification.

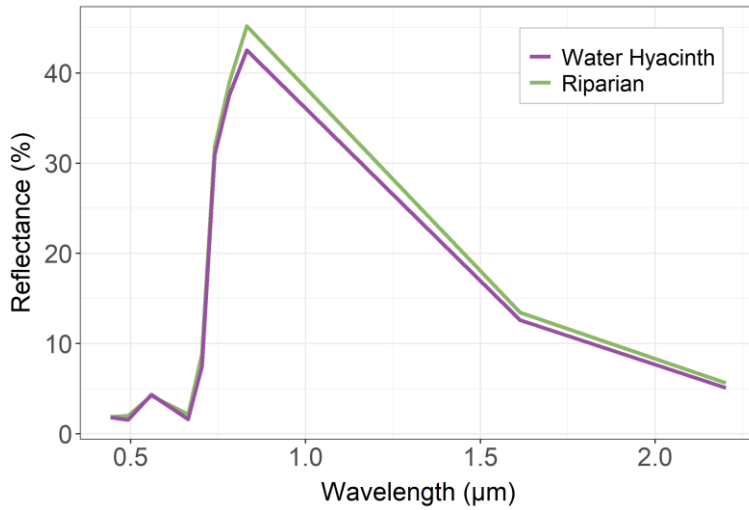


Figure 3-5. Spectral response of a riparian vegetation pixel that was misclassified as water hyacinth and a water hyacinth pixel.

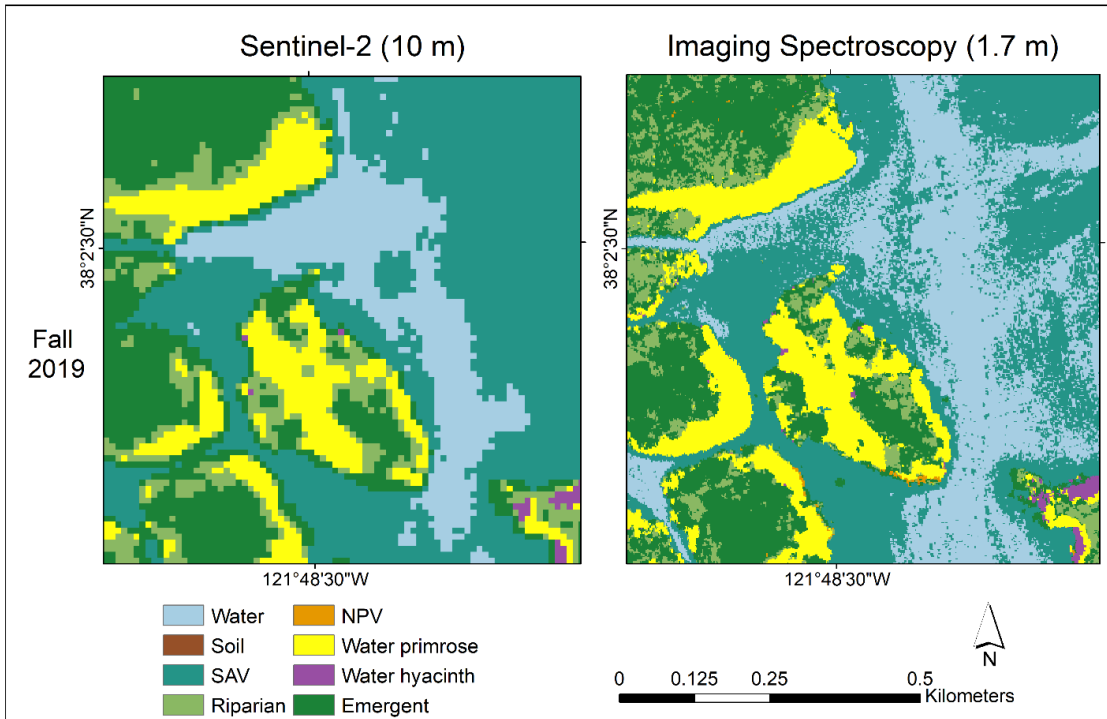


Figure 3-6. Comparison of the impact of limited spatial resolution in S2 data using water primrose patches. Coarse pixel resolution is more likely to cause misclassification at class boundaries due to pixel mixing.

3.4.4 *Impact of environmental conditions: tidal stage*

Other large mismatches in visual and percent area assessments occurred for the SAV and water classes, these differences are likely explained by differences in tidal stage during image acquisition rather than S2 misclassification. **Figure 3-8** explores the impact of tide-stage mismatch between datasets more extensively by comparing a good tidal match-up date (fall 2019) with one of lesser quality (fall 2018). Fall 2018 Sentinel-2 acquisition occurred during a flood tide, which impedes detection of full SAV extent. Fall 2019 Sentinel-2 acquisition occurred at a low tide and shows a much closer match-up between S2 and AIS maps. This indicates that SAV is detectable with Sentinel-2, but images should be selected at low tide to reduce the impacts of water height and increased turbidity, which inhibit detection of the full extent for SAV coverage. Such an approach would mirror the current operations for AIS-based SAV mapping, which only acquires data during periods of low tide and during times of the day that avoid effects from sunglint (Khanna et al. 2018, Hestir et al. 2008). Tidal stage did not strongly impact FAV mapping because the leaves are above the water column hence spectral reflectance is not affected by tidal stage. Both water hyacinth and water primrose exhibit a good visual match and smaller quantitative differences as listed in **Table 3-6**.

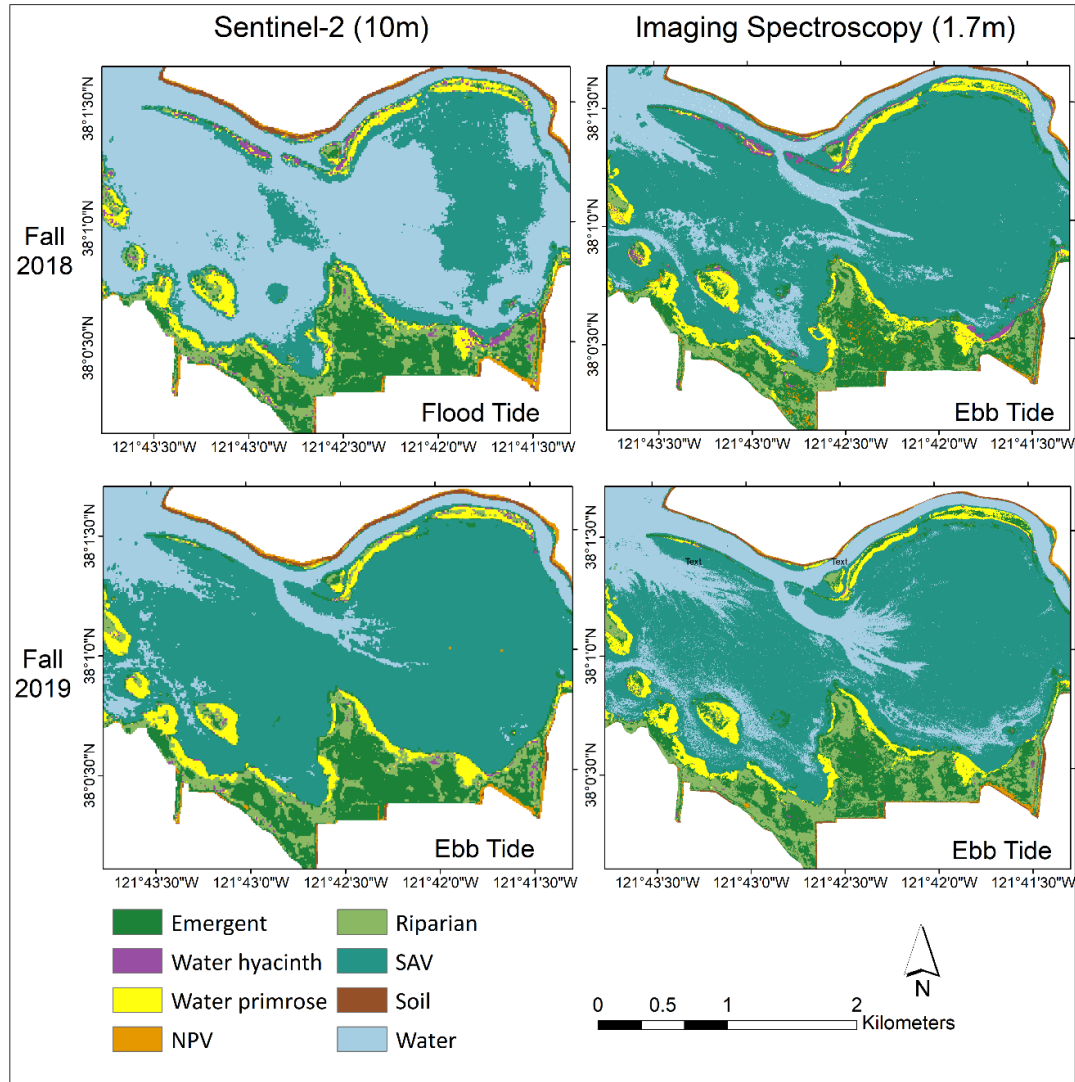


Figure 3-7. Tidal stage comparison for fall match-ups at Big Break. Fall 2018 Sentinel-2 acquisition occurs during a flood tide which impedes detection of full SAV extent. Fall 2019 Sentinel-2 acquisition occurs at a low tide and shows a much closer match-up between S2 and imaging spectrometer maps.

3.4.5 Sentinel-2 characteristics that enable differentiation between FAV classes and the neighboring vegetation

The detection of water hyacinth and water primrose in this spatially complex system of wetlands was possible due to the 10-20m pixel size of S2 images and the moderate spectral resolution. While some previous multi-spectral RS studies targeting water hyacinth detection have successfully used Landsat (30m pixels; 7 bands),– (Singh et al., 2020)– these studies occurred in simpler systems with fewer target species. Thamaga and Dube (2018b) compared the performance of Landsat and S2 and determined that S2 resulted in higher class accuracies. In an environment as spatially complex as the Delta,

the 10 m spatial resolution of S2 supports water primrose and water hyacinth detection because these vegetation patches are generally small (~40-60 m) wide with few large patches (90-100 m). Large patches would be contained within a single 30m pixel, but smaller patches would not.

Spectral resolution and range also play important roles in FAV separation. Although the three S2 red-edge bands were not ranked as high as several spectral indexes or spectral bands in S2 RF model variable importance, the mean decrease accuracy values (~20%) suggest that the red edge bands still played an important role in class discrimination. The importance of the red edge bands to aquatic vegetation classification has been demonstrated in other studies (Thamaga and Dube, 2018c; Tian et al., 2020). These works, like ours, determined that spectral indexes and other VSWIR spectral bands are more important to classification accuracy than red edge bands, but this does not negate the usefulness of these additional S2 bands. However, red edge indices were consistently among the least important variables, their importance has varied in other aquatic vegetation classification studies (Amani et al., 2018; Tian et al., 2020). Additional testing is recommended to determine if these red edge indexes could be excluded in future models. Spectral range is also an important consideration. The SWIR region, and spectral indexes calculated with SWIR bands were important for RF model performance. Previous work has also documented the importance in the SWIR region for discriminating aquatic vegetation from water (Hestir et al. 2012, Khanna et al. 2012).

3.5 Conclusions

Analysis of Sentinel-2 classifications maps demonstrates two types of invasive floating aquatic vegetation, water hyacinth and water primrose, can be distinguished in heterogeneous wetlands during summer and fall. Our results indicate that Sentinel-2 imagery can supplement AIS mapping efforts by filling temporal gaps and enabling studying of annual and intra-annual changes in FAV community composition as a response to environmental or anthropogenic disturbance events. Extensive time series will in particular enhance the understanding of invasion processes. Future research should investigate differences in spring and winter and incorporate a riparian vegetation mask to reduce misclassification of floating vegetation. Further, the near-operational pipeline developed during this study will lead to an operational mapping pipeline for generating wetland vegetation maps for California agencies that enable new methods of management and monitoring to identify where aquatic invasive species control is effective.

3.6 Acknowledgements and funding

We thank the Delta Stewardship Council agreement number 18201 for funding this research.

3.7 Appendix

A1. Percent coverage

Table A1. Percent coverage of each class by sensor

Date		Water Hyacinth		Water Primrose		Emergent		Riparian		SAV		Water	
		S2	AIS	S2	AIS	S2	AIS	S2	AIS	S2	AIS	S2	AIS
2018	Ward Cut	1.2	1.4	5.0	5.3	14.7	17.6	10.3	7.5	19.5	18.8	39.6	41.7
	Rhode	5.0	4.6	32.3	38.8	4.1	5.4	14.7	4.3	19.1	17.2	22.2	27.4
	Big Break	1.5	1.3	5.6	6.4	11.0	13.2	7.7	5.9	19.1	50.6	51.8	19.7
	Liberty	0.3	0.3	1.9	2.4	21.9	23.2	7.2	4.6	24.2	26.4	42.1	39.4
	Delta	0.9	0.7	1.6	2.2	11.8	14.5	7.5	5.5	13.6	19.4	49.9	50.4
2019	Ward Cut	1.4	1.6	6.0	6.2	14.2	11.9	10.8	13.4	13.6	14.0	45.0	45.1
	Rhode	5.8	4.0	30.0	31.9	6.0	8.2	17.4	12.0	15.6	14.8	22.4	24.5
	Big Break	0.7	0.4	6.6	6.6	12.0	11.9	6.8	7.9	53.4	46.7	17.3	23.5
	Liberty	0.4	0.2	1.6	2.3	25.5	19.2	5.5	12.3	33.2	26.2	32.4	36.9
	Delta	0.6	0.7	1.7	2.0	15.7	11.6	6.1	10.7	15.5	17.9	47.2	47.1
2020	Ward Cut	2.0	1.6	5.0	6.9	13.3	10.8	13.2	12	14.9	17.6	41.8	42.8
	Rhode	6.0	4.9	30.7	34.4	6.0	4.9	30.7	34.4	6.0	4.9	30.7	34.4
	Big Break	1.4	1.1	5.9	5.3	12.2	12.7	7.6	8.0	42.6	50.6	27.1	17.8
	Liberty	0.5	0.5	1.9	0.8	25.3	19.6	5.9	9.0	38.1	30.3	26.1	34.4
	Delta	1.4	1.0	1.5	1.9	15.4	10.1	6.9	10.2	13.1	13.5	47.5	53.8

3.8 References

- Adam, E., Mutanga, O., Rugege, D., 2010. Multispectral and hyperspectral remote sensing for identification and mapping of wetland vegetation: A review. *Wetl. Ecol. Manag.* 18, 281–296. <https://doi.org/10.1007/S11273-009-9169-Z/TABLES/2>
- Amani, M., Salehi, B., Mahdavi, S., Brisco, B., 2018. Spectral analysis of wetlands using multi-source optical satellite imagery. *ISPRS J. Photogramm. Remote Sens.* 144, 119–136. <https://doi.org/10.1016/J.ISPRSJPRS.2018.07.005>
- Berhane, T.M., Lane, C.R., Wu, Q., Autrey, B.C., Anenkhonov, O.A., Chepinoga, V. V., Liu, H., 2018. Decision-Tree, Rule-Based, and Random Forest Classification of High-Resolution Multispectral Imagery for Wetland Mapping and Inventory. *Remote Sens.* 2018, Vol. 10, Page 580 10, 580. <https://doi.org/10.3390/RS10040580>
- Bolch, E.A., Hestir, E.L., Khanna, S., 2021. Performance and Feasibility of Drone-Mounted Imaging Spectroscopy for Invasive Aquatic Vegetation Detection. *Remote*

- Sens. 2021, Vol. 13, Page 582 13, 582. <https://doi.org/10.3390/RS13040582>
- Cohen, A.N., Carlton, J.T., 1998. Accelerating Invasion Rate in a Highly Invaded Estuary. *Science* (80-.). 279, 555–558. <https://doi.org/10.1126/science.279.5350.555>
- DBW, 2019. Aquatic Invasive Plant Control Program 2019 Annual Monitoring Report.
- Dersseh, M.G., Tilahun, S.A., Worqlul, A.W., Moges, M.A., Abebe, W.B., Mhired, D.A., Melesse, A.M., 2020. Spatial and Temporal Dynamics of Water Hyacinth and Its Linkage with Lake-Level Fluctuation: Lake Tana, a Sub-Humid Region of the Ethiopian Highlands. *Water* 2020, Vol. 12, Page 1435 12, 1435. <https://doi.org/10.3390/W12051435>
- Dogliotti, A.I., Ruddick, K., Guerrero, R., 2016. Seasonal and inter-annual turbidity variability in the Río de la Plata from 15 years of MODIS: El Niño dilution effect. *Estuar. Coast. Shelf Sci.* 182, 27–39. <https://doi.org/https://doi.org/10.1016/j.ecss.2016.09.013>
- Dong, D., Wang, C., Yan, J., He, Q., Zeng, J., Wei, Z., 2020. Combining Sentinel-1 and Sentinel-2 image time series for invasive *Spartina alterniflora* mapping on Google Earth Engine: a case study in Zhangjiang Estuary. *J. Appl. Remote Sens.* 14, 1–18. <https://doi.org/10.1117/1.JRS.14.044504>
- Drusch, M., Del Bello, U., Carlier, S., Colin, O., Fernandez, V., Gascon, F., Hoersch, B., Isola, C., Laberinti, P., Martimort, P., 2012. Sentinel-2: ESA’s optical high-resolution mission for GMES operational services. *Remote Sens. Environ.* 120, 25–36.
- Everitt, J.H., Yang, C., Summy, K.R., Owens, C.S., Glomski, L.M., Smart, R.M., 2011. Using in situ hyperspectral reflectance data to distinguish nine aquatic plant species. <http://dx.doi.org/10.1080/10106049.2011.591944> 26, 459–473. <https://doi.org/10.1080/10106049.2011.591944>
- Fernández-Manso, A., Fernández-Manso, O., Quintano, C., 2016. SENTINEL-2A red-edge spectral indices suitability for discriminating burn severity. *Int. J. Appl. Earth Obs. Geoinf.* 50, 170–175. <https://doi.org/https://doi.org/10.1016/j.jag.2016.03.005>
- Foody, G.M., 2020. Explaining the unsuitability of the kappa coefficient in the assessment and comparison of the accuracy of thematic maps obtained by image classification. *Remote Sens. Environ.* 239, 111630. <https://doi.org/10.1016/J.RSE.2019.111630>
- Frazier, A.E., 2015. Landscape heterogeneity and scale considerations for super-resolution mapping. <http://dx.doi.org/10.1080/2150704X.2015.1040130> 36, 2395–2408. <https://doi.org/10.1080/2150704X.2015.1040130>
- Gallant, A.L., 2015. The challenges of remote monitoring of wetlands. *Remote Sens.* <https://doi.org/10.3390/rs70810938>
- Gao, B., 1996. NDWI—A normalized difference water index for remote sensing of vegetation liquid water from space. *Remote Sens. Environ.* 58, 257–266. [https://doi.org/https://doi.org/10.1016/S0034-4257\(96\)00067-3](https://doi.org/https://doi.org/10.1016/S0034-4257(96)00067-3)
- Gitelson, A., Merzlyak, M.N., 1994. Spectral Reflectance Changes Associated with Autumn Senescence of *Aesculus hippocastanum* L. and *Acer platanoides* L. Leaves. Spectral Features and Relation to Chlorophyll Estimation. *J. Plant Physiol.* 143, 286–292. [https://doi.org/10.1016/S0176-1617\(11\)81633-0](https://doi.org/10.1016/S0176-1617(11)81633-0)

- Gong, Z., Zhang, C., Zhang, L., Bai, J., Zhou, D., 2021. Assessing spatiotemporal characteristics of native and invasive species with multi-temporal remote sensing images in the Yellow River Delta, China. *L. Degrad. Dev.* 32, 1338–1352. <https://doi.org/10.1002/ldr.3799>
- Grewell, B.J., Gillard, M.B., Futrell, C.J., Castillo, J.M., 2019. Seedling Emergence from Seed Banks in *Ludwigia hexapetala*-Invaded Wetlands: Implications for Restoration. *Plants* 2019, Vol. 8, Page 451 8, 451. <https://doi.org/10.3390/PLANTS8110451>
- Guo, M., Li, J., Sheng, C., Xu, J., Wu, L., 2017. A review of wetland remote sensing. *Sensors (Switzerland)*. <https://doi.org/10.3390/s17040777>
- Hestir, E.L., Khanna, S., Andrew, M.E., Santos, M.J., Viers, J.H., Greenberg, J.A., Rajapakse, S.S., Ustin, S.L., 2008. Identification of invasive vegetation using hyperspectral remote sensing in the California Delta ecosystem. *Remote Sens. Environ.* 112, 4034–4047. <https://doi.org/10.1016/J.RSE.2008.01.022>
- Huete, A.R., 1988. A soil-adjusted vegetation index (SAVI). *Remote Sens. Environ.* 25, 295–309.
- Jetter, K.M., Nes, K., Tahoe, L., 2018. The cost to manage invasive aquatic weeds in the California Bay-Delta. *ARE Updat.* 21, 9–11.
- Khanna, S., Acuna, S., Contreras, D., Griffiths, W.K., Lesmeister, S., Reyes, R.C., Schreier, B., Wu, B.J., 2019. Invasive aquatic vegetation impacts on Delta operations, monitoring, and ecosystem and human health. *Interag. Ecol. Progr. Newsl.*
- Khanna, S., Santos, M.J., Boyer, J.D., Shapiro, K.D., Bellvert, J., Ustin, S.L., 2018. Water primrose invasion changes successional pathways in an estuarine ecosystem. *Ecosphere* 9, e02418. <https://doi.org/https://doi.org/10.1002/ecs2.2418>
- Khanna, Shrutti, Santos, M.J., Boyer, J.D., Shapiro, K.D., Bellvert, J., Ustin, S.L., 2018. Water primrose invasion changes successional pathways in an estuarine ecosystem. *Ecosphere* 9, e02418. <https://doi.org/10.1002/ECS2.2418>
- Khanna, S., Santos, M.J., Hestir, E.L., Ustin, S.L., 2012. Plant community dynamics relative to the changing distribution of a highly invasive species, *Eichhornia crassipes*: A remote sensing perspective. *Biol. Invasions* 14, 717–733. <https://doi.org/10.1007/s10530-011-0112-x>
- Khanna, S., Santos, M.J., Ustin, S.L., Haverkamp, P.J., 2011. An integrated approach to a biophysiological based classification of floating aquatic macrophytes. <https://doi.org/10.1080/01431160903505328> 32, 1067–1094. <https://doi.org/10.1080/01431160903505328>
- Khanna, S., Ustin, S.L., Hestir, E.L., Santos, M.J., Andrew, M., Lay, M., Tuil, J., Bellvert, J., Greenberg, J., Shapiro, K.D., Rajapakse, S., 2022. The Sacramento-San Joaquin Delta genus and community level classification maps derived from airborne spectroscopy data. <https://doi.org/10.5063/F1K9360F>
- Kleinschroth, F., Winton, R.S., Calamita, E., Niggemann, F., Botter, M., Wehrli, B., Ghazoul, J., 2021. Living with floating vegetation invasions. *Ambio* 50, 125–137. <https://doi.org/10.1007/S13280-020-01360-6/FIGURES/7>
- Knight, J.F., Lunetta, R.S., 2003. An experimental assessment of minimum mapping unit size. *IEEE Trans. Geosci. Remote Sens.* 41, 2132–2134. <https://doi.org/10.1109/TGRS.2003.816587>

- Kuhn, M., 2008. Building predictive models in R using the caret package. *J Stat Softw* 28, 1–26.
- Liaw, A., Wiener, M., 2002. Classification and regression by randomForest. *R news* 2, 18–22.
- Magidi, J., Nhamo, L., Mpandeli, S., Mabhaudhi, T., 2021. Application of the Random Forest Classifier to Map Irrigated Areas Using Google Earth Engine. *Remote Sens.* 2021, Vol. 13, Page 876 13, 876. <https://doi.org/10.3390/RS13050876>
- Mahdianpari, M., Salehi, B., Mohammadimanesh, F., Motagh, M., 2017. Random forest wetland classification using ALOS-2 L-band, RADARSAT-2 C-band, and TerraSAR-X imagery. *ISPRS J. Photogramm. Remote Sens.* 130, 13–31. <https://doi.org/10.1016/J.ISPRSJPRS.2017.05.010>
- Malik, A., 2007. Environmental challenge vis a vis opportunity: The case of water hyacinth. *Environ. Int.* 33, 122–138. <https://doi.org/10.1016/J.ENVINT.2006.08.004>
- McFeeters, S.K., 1996. The use of the Normalized Difference Water Index (NDWI) in the delineation of open water features. *Int. J. Remote Sens.* 17, 1425–1432.
- Morrison, B.D., Heath, K., Greenberg, J.A., 2019. Spatial scale affects novel and disappeared climate change projections in Alaska. *Ecol. Evol.* 9, 12026–12044. <https://doi.org/10.1002/ECE3.5511>
- Ongore, C.O., Aura, C.M., Ogari, Z., Njiru, J.M., Nyamweya, C.S., 2018. Spatial-temporal dynamics of water hyacinth, *Eichhornia crassipes* (Mart.) and other macrophytes and their impact on fisheries in Lake Victoria, Kenya. *J. Great Lakes Res.* 44, 1273–1280. <https://doi.org/10.1016/J.JGLR.2018.10.001>
- Penfound, W.T., Earle, T.T., 1948. The Biology of the Water Hyacinth. *Ecol. Monogr.* 18, 447–472. <https://doi.org/10.2307/1948585>
- Pimentel, D., Zuniga, R., Morrison, D., 2005. Update on the environmental and economic costs associated with alien-invasive species in the United States. *Ecol. Econ.* 52, 273–288. <https://doi.org/10.1016/J.ECOLECON.2004.10.002>
- Ranghetti, L., Boschetti, M., Nutini, F., Busetto, L., 2020. “sen2r”: An R toolbox for automatically downloading and preprocessing Sentinel-2 satellite data. *Comput. Geosci.* 139, 104473. <https://doi.org/10.1016/J.CAGEO.2020.104473>
- Rejmánková, E., 1992. Ecology of creeping macrophytes with special reference to *Ludwigia peploides* (H.B.K.) Raven. *Aquat. Bot.* 43, 283–299. [https://doi.org/10.1016/0304-3770\(92\)90073-R](https://doi.org/10.1016/0304-3770(92)90073-R)
- Rouse, J.W., Haas, R.H., Schell, J.A., Deering, D.W., 1974. Monitoring vegetation systems in the Great Plains with ERTS. *NASA Spec. Publ.* 351, 309.
- Roy, D.P., Li, J., Zhang, H.K., Yan, L., 2016. Best practices for the reprojection and resampling of Sentinel-2 Multi Spectral Instrument Level 1C data. <http://dx.doi.org/10.1080/2150704X.2016.1212419> 7, 1023–1032. <https://doi.org/10.1080/2150704X.2016.1212419>
- Santos, M.J., Hestir, E.L., Khanna, S., Ustin, S.L., 2012. Image spectroscopy and stable isotopes elucidate functional dissimilarity between native and nonnative plant species in the aquatic environment. *New Phytol.* 193. <https://doi.org/10.1111/j.1469-8137.2011.03955.x>
- Schmidt, K.S., Skidmore, A.K., 2003. Spectral discrimination of vegetation types in a coastal wetland. *Remote Sens. Environ.* 85, 92–108.

- [https://doi.org/https://doi.org/10.1016/S0034-4257\(02\)00196-7](https://doi.org/https://doi.org/10.1016/S0034-4257(02)00196-7)
- Singh, G., Reynolds, C., Byrne, M., Rosman, B., 2020. A Remote Sensing Method to Monitor Water, Aquatic Vegetation, and Invasive Water Hyacinth at National Extents. *Remote Sens.* 2020, Vol. 12, Page 4021 12, 4021. <https://doi.org/10.3390/RS12244021>
- Thamaga, K.H., Dube, T., 2019. Understanding seasonal dynamics of invasive water hyacinth (*Eichhornia crassipes*) in the Greater Letaba river system using Sentinel-2 satellite data. <https://doi.org/10.1080/15481603.2019.1646988> 56, 1355–1377. <https://doi.org/10.1080/15481603.2019.1646988>
- Thamaga, K.H., Dube, T., 2018a. Remote sensing of invasive water hyacinth (*Eichhornia crassipes*): A review on applications and challenges. *Remote Sens. Appl. Soc. Environ.* <https://doi.org/10.1016/j.rsase.2018.02.005>
- Thamaga, K.H., Dube, T., 2018b. Remote sensing of invasive water hyacinth (*Eichhornia crassipes*): A review on applications and challenges. *Remote Sens. Appl. Soc. Environ.* 10, 36–46. <https://doi.org/10.1016/J.RSASE.2018.02.005>
- Thamaga, K.H., Dube, T., 2018c. Testing two methods for mapping water hyacinth (*Eichhornia crassipes*) in the Greater Letaba river system, South Africa: discrimination and mapping potential of the polar-orbiting Sentinel-2 MSI and Landsat 8 OLI sensors. <https://doi.org/10.1080/01431161.2018.1479796> 39, 8041–8059. <https://doi.org/10.1080/01431161.2018.1479796>
- Thouvenot, L., Haury, J., Thiebaut, G., 2013a. A success story: water primroses, aquatic plant pests. *Aquat. Conserv. Mar. Freshw. Ecosyst.* 23, 790–803. <https://doi.org/10.1002/AQC.2387>
- Thouvenot, L., Haury, J., Thiébaud, G., 2013b. Seasonal plasticity of *Ludwigia grandiflora* under light and water depth gradients: An outdoor mesocosm experiment. *Flora - Morphol. Distrib. Funct. Ecol. Plants* 208, 430–437. <https://doi.org/10.1016/J.FLORA.2013.07.004>
- Tian, Y., Jia, M., Wang, Z., Mao, D., Du, B., Wang, C., 2020. Monitoring Invasion Process of *Spartina alterniflora* by Seasonal Sentinel-2 Imagery and an Object-Based Random Forest Classification. *Remote Sens.* 2020, Vol. 12, Page 1383 12, 1383. <https://doi.org/10.3390/RS12091383>
- Ustin, S.L., Khanna, S., Lay, M., 2021. Remote sensing of the Sacramento-San Joaquin Delta to enhance mapping for invasive and native aquatic plant species. University of California, Davis. Report to The Delta Stewardship Council.
- Vanderbilt, V.C., Khanna, S., Ustin, S.L., 2007. Impact of pixel size on mapping surface water in subsolar imagery. *Remote Sens. Environ.* 109, 1–9. <https://doi.org/10.1016/J.RSE.2006.12.009>
- Villa, P., Bresciani, M., Bolpagni, R., Pinardi, M., Giardino, C., 2015. A rule-based approach for mapping macrophyte communities using multi-temporal aquatic vegetation indices. *Remote Sens. Environ.* 171, 218–233. <https://doi.org/10.1016/J.RSE.2015.10.020>
- Villa, P., Laini, A., Bresciani, M., Bolpagni, R., 2013. A remote sensing approach to monitor the conservation status of lacustrine *Phragmites australis* beds. *Wetl. Ecol. Manag.* 21, 399–416.
- Villa, P., Mousivand, A., Bresciani, M., 2014. Aquatic vegetation indices assessment

- through radiative transfer modeling and linear mixture simulation. *Int. J. Appl. Earth Obs. Geoinf.* 30, 113–127. <https://doi.org/https://doi.org/10.1016/j.jag.2014.01.017>
- Wang, L., Dronova, I., Gong, P., Yang, W., Li, Y., Liu, Q., 2012. A new time series vegetation-water index of phenological-hydrological trait across species and functional types for Poyang Lake wetland ecosystem. *Remote Sens. Environ.* 125, 49–63. <https://doi.org/10.1016/j.rse.2012.07.003>
- Xu, H., 2006. Modification of normalised difference water index (NDWI) to enhance open water features in remotely sensed imagery. *Int. J. Remote Sens.* 27, 3025–3033. <https://doi.org/10.1080/01431160600589179>
- Zheng, H., Du, P., Chen, J., Xia, J., Li, E., Xu, Z., Li, X., Yokoya, N., 2017. Performance Evaluation of Downscaling Sentinel-2 Imagery for Land Use and Land Cover Classification by Spectral-Spatial Features. *Remote Sens.* 2017, Vol. 9, Page 1274–1274. <https://doi.org/10.3390/RS9121274>

4. Chapter 3: Priority effects, niche breadth and environmental plasticity of invasive floating aquatic vegetation phenology revealed by satellite remote sensing*

Abstract

Phenology may play an important role in the success of invasive aquatic vegetation species, which can be explained by four ecological theories- vacant niche, priority effects, niche breadth, and plasticity. In order to understand the link between growth cycles and invasions in aquatic ecosystems, we analyzed Sentinel-2 derived phenology metrics of competing invasive floating vegetation, water primrose (*Ludwigia* spp) and water hyacinth (*Eichhornia crassipes*) and emergent macrophytes at the community level in the Sacramento San Joaquin Delta. Results show that water primrose has the earliest start of the growing seasons, higher rates of increase and decrease, longer growing seasons and later end dates than water hyacinth or emergent vegetation, thereby, providing examples of priority effects, niche breadth and environmental plasticity. We also noted several spatial patterns and within-class variability, which highlights the need for spatially resolved phenology metrics, especially in spatio-temporally complex areas like wetlands. Our results help to shed light on the link between phenology dynamics and invasion processes and contribute to the development and prioritization of spatial management strategies using remote sensing.

4.1 Introduction

Phenology, the timing of growth, plays an important role in structuring population and community dynamics as it influences resource access, mating success, vulnerability to herbivores, and competition (Thackeray et al., 2016; Visser and Both, 2005; Wolkovich and Cleland, 2014). Differences in phenology of invasive species relative to native species can enhance their ability to capture and utilize resources, which may change under projected climate-change and disturbance regimes (Piao et al., 2019; Wolkovich and Cleland, 2014, 2011). The link between phenology and invasion success can be explained by four non-mutually exclusive hypotheses proposed by Wolkovich and Cleland, 2011, all of which may be impacted by global warming: vacant niche, priority effects, niche breadth, and plasticity.

These mechanisms of invasion related to phenology are currently underexplored for aquatic plant communities (Fleming and Dibble, 2015). Some studies have compared the phenology of invasive aquatic species relative to native species and their phenological response to warming within submerged (Calero and Rodrigo, 2019; Verhoeven et al., 2020), floating (Peeters et al., 2013) and emergent communities (Alahuhta et al., 2011; Harms and Cronin, 2021), while others examined relationships across multiple growth forms (Gillard et al., 2021). However, the vast majority of studies are focused on in-situ observations of vegetation density and biomass; therefore, they are not generalizable across large spatial and temporal scales. The ability to map key phenological metrics, such as start, duration, and end of the growing season, with spatial and temporal continuity would enhance our understanding of aquatic vegetation community invasion and the responses of different plant community types or species environmental characteristics and drivers of change (Dronova et al., 2021; Pinardi et al., 2021; Tóth et al., 2019)

Remotely sensed (RS) phenology metrics have already provided key insights on ecosystem sensitivity to climatic fluctuations, shifts in species composition, and general ecosystem health (Piao et al., 2019; Richardson et al., 2013). However, most of these studies are focused on terrestrial ecosystems and there is less information available about extracting RS phenology metrics in aquatic ecosystems. Although, there are RS studies centered around aquatic vegetation phenology they primarily focus on improving classification map accuracy (Ai et al., 2017; Luo et al., 2016; Sun et al., 2021; Wang et al., 2012), extract phenology metrics at the community level (Dronova et al., 2021; Miller et al., 2021; Taddeo and Dronova, 2020), or occur at too large of spatial scales to monitor smaller scale invasions process (O'Connell et al., 2017; Zhao et al., 2009).

The sparsity of aquatic RS phenology studies is related to the spatial and temporal heterogeneity of wetland environments, and a long-standing mismatch between the sensor resolution requirements for observing these ecosystems and actively available sensors. However, recent advancements provided by the high temporal resolution and spatial resolution of Sentinel-2 enabled researchers to map RS derived phenology metrics in aquatic systems and link these variables to species invasions. Villa et al., 2018 and Tóth et al., 2019 derived seasonal dynamics in a shallow freshwater lake using Sentinel-2 and determined that *Ludwigia hexapetala* may have phenological advantages over native floating species. Specifically, it was observed that *L. hexapetala* has a longer growth season

than native species by extending growth longer into the fall – providing an example of niche breadth. Several studies have confirmed that *Ludwigia* spp. has high morphological and seasonal plasticity, which allows it to tolerate and efficiently colonize over a broad range of environmental conditions (Lambert et al., 2010; Thouvenot et al., 2013). It is unknown if the results and approach by Tóth et al. 2019 apply to other aquatic ecosystems invaded by water primrose, such as the Sacramento San-Joaquin Delta in California. Additionally, there are no previous studies examining invasive floating aquatic species interactions in a tidally influenced system using RS phenology metrics.

The Sacramento San-Joaquin Delta is the largest tidal freshwater estuary in the western United States and is heavily invaded by water primrose (*Ludwigia* spp.) and water hyacinth (*Eichhornia crassipes*). Water primrose increased in coverage four-fold in the Sacramento San Joaquin Delta (The Delta, henceforth), replacing water hyacinth as the most dominate floating invasive species, between 2004 and 2016 as observed by airborne imaging spectroscopy (AIS) (Khanna et al 2018). Two growth forms, aquatic and terrestrialized, extend the adaptive capabilities of water primrose by allowing it to first populate open water and when running out of suitable habitat, the terrestrialized form can invade regions of emergent vegetation (Khanna et al. 2018). Spatially resolved maps of phenology dynamics may be able to provide more information about underlying mechanisms of the invasion process related to phenology and the more recent success of *Ludwigia* spp, as well as, providing management with information on concerning timing of pesticide treatments.

The objective of this work is to use RS derived phenology metrics to quantitatively examine differences in phenology for competing invasive floating aquatic vegetation at the genus level, water hyacinth and water primrose, and emergent vegetation at the community level in the Delta. And assess how these differences may be influencing the invasion process in the Delta relative to the four hypotheses delineated in Figure 1.

We hypothesize that: 1) The relationship between water primrose and emergent vegetation may show an example of niche breadth and priority effects based on the works of Tóth et al., 2019 and Khanna et al., 2018. 2) The relationship between water primrose and water hyacinth may demonstrate priority effects or niche in favor of water primrose based on estimates Tóth et al., 2019 and observations of water hyacinth growth in the Delta by (CDBW, 2012).

4.2 Study Site

The Sacramento San Joaquin is the largest tidal freshwater estuary in the western United States, spanning approximately 2220 km² in Northern and Central California (**Figure 4-1**). It is a heavily managed system including complex waterways and several flooded islands that support lake-like and wetland environments. The Delta is also one of the most invaded ecosystems in the world, and the spread and persistence of invasive aquatic vegetation species has been determinantal to water quality, water pumping and native species (DBW, 2019; Jetter et al., 2018).

Aquatic vegetation in the Delta consists of three plant community types: floating, emergent and submerged. The majority of the floating aquatic vegetation community is comprised of competing invasive species - water primrose and water hyacinth (Ustin et al., 2021). Water hyacinth and water primrose are in the top 200 invasive aquatic plants

globally (Cronk and Fuller, 2014). Water primrose, although nominally rooted, forms floating canopies (Rejmánková, 1992). Water hyacinth is a free-floating aquatic macrophyte – often anchoring itself to nearby emergent vegetation (Penfound and Earle, 1948). The emergent vegetation community in the Delta primarily consists of two cattail species (*Typha latifolia* and *Typha angustifolia*) and two tule species (*Schoenoplectus acutus* and *Schoenoplectus californicus*) and their hybrids, and the invasive *Phragmites australis* (Khanna et al., 2012). While invasive submerged aquatic vegetation is highly prevalent in the Delta, it was excluded from analysis because detected changes in RS phenology metrics dynamics would likely reflect changes in water height rather than vegetation growth.

Although statistics are reported Delta wide, our analysis and visualizations focus on three study sites, Liberty Island, Rhode Island, and Lower Sherman Island, which are representative of a range of hydrological and environmental characters present in the Delta (**Figure 4-1**).

Lower Sherman Island is located at the confluence of the Sacramento and the San Joaquin Delta and is the most tidally influenced of the three sites. This area receives a considerable amount of freshwater input and has low salinity during wet years and high inflow periods (winter), but during dry years and summer becomes brackish (8,000 to 10,000 $\mu\text{S}/\text{cm}$) (Tuxen et al., 2011).

Rhode Island is a small partially submerged island located along Old River in the central Delta. Between 2004 and 2017 there was a major shift from submerged aquatic community to floating aquatic community (Ustin et al., 2017). Between 2015 to 2019, water primrose dominated the area, likely due to a reduction in water hyacinth from treatment (Ustin et al. 2021). This site was selected because it is one of few areas with large persistent water hyacinth patches.

Liberty Island is a naturally restored freshwater shallow tidal wetland created by flooding a reclaimed agricultural tract. The emergent marsh forms triangular areas that are separated by the original roads between agricultural fields. Differences in stream flow, tidal exposure, elevation have facilitated emergent vegetation to recolonize more rapidly in northern and western portions of the island than the eastern side (Whitley and Bollens, 2014). Water primrose has been documented in the area for at least two decades, but has substantially increased its coverage since 2004, and in recent years has been encroaching on emergent marsh habitats (Khanna et al. 2012, Khanna et al. 2018).

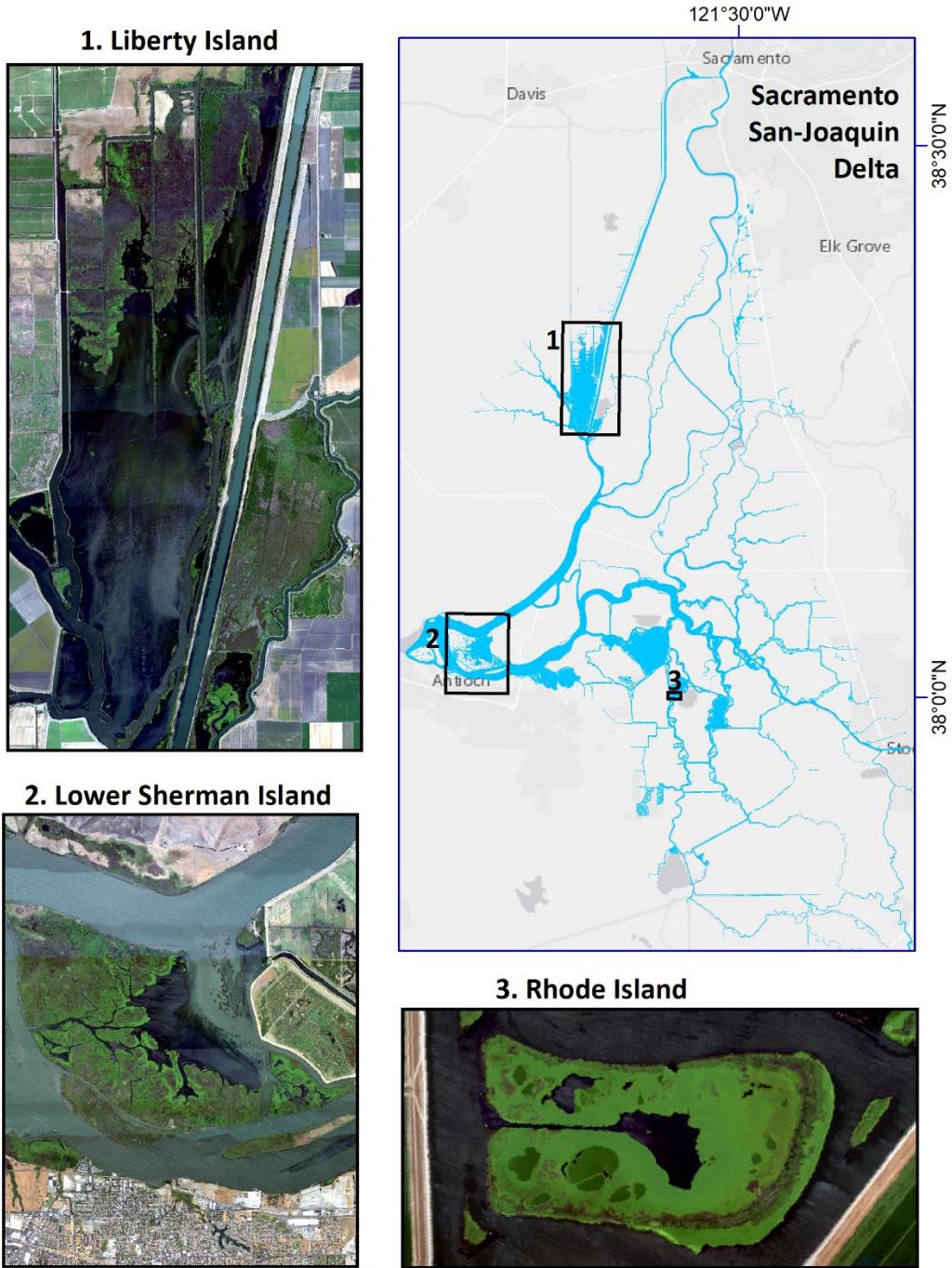


Figure 4-1. The three sub study areas in the Delta.

4.3 Methods

4.3.1 Acquisition and pre-processing of Sentinel-2 Imagery

All Level-1C top of atmosphere (TOA) reflectance products from 2018–2020 of the 10SFH Sentinel-2 tile with cloud cover less than 25% were downloaded from the European Space Agency Copernicus Hub. Following additional cloud screening and quality control, 79 dates were atmospherically corrected to Level-2A bottom of atmosphere (BOA) reflectance using Sen2cor v2.8. (**Figure 4-2**) Sentinel-2A and 2B collect information in 13 spectral bands at 10, 20, and 60 m resolutions (**Table 4-1**). Here, only bands collected at the 10 m spatial resolution were used. The 10,000 scale factor was applied and any pixels with reflectance greater than 1 were marked as NA.

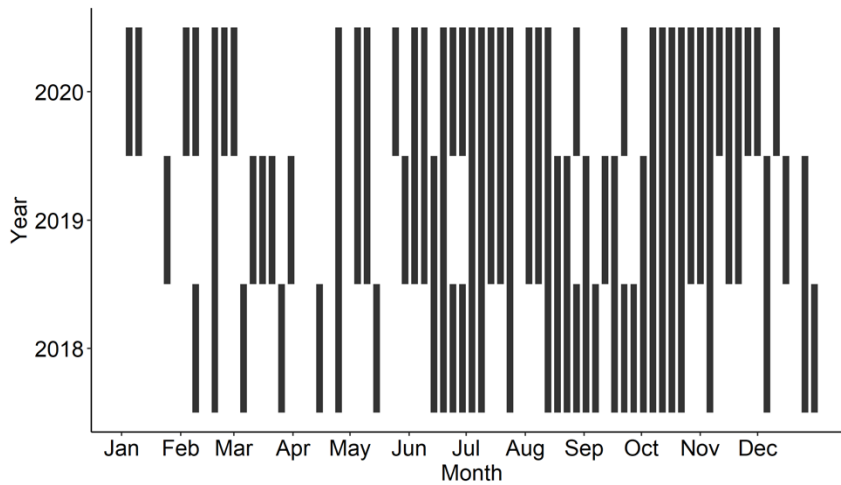


Figure 4-2. Sentinel-2 image dates used in time series analysis.

Table 4-1. Sentinel-2 band characteristics. Asterisk indicates band was used in vegetation index calculation.

<i>Sentinel-2 Bands</i>	<i>Wavelengths (μm)</i>	<i>Spatial Resolution (m)</i>
<i>Band 2-Blue*</i>	0.440-0.538	10
<i>Band 3-Green*</i>	0.537-0.582	10
<i>Band 4-Red*</i>	0.646-0.684	10
<i>Band 8-NIR*</i>	0.733-0.908	10

4.1.1 Seasonal Dynamics Maps

Variations in the vegetation growth cycle are manifested in changes of spectral indicators, vegetation indexes (VIs), of plant greenness (Gu et al., 2003; Richardson et al., 2013). Here, we report findings using the Enhanced Vegetation Index (EVI), which indicates vegetation abundance based on the ratio of red light absorbed by plant chlorophyll

and near infrared light reflected by cells in the spongy mesophyll, while correcting for soil background and atmospheric effects (Huete et al., 2002). EVI was selected due to its wide use in RS phenology studies (Klosterman et al., 2014; Toomey et al., 2015) and previous use in Delta phenology studies (Dronova et al., 2021; Miller et al., 2021), including field-based studies which indicated a higher correlation between EVI and biomass than other VIs (Knox et al., 2017).

$$EVI = 2.5 \frac{\rho_{NIR} - \rho_{RED}}{\rho_{NIR} + C1 * \rho_{RED} - C2 * \rho_{BLUE} + L}$$

C1 = 6; C2 = 7.5; L = 1

Eq 1. Enhanced vegetation index.

Quantitative maps of phenology metrics were derived for each year 2018 – 2020 using TIMESAT (Eklundh and Jönsson, 2015). TIMESAT enables users to input VI time series and select a model fitting function from which phenology metrics can be extracted (**Figure 4-3**). Five TIMESAT metrics of seasonal dynamics were considered: 1) start of the growing season (SoS, expressed as the day of the year: DOY), 2) end of the growing season (EoS), 3) length of growing season (LoS), 4) rate of increase during early growth (Growth rate), and 5) rate of decrease during senescence (Senescence rate) (**Figure 4-3, Table 4-2**).

Following Villa et al. 2020, TIMESAT was set to run with no spike filtering, asymmetric Gaussian curves as the fitting method, with two iterations envelope fitting (Gao et al., 2008; Villa et al., 2018), and start date and end date were defined as 0.5 of the seasonal amplitude. The minimum index value was set to 0 and all missing dates were filled with void layers (value = -1) that were assigned a weight of 0 during the fitting process.

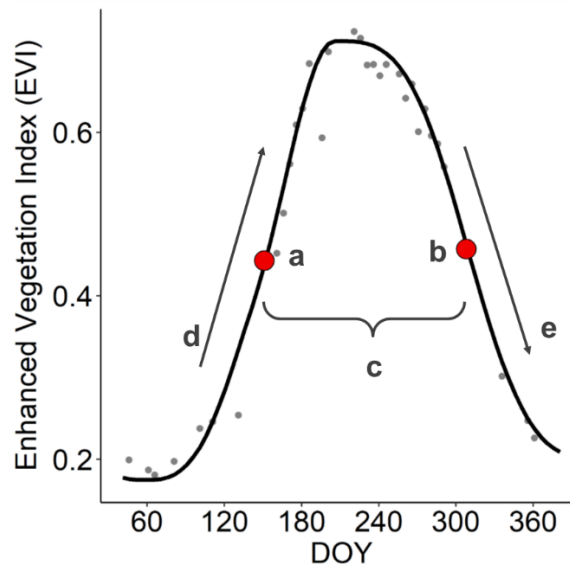


Figure 4-3. Metrics of seasonal dynamics derived from EVI time series using TIMESAT (a) Start of growing season (SoS), (b) end of growing season (EoS), (c) length of growing season, (d)

Growth rate at beginning of season, (e) Senescence rate at end of growing season. Grey dots represent EVI derived from satellite time series for a single water hyacinth pixel in Rhode Island. Black line represents the fitted asymmetric gaussian curve calculated by TIMESAT. Figure adapted from (Eklundha and Jönsson, 2017).

Table 4-2. Phenology metrics extracted from TIMESAT and corresponding definitions.

Phenology parameter	Definition
Start of the growing season (SoS)	Day of year for which the left edge has increased to a user defined threshold (here 0.5) of the seasonal amplitude measured from the left minimum level.
End of the growing season (EoS)	Day of year for which the right edge has decreased to user defined threshold (here 0.5) of the seasonal amplitude measured from the right minimum level.
Length of growing season (LoS)	Time from the start to end of the season (number of days)
Rate of increase at the beginning of the growing season (Growth rate)	The ratio of the difference between the left 20% and 80% levels and the corresponding time difference
Rate of decrease at the end of the growing season (Senescence rate)	The ratio of the difference between the right 20% and 80% levels and the corresponding time difference (positive value)

4.3.3 Vegetation regions of interest statistical analysis

Phenology metrics were extracted for water hyacinth, water primrose, and emergent vegetation across the three years and statistical differences between groups were evaluated (**Figure 4-4**). Floating aquatic vegetation genus-level classification maps (described in Chapter 2) were used to create regions of interest (ROIs) for these three vegetation classes. To reduce the influence of mixed pixels and misclassified pixels in comparisons, all maps were converted to a polygon layer and buffered inwards by 10 meters using ENVI 5.5 and R 4.3.1, respectively. Through this process most riparian vegetation pixels that were misclassified as water hyacinth were removed. For regions where the buffer eliminated most emergent vegetation pixels (e.g Rhode Island), additional polygons were added using classification maps and expert knowledge of the area. Pixels with start dates greater than 190 days were removed, as this suggests the pixel was not vegetated for over half the year. These pixels typically corresponded to floating vegetation facing the SAV/water edge, which may indicate areas of new growth.

Statistical analysis of median differences between vegetation classes, sites and years, was preformed using R v.4.1.3 with FSA v0.9.3 and rcompanion v2.4.15 packages. Due to non-normality of samples, multivariate differences within years were tested using Kruskal-Wallis One Way Analysis of Variance on Ranks. Post-hoc pairwise multiple comparisons were performed using Dunn’s test and adjusted p-value scores were calculated using the Benjamin-Hochberg method (Dunn, 1964). Effect size of pairwise sample differences between vegetation classes were calculated using Vargha and Delaney’s A (VDA) (Vargha and Delaney, 2000). VDA scores range from 0 to 1, where 0.5 indicates the two groups are stochastically equal while and extreme values indicate dominance of

one group over the other. VDA values less than 0.29 and greater than 0.71 indicate large effects.

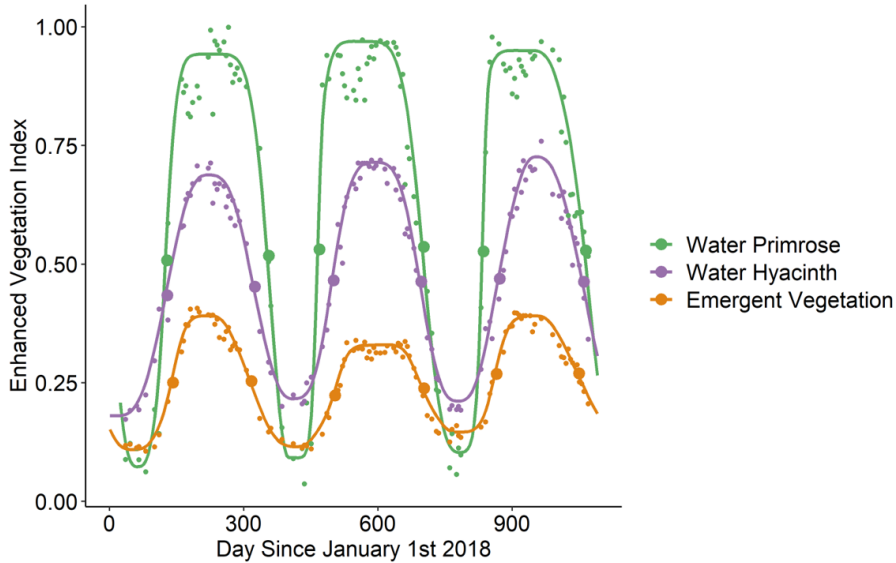


Figure 4-4. Example of TIMESAT extracted start dates and end dates throughout the three-year time series for water primrose (green), water hyacinth (purple), and emergent vegetation (orange). Large dots on the left side of curves represent TIMESAT extract start dates while those on the right indicate end dates.

4.4 Results

Maps of macrophyte seasonal dynamics derived from 2020 for Liberty Island, Rhode Island, and Sherman Island along with classification maps from Chapter 2 are shown in Figure 6. additional maps for the remaining years are shown in supplementary materials by site (4A-1, 4A-2, 4A-3). **Figure 4-6** and **Figure 4-7** display violin plots of extracted metrics from vegetation ROIs across the three sites and for all water ways, respectively. Estimated phenology metrics differed across aquatic vegetation groups, sites and years with notable spatial patterns.

Across all years and sites water primrose had the earliest median start dates ranging from late March to early May (83- 123 DOY), followed by emergent vegetation from mid-April- May (109-135 DOY) and water hyacinth mid-May- early June (129-159 DOY). Median rates of increase were also highest for water primrose (0.059-0.104) followed by water hyacinth (0.027-0.052) and emergent vegetation (0.014-0.025), indicating water primrose not only starts greening earlier, but faster. Median EoS dates were later for water primrose (313-362 DOY) than water hyacinth (306-341 DOY) and emergent vegetation (291-307 DOY). EoS dates were more similar between water hyacinth and water primrose than other phenology metric. Differences in rate of decrease were smaller between classes than those in rate of increase, but water primrose patches senesced more rapidly even

though they have a later EoS. Resulting from both earlier SoS and later EoS dates, water primrose also had the longest growth cycle (214-238), followed by water hyacinth (179-209) and then emergent vegetation (153-182).

Some within class variation in statistical comparisons may stem from misclassification or mixed pixels. Although the influence of mixed pixels was minimized by creating a 10 meter inward buffer, the two floating classes are mobile and may shift throughout the season resulting in poorly fitted curves or pixels with mixed phenologies (Chen et al., 2018). Classification maps from 2020 may be better aligned with vegetation patches because they are derived from summer rather than fall imagery.

Spatially, emergent vegetation community had the highest variability across all metrics, which is expected as it is comprised of more species than either of the two floating classes and occupies the largest area (Ta et al., 2017). Water primrose also exhibited spatial differences within patches, which were most evident in Rhode and Liberty Island (Figure 6). For several primrose patches, the outer edge had earlier EoS dates, higher rates of increase and decrease, and longer growing seasons. Some of the variability within both classes may be related to documented encroachment of water primrose into tule and cattail marshes (Khanna et al. 2018). These areas may lead to possible overlaps in the ROI extracted phenology metrics of water primrose and emergent vegetation.

Rhode Island is the only site that clearly depicts water hyacinth patches and differences are most visible for SoS and rate of increase. Length, rate of decrease, and EoS also show detectable differences, but water hyacinth and the inner group of water primrose more closely resemble each other (**Figure 4-5**). Although not clearly visible in Sherman and Liberty Island maps, extracted statistics for water hyacinth patches show a similar pattern across all sites which further confirmed by the results across the Delta (**Figure 4-7**). Water hyacinth in these two areas generally occurs in thinner patches, which are more likely to be influenced by neighboring pixels resulting in mixed phenologies or poor curve fits possibly explaining the higher variation in extracted metrics.

All results were statistically significant with a p-value less than 0.05 except for comparisons between water primrose and water hyacinth for 1) Liberty Island rates of increase and decrease in all years and 2018 EoS, 2) Sherman Island 2018 EoS, rate of increase and decrease, and water hyacinth and emergent vegetation length for Rhode Island 2020. This was reflected in the VDA analysis for Sherman 2018 end (0.557) and Liberty Island 2018 rate of increase (0.599).

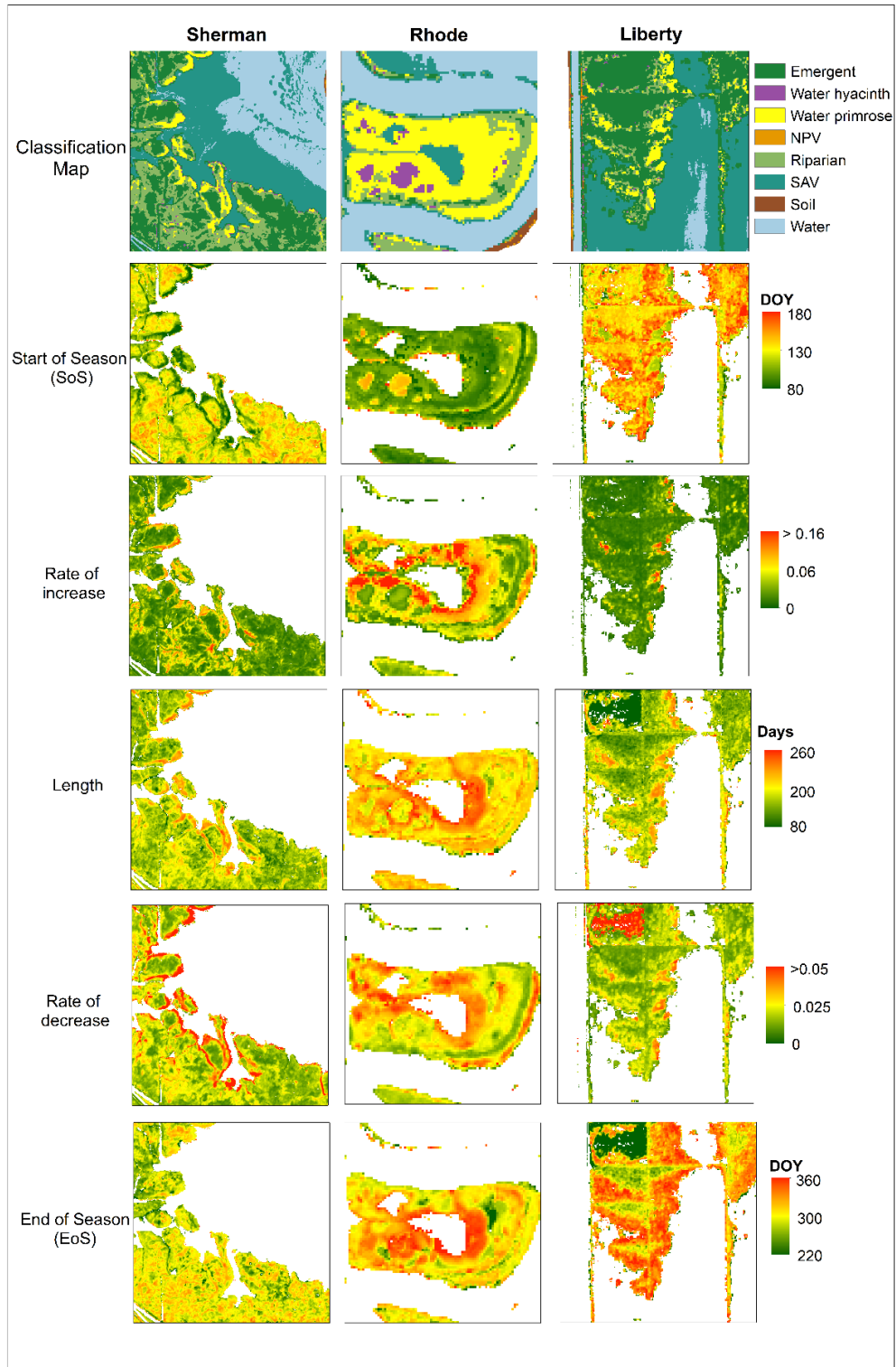


Figure 4-5. The classification map and five phenology metrics extracted for Sherman Island, Rhode Island, and Liberty Island for 2020.

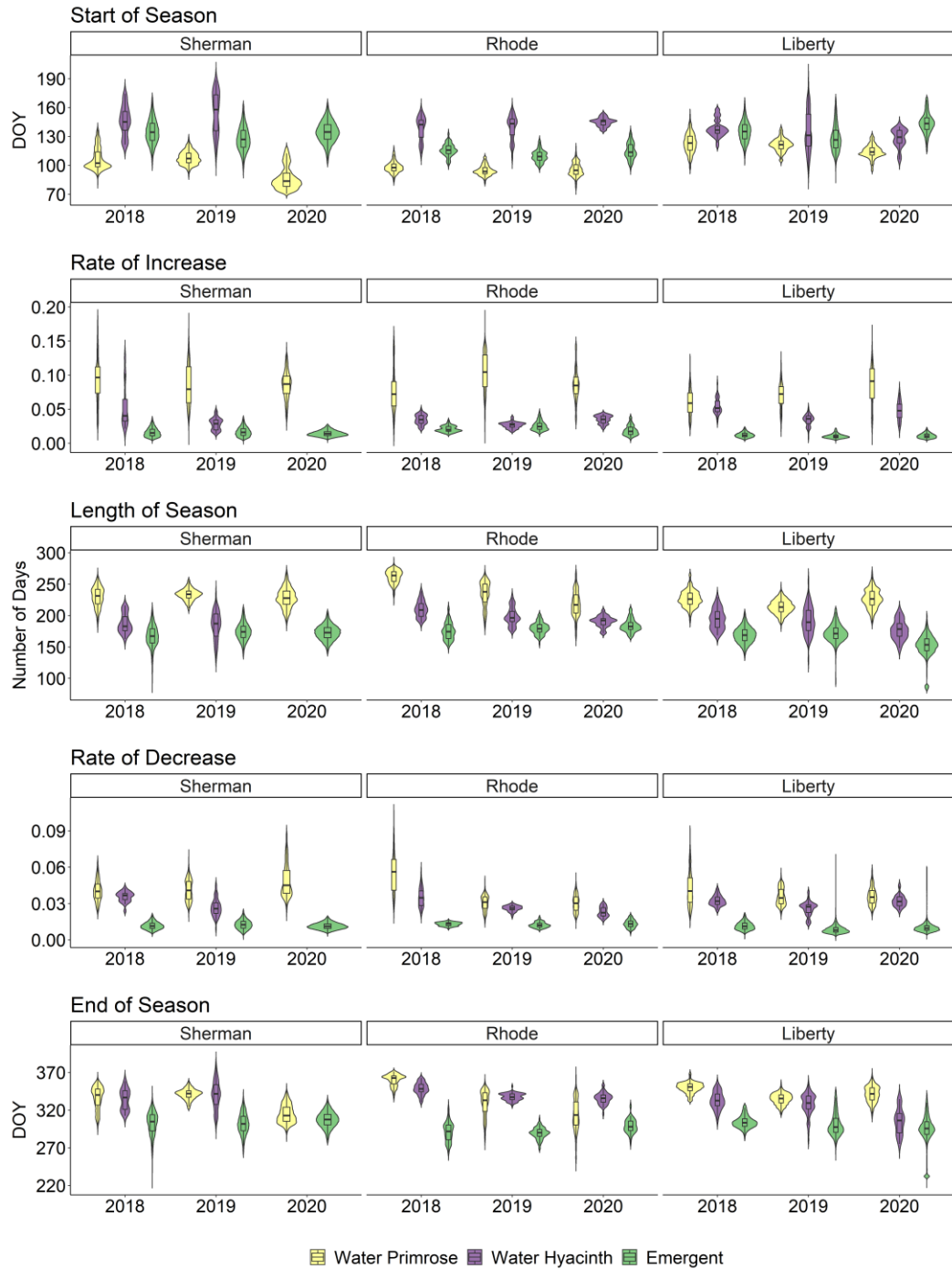


Figure 4-6. Violin plots with encompassed box plots of seasonal dynamics across the Sherman Island, Rhode Island, and Liberty Island for water primrose, water hyacinth, and emergent vegetation from 2018 – 2020.

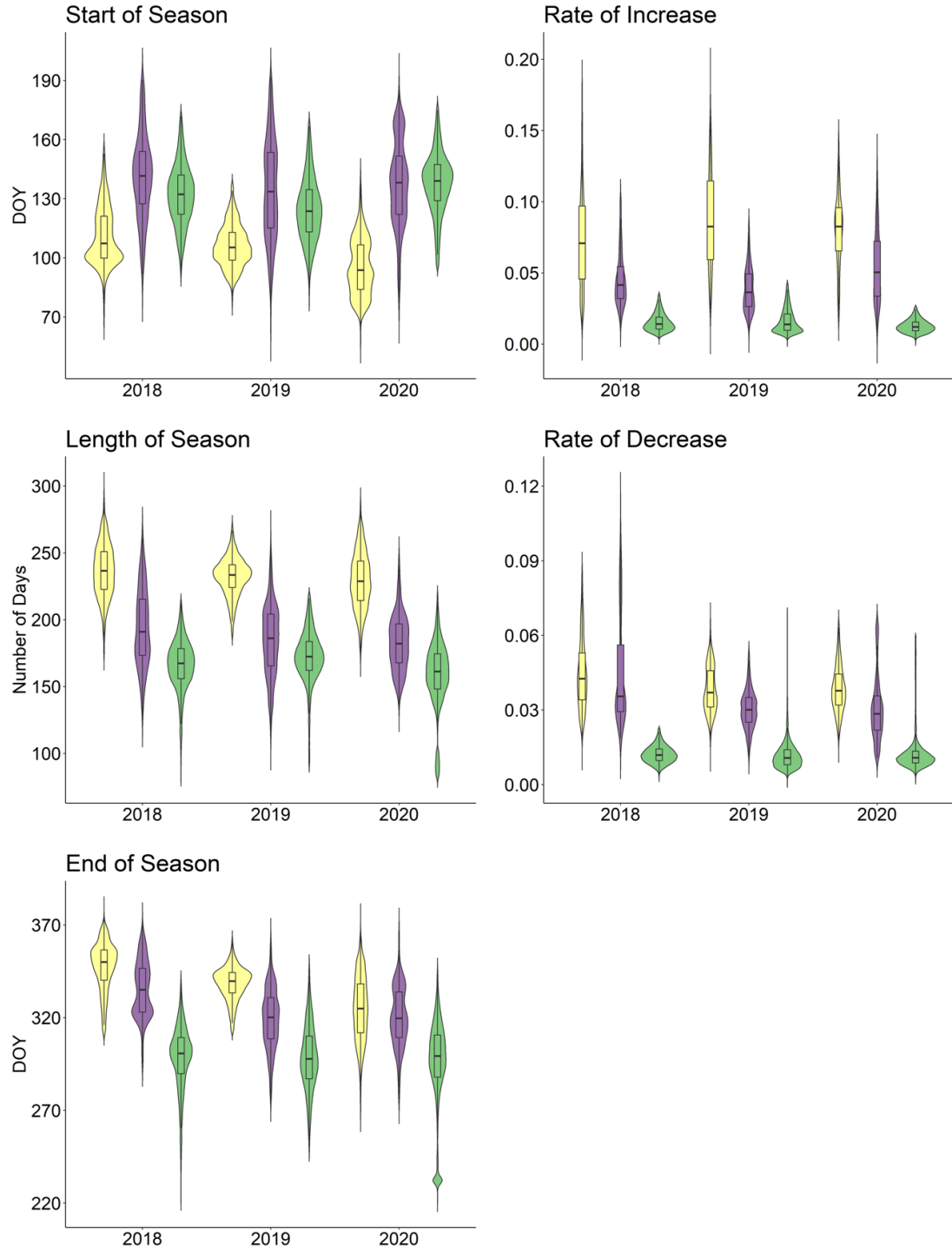


Figure 4-7. Violin plots with encompassed box plots of seasonal dynamics across the Delta for water primrose, water hyacinth, and emergent vegetation from 2018 – 2020.

4.5 Discussion

Phenology metrics derived from satellite RS provide a synoptic view of vegetation growth dynamics and can substantially improve our knowledge of the link between vegetation phenology and aquatic species invasion. However, studies focused on RS based phenology metrics are limited for aquatic macrophytes. Here, we mapped phenology metrics using TIMESAT for a three year Sentinel-2 timeseries and used previously created classification maps (Chapter 2) to compare derived phenology metrics for water primrose and water hyacinth at the genus level and emergent vegetation at the community level. We discuss our results in relation to other aquatic RS phenology studies and then frame our results in context of the four phenology niche theories- vacant niche, priority effects, niche breadth, plasticity and climate presented by Wolkovich and Cleland 2011.

4.5.1 Selective comparison to prior RS studies

As discussed in the introduction, Toth et al provides an example of niche breadth as a mechanism of invasion between two floating species in a freshwater site. We compare our results to see if we see similarities. Specifically, one species of water primrose (*Ludwigia hexapetala*) had later EoS and thus a longer growing season than other native floating species by 40 – 60 days thereby providing it with a phenological advantage (Tóth et al., 2019). Although the locations and abundance of specific water primrose species is not well documented in the Delta, we compare our SoS, length, and EoS metrics to those reported by Tóth et al. 2019. Overall, our results have higher variability in all extracted phenology metrics, which may relate to local or yearly environmental conditions or reflect variation and abundance of different water species. Liberty Island, our most freshwater site, had median SoS of 114-123 DOY which was in line with dates of 116-30 reported by Toth et al. 2018. While our more brackish/central sites, Rhode Island and Sherman Island, had earlier start dates: 95-98 and 83-107, respectively. EoS dates for Sherman and Rhode Island 2020 were similar to those reported by Toth et al 2018., but generally all sites had later median EoS with some sites ending in early December compared end dates of September in the Mantua system. Thus, the duration of water primrose growth in the Delta was also longer than Toth et al. 2018 by 21 – 71 days (~40 on average). Differences in SoS between sites suggest that water temperature or salinity levels may influence extracted dates, since Rhode Island likely has warmer water conditions and Sherman Island has a higher salinity than Liberty Island (Vroom et al., 2017). Due to the relatively short time series available from Sentinel-2, we cannot currently confirm if some of the site or yearly differences are due to specific environmental conditions, species traits, or image processing.

Additionally, we compare to field observations and confirm that the start of season for water hyacinth in the Delta is around May – end of June (CBDW 2012; Spencer and Ksander 2005). Dronova et al., 2021 computed phenology metrics for managed freshwater restoration sites in the Delta dominated by cattails (*Typha* spp.) and tule (*Schoenoplectus acutus*) reeds. Although all three sites contain similar emergent vegetation, a direct comparison between Dronova et al., 2021 and this study is not possible because of differences in the selection and definition of phenology metrics. Rather than defining start and end at 50% of the amplitude metrics Dronova et al., 2021 extracts the start of greening, end of greening, start of senescence and end of senescence using the first and second major curvature points in VI time series. Thus, our SoS and EoS values should lie in between

these two estimates. Approximate median values for start ranged from 75-50 DOY and end from 275-330 DOY (Dronova et al. 2021). SoS EMR values ranged from 109-144 and EoS from 290-308, indicating that our values are within the acceptable ranges although both might be a bit higher than Dronova et al. 2021.

4.5.2 Phenology & potential mechanisms of invasion success

Here, we discuss our results in the context of the four phenology niche theories presented in Wolkovich and Cleland 2014 by sharing examples from Liberty and Rhode Island.

Liberty Island shows at least two distinct sub-groups of emergent vegetation and water primrose across years (**Figure 4-5, Figure 4A-3**). **Figure 4-8** shows example TIMESAT fitted phenology curves for aquatic and terrestrial water primrose, and emergent tulle and cattail. Aquatic primrose shows a higher rate of increase and earlier start date than terrestrial primrose (**Figure 4-8**) which supports findings by Khanna et al. (2018), who demonstrated the marsh encroachment of water primrose and proposed a bilateral expansion mechanism of invasion in which water primrose expanded into marsh after exhausting available niche space in aquatic environments. Both forms have also been observed in other systems with the terrestrial form exhibiting slower growth than the aquatic (Haury et al., 2014; Lambert et al., 2010; Meisler, 2009). Both types of water primrose exhibit earlier SoS dates, rates of increase and length of growing season compared to tulle and cattail – providing examples of priority effects and niche breadth (**Figure 4-8**). The earlier start date and longer growing season allows water primrose to plausibly establish an advantage in terms of productivity and resource competitiveness over emergent vegetation early in the growing season (Wolkovich and Cleland 2011; Tóth et al. 2019). Thereby, allowing water primrose the time and resources to grow taller and overtake emergent vegetation prior to the start of its growth cycle (Khanna et al., 2018). However, it appears that cattail has an earlier growing season compared to tulle and the start of its growth matches more closely to water primrose, especially in 2019 which was a wet year (**Figure 4-8**). Thus, suggesting that Cattail patches may be more resistant to invasion by water primrose than Tulle, but this may vary due to yearly precipitation and flow conditions. However, this difference between emergent types needs to be validated by a larger scale comparison in terms of both time and space and supplemented with field data.

Rhode Island maps show clear differences between SoS of water hyacinth and water primrose, but remaining metrics suggest the presence of two water primrose groups (**Figure 4-5, Figure 4-9**). The outer edge of the detected primrose patch (Prim_out) shows faster rates of increase, longer duration and a later EoS than the inner edge (Prim_in) (**Figure 4-9**). Thus, the relationship between water hyacinth and Prim_out also demonstrates priority effects and niche breadth in favor of water primrose. Providing a phenology explanation for water primrose overtaking water hyacinth as the dominant floating invasive species in the Delta over the past decade in addition to herbicide treatments (Ustin et al., 2021). Water hyacinth and Prim_in show a similar duration of growth, but water hyacinth peaks later and has a later EoS (**Figure 4-9**). Thereby, potentially demonstrating niche partitioning rather than priority effects, in which resources are shared by the two invasive species at different times. This may explain why water hyacinth patches continue to expand in size across our time series, despite the earlier SoS date of water primrose (**Figure 4-9, 4A-2**). Although niche partitioning was not one of the

four niche theories discussed in Wolkovich and Cleland, 2011, we suggest that it may be added in the case of competing invasive species. However, future research is required to confirm the different water primrose species, locations of sites treated by herbicide, and environmental characteristics across the Delta to supplement this suggestion.

Both examples shown discussed here and general mapping results also indicate that water primrose also exhibits environmental plasticity which is expected to increase under climate change (Gillard et al., 2021) and is confirmed by several other field studies (Lambert et al., 2010; Skaer Thomason et al., 2018), including Thouvenot et al., 2013a who reported higher biomass and morphological plasticity was found particularly at the beginning of the life cycle when considering water depth and light intensity. Offering a potential explanation for differing EoS across sites and years. Although, the current S2 time-series is too short to determine if any differences are related to environmental characteristics or the curve fitting process. Examples of vacant niche theory may also be present in the Delta (especially when considering the impacts of herbicide treatment); however, we do not possess the ancillary data required to investigate this specific theory.

Additional work is required to characterize the phenology of classes and sub-classes over time and their relation to yearly environmental variation and site characteristics, since the phenology of any species varies in type due to fluctuations in local environment (Diez et al., 2012; Rudolf, 2019). Future research should consider the effects of precipitation and flow (e.g., wet versus dry years), as well as the influence of site-level and annual variability in salinity, water depth, water temperature, air temperature, light availability, and herbicide control.

To provide support for ecosystem management regarding timing of herbicide application; additional quantification of uncertainty regarding estimated SoS and EoS dates in the Delta is recommended. This includes exploration of uncertainty related to image timing and frequency (Villa et al., 2018; Vrieling et al., 2018), curve fitting and VI selection (Hill et al., 2021; Sun et al., 2020), and additional or alternative definitions of the RS phenology metrics presented here (Dronova et al., 2021; Eklundh and Jönsson, 2015).

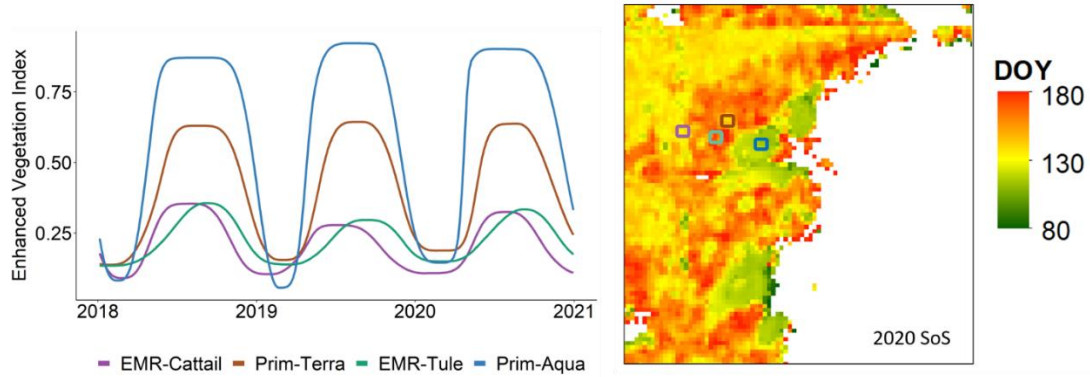


Figure 4-8. Differences in phenology between two emergent vegetation genus types (EMR-Cattail and EMR-Tule) and aquatic and terrestrialized water primrose (Prim-Aqua and Prim-Terra) present in Liberty Island. Points were selected via field data and photointerpretation. Phenology curves for both types of water primrose show breadth and priority effects relative to Cattail and Tule. However, tule patches neighboring terrestrialized water primrose have later shifted phenologies compared to Cattail, which may make tule more susceptible to invasion by water primrose.

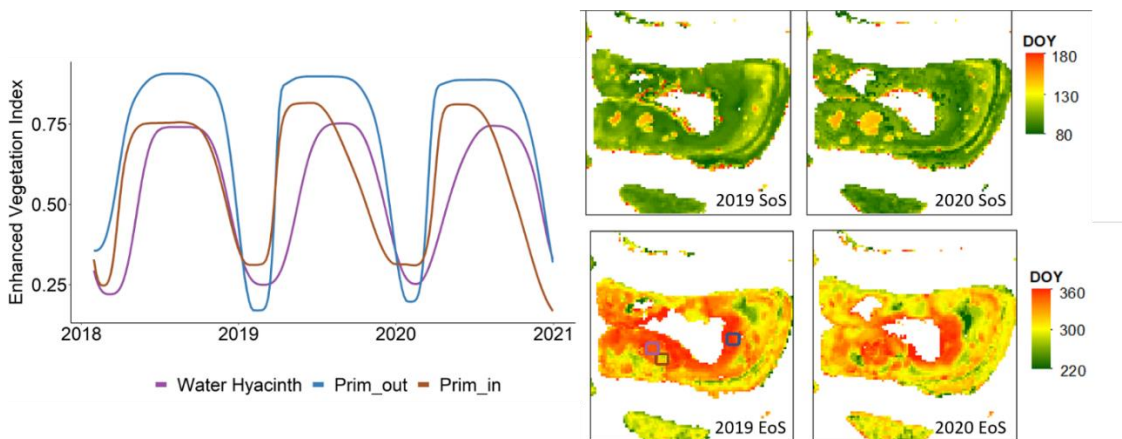


Figure 4-9. Differences in phenology between two sub-classes of water primrose from the outer (Prim_out) and inner patch (Prim_in) and water hyacinth in Rhode Island. Points were selected via field data and photointerpretation. Prim_out and water hyacinth phenologies demonstrate examples of niche breadth and priority effects, while Prim_in and water hyacinth suggest potential niche partition between the two invasive.

4.6 Conclusion

We observed that water primrose may have a phenological advantage compared to water hyacinth and emergent vegetation through the following invasion mechanisms - priority effects and niche breadth. We also found potential evidence of niche partitioning between water hyacinth and water primrose in one site. Water primrose patches exhibited earlier SoS, higher rates of increase and decrease, longer growing seasons and later EoS than water hyacinth or emergent vegetation. The earlier start date and rate of increase allow water primrose to establish an advantage in terms of productivity and resource

competitiveness over water hyacinth and emergent vegetation early in the growing season. Our results also highlight the need for spatially resolved phenology metrics for improved understanding of the link between phenology and invasion processes in aquatic systems and have the potential to provide management support for planning herbicide treatment application.

4.7 Appendix

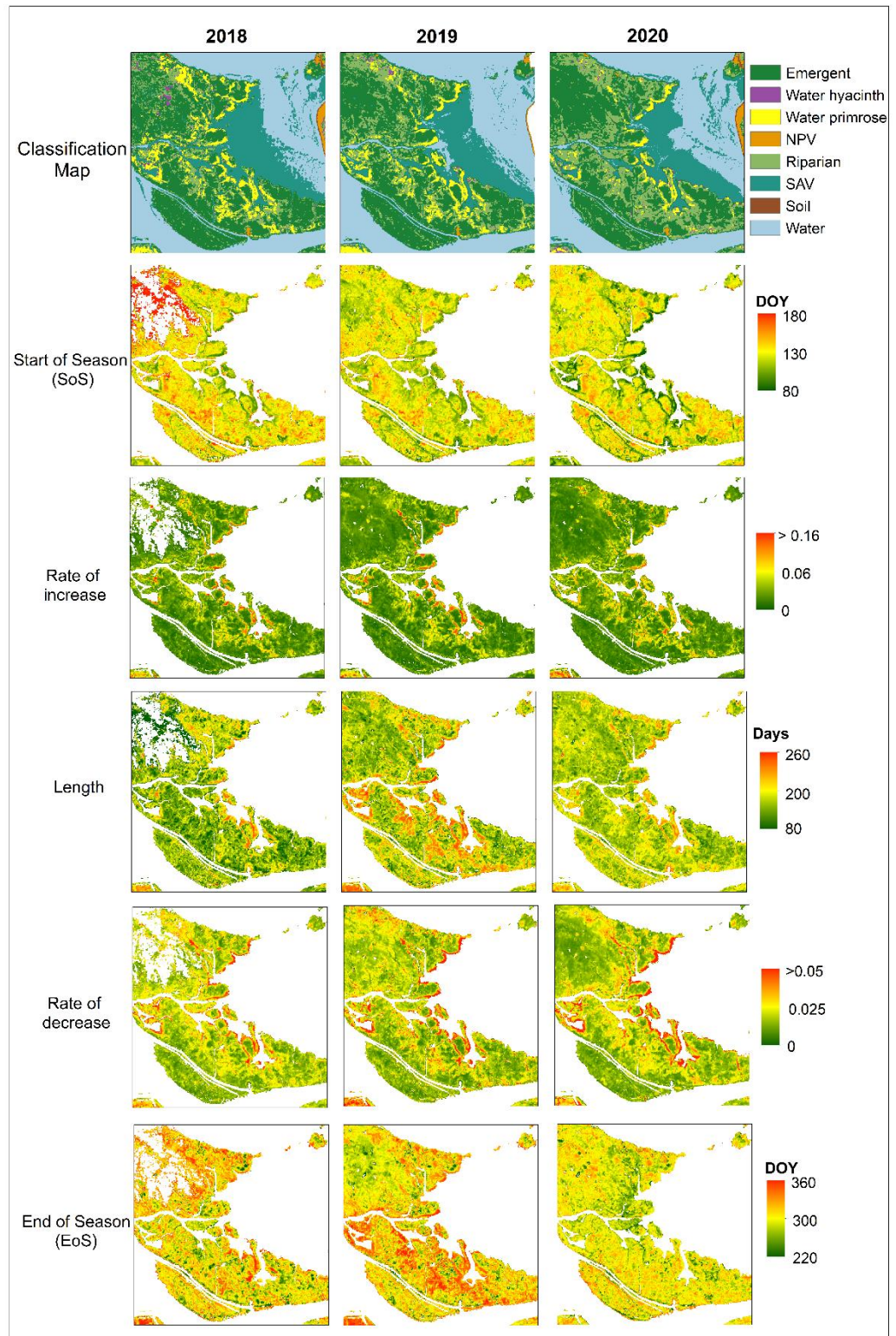


Figure 4A-1. The classification map and five phenology metrics extracted for Sherman Island across 2018 – 2020.

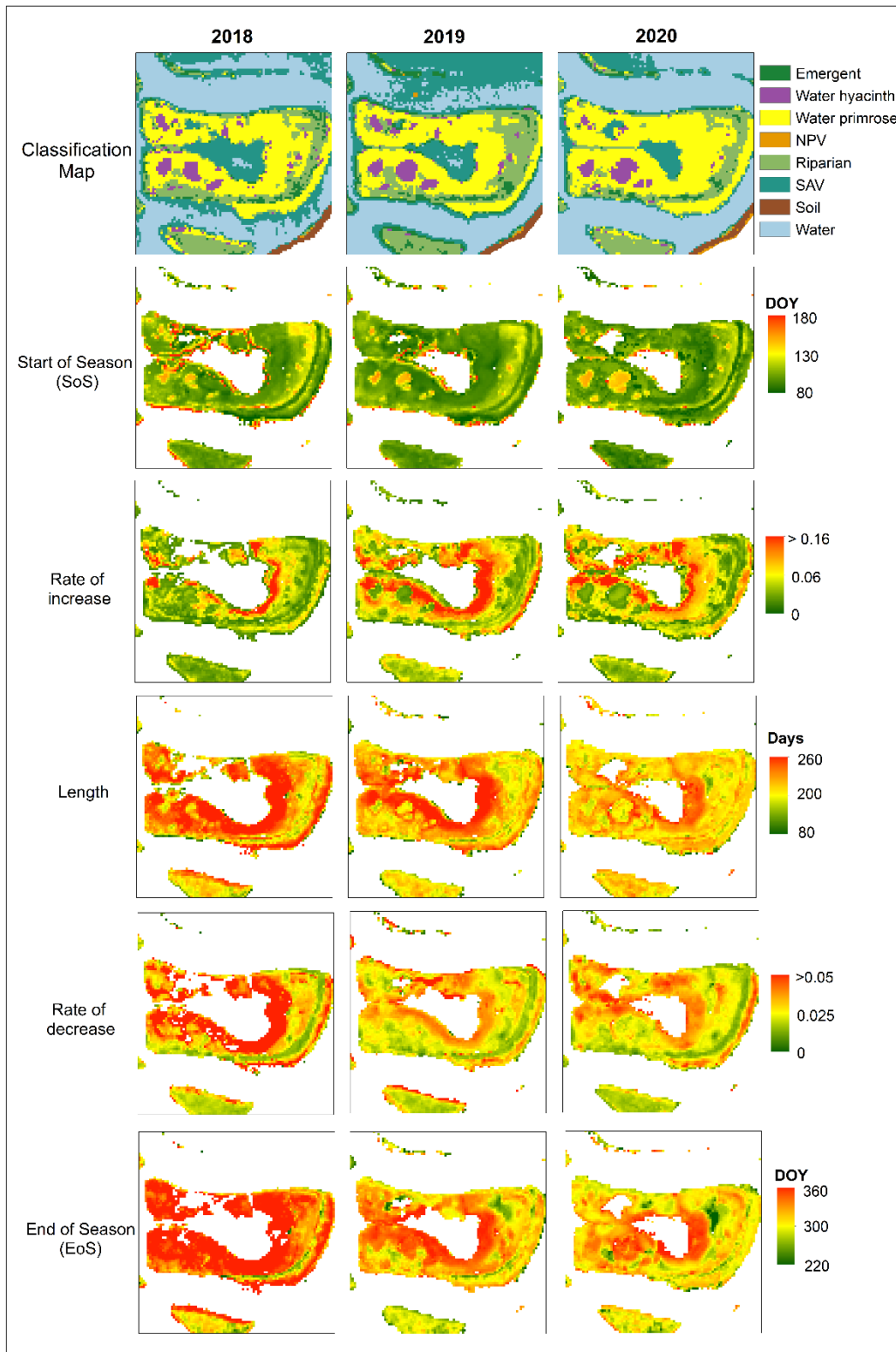


Figure 4A-2 The classification map and five phenology metrics extracted for Rhode Island across 2018 – 2020.

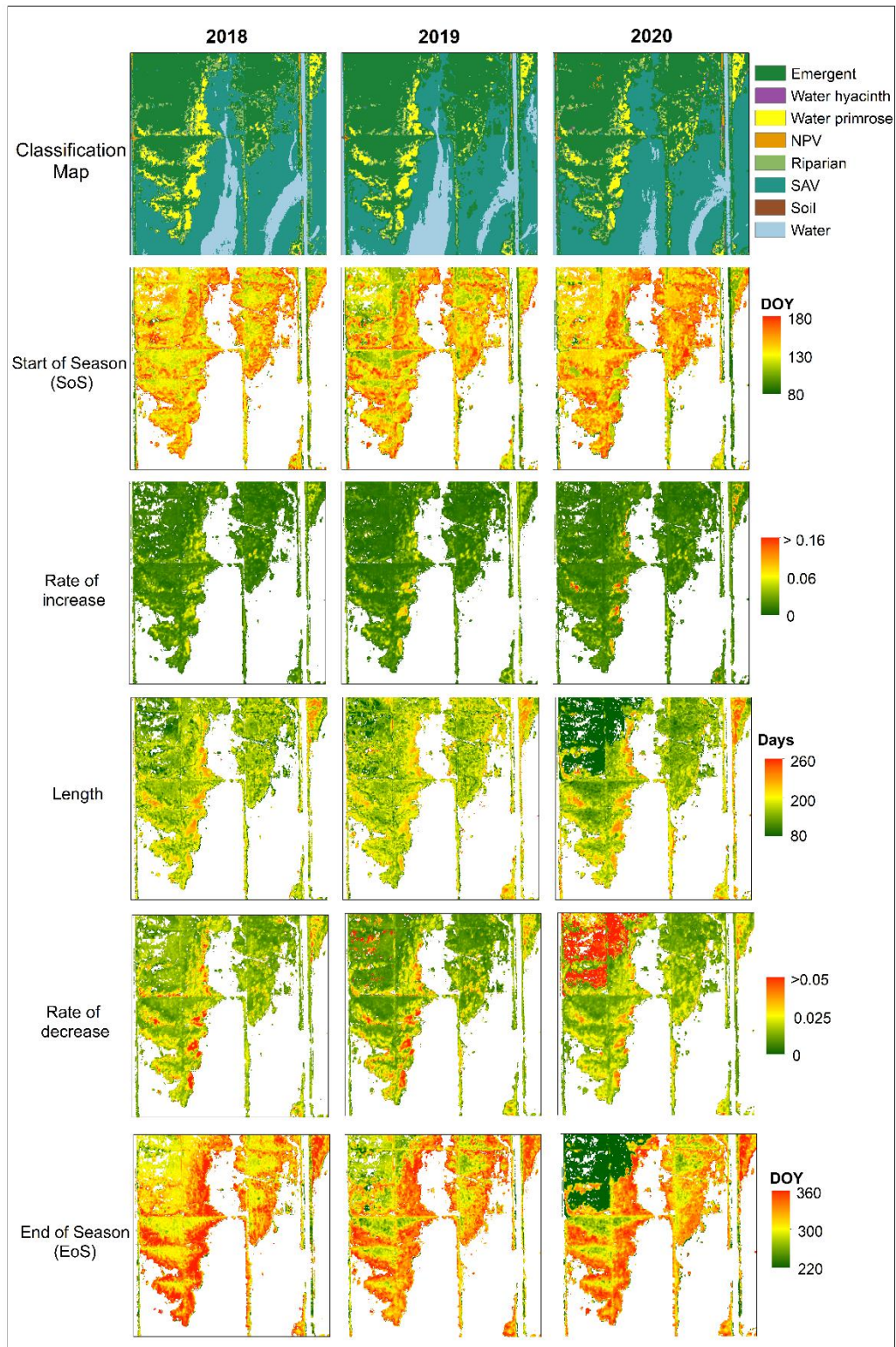


Figure 4A-3. The classification map and five phenology metrics extracted for Rhode Island across 2018 – 2020.

4.8 References

- Ai, J., Gao, W., Gao, Z., Shi, R., Zhang, C., 2017. Phenology-based *Spartina alterniflora* mapping in coastal wetland of the Yangtze Estuary using time series of GaoFen satellite no. 1 wide field of view imagery. <https://doi.org/10.1117/1.JRS.11.026020>
- Alahuhta, J., Heino, J., Luoto, M., 2011. Climate change and the future distributions of aquatic macrophytes across boreal catchments. *J. Biogeogr.* 38, 383–393. <https://doi.org/10.1111/J.1365-2699.2010.02412.X>
- biology, C.P.-G. change, 2007, undefined, 2007. Influences of species, latitudes and methodologies on estimates of phenological response to global warming. *Wiley Online Libr.* 13, 1860–1872. <https://doi.org/10.1111/j.1365-2486.2007.01404.x>
- Calero, S., Rodrigo, M.A., 2019. Reproductive phenology of submerged macrophytes: A tracker of year-to-year environmental variations. *J. Veg. Sci.* 30, 1217–1227. <https://doi.org/10.1111/JVS.12801>
- CDBW, 2012. Water hyacinth control program biological assesment. Sacramento CA.
- Chen, X., Wang, D., Chen, J., Wang, C., Shen, M., 2018. The mixed pixel effect in land surface phenology: A simulation study. *Remote Sens. Environ.* 211, 338–344. <https://doi.org/10.1016/J.RSE.2018.04.030>
- Cronk, Q., Fuller, J., 2014. Plant invaders: the threat to natural ecosystems.
- DBW, 2019. Aquatic Invasive Plant Control Program 2019 Annual Monitoring Report.
- Diez, J.M., Ibáñez, I., Miller-Rushing, A.J., Mazer, S.J., Crimmins, T.M., Crimmins, M.A., Bertelsen, C.D., Inouye, D.W., 2012. Forecasting phenology: from species variability to community patterns. *Ecol. Lett.* 15, 545–553. <https://doi.org/10.1111/J.1461-0248.2012.01765.X>
- Dronova, I., Taddeo, S., Hemes, K.S., Knox, S.H., Valach, A., Oikawa, P.Y., Kasak, K., Baldocchi, D.D., 2021. Remotely sensed phenological heterogeneity of restored wetlands: linking vegetation structure and function. *Agric. For. Meteorol.* 296, 108215. <https://doi.org/10.1016/J.AGRFORMET.2020.108215>
- Dunn, O., 1964. Multiple comparisons using rank sums. *Technometrics* 6, 241–252. <https://doi.org/10.1080/00401706.1964.10490181>
- Eklundh, L., Jönsson, P., 2015. TIMESAT: A software package for time-series processing and assessment of vegetation dynamics, in: *Remote Sensing Time Series*. Springer, pp. 141–158.
- Eklundha, L., Jönsson, P., 2017. TIMESAT 3.3 with seasonal trend decomposition and parallel processing Software Manual.

- Fleming, J.P., Dibble, E.D., 2015. Ecological mechanisms of invasion success in aquatic macrophytes. *Hydrobiologia* 746, 23–37. <https://doi.org/10.1007/S10750-014-2026-Y/FIGURES/1>
- Gillard, M.B., Caudal, J.P., Deleu, C., Thiébaud, G., 2021. Heterogeneous Impact of Water Warming on Exotic and Native Submerged and Emergent Plants in Outdoor Mesocosms. *Plants* 2021, Vol. 10, Page 1324 10, 1324. <https://doi.org/10.3390/PLANTS10071324>
- Gu, L., Post, W.M., Baldocchi, D., Black, T.A., Verma, S.B., Vesala, T., Wofsy, S.C., 2003. Phenology of vegetation photosynthesis. Springer.
- Harms, N.E., Cronin, J.T., 2021. Phenology of Competitive Interactions and Implications for Management of the Invasive Wetland Plant *Alternanthera philoxeroides*.
- Haury, J., Druel, A., Cabral, T., Paulet, Y., Bozec, M., Coudreuse, J., 2014. Which adaptations of some invasive *Ludwigia* spp. (Rosidae, Onagraceae) populations occur in contrasting hydrological conditions in Western France? *Hydrobiologia* 737, 45–56. <https://doi.org/10.1007/S10750-014-1815-7/TABLES/5>
- Hill, A.C., Vázquez-Lule, A., Vargas, R., 2021. Linking vegetation spectral reflectance with ecosystem carbon phenology in a temperate salt marsh. *Agric. For. Meteorol.* 307, 108481. <https://doi.org/10.1016/J.AGRFORMET.2021.108481>
- Huete, A., Didan, K., Miura, T., Rodriguez, E.P., Gao, X., Ferreira, L.G., 2002. Overview of the radiometric and biophysical performance of the MODIS vegetation indices. *Remote Sens. Environ.* 83, 195–213. [https://doi.org/10.1016/S0034-4257\(02\)00096-2](https://doi.org/10.1016/S0034-4257(02)00096-2)
- Khanna, S., Santos, M.J., Boyer, J.D., Shapiro, K.D., Bellvert, J., Ustin, S.L., 2018. Water primrose invasion changes successional pathways in an estuarine ecosystem. *Ecosphere* 9, e02418. <https://doi.org/https://doi.org/10.1002/ecs2.2418>
- Khanna, S., Santos, M.J., Hestir, E.L., Ustin, S.L., 2012. Plant community dynamics relative to the changing distribution of a highly invasive species, *Eichhornia crassipes*: A remote sensing perspective. *Biol. Invasions* 14, 717–733. <https://doi.org/10.1007/s10530-011-0112-x>
- Klosterman, S.T., Hufkens, K., Gray, J.M., Melaas, E., Sonnentag, O., Lavine, I., Mitchell, L., Norman, R., Friedl, M.A., Richardson, A.D., 2014. Evaluating remote sensing of deciduous forest phenology at multiple spatial scales using PhenoCam imagery. *bg.copernicus.org* 11, 4305–4320. <https://doi.org/10.5194/bg-11-4305-2014>
- Knox, S.H., Dronova, I., Sturtevant, C., Oikawa, P.Y., Matthes, J.H., Verfaillie, J.,

- Baldocchi, D., 2017. Using digital camera and Landsat imagery with eddy covariance data to model gross primary production in restored wetlands. *Agric. For. Meteorol.* 237–238, 233–245. <https://doi.org/10.1016/J.AGRFORMET.2017.02.020>
- Lambert, E., Dutartre, A., Coudreuse, J., Haury, J., 2010. Relationships between the biomass production of invasive *Ludwigia* species and physical properties of habitats in France. *Hydrobiologia* 656, 173–186. <https://doi.org/10.1007/S10750-010-0440-3/FIGURES/3>
- Luo, J., Li, X., Ma, R., Li, F., Duan, H., Hu, W., Qin, B., Huang, W., 2016. Applying remote sensing techniques to monitoring seasonal and interannual changes of aquatic vegetation in Taihu Lake, China. *Ecol. Indic.* 60, 503–513. <https://doi.org/10.1016/J.ECOLIND.2015.07.029>
- Meisler, J., 2009. Controlling *Ludwigia hexaplata* in Northern California. <https://doi.org/10.1672/055.026.0404> 26, 15–19. <https://doi.org/10.1672/055.026.0404>
- Miller, G.J., Dronova, I., Oikawa, P.Y., Knox, S.H., Windham-Myers, L., Shahan, J., Stuart-Haëntjens, E., 2021. The Potential of Satellite Remote Sensing Time Series to Uncover Wetland Phenology under Unique Challenges of Tidal Setting. *Remote Sens.* 2021, Vol. 13, Page 3589 13, 3589. <https://doi.org/10.3390/RS13183589>
- O’Connell, J.L., Mishra, D.R., Cotten, D.L., Wang, L., Alber, M., 2017. The Tidal Marsh Inundation Index (TMII): An inundation filter to flag flooded pixels and improve MODIS tidal marsh vegetation time-series analysis. *Remote Sens. Environ.* 201, 34–46. <https://doi.org/10.1016/J.RSE.2017.08.008>
- Peeters, E.T.H.M., van Zuidam, J.P., van Zuidam, B.G., Van Nes, E.H., Kosten, S., Heuts, P.G.M., Roijackers, R.M.M., Netten, J.J.C., Scheffer, M., 2013. Changing weather conditions and floating plants in temperate drainage ditches. *J. Appl. Ecol.* 50, 585–593. <https://doi.org/10.1111/1365-2664.12066>
- Piao, S., Liu, Q., Chen, A., Janssens, I.A., Fu, Y., Dai, J., Liu, L., Lian, X., Shen, M., Zhu, X., 2019. Plant phenology and global climate change: Current progresses and challenges. *Glob. Chang. Biol.* 25, 1922–1940. <https://doi.org/10.1111/GCB.14619>
- Pinardi, M., Villa, P., Free, G., Giardino, C., Bresciani, M., 2021. Evolution of Native and Alien Macrophytes in a Fluvial-wetland System Using Long-term Satellite Data. *Wetlands* 41, 1–14. <https://doi.org/10.1007/S13157-021-01395-9/FIGURES/7>
- Rejmánková, E., 1992. Ecology of creeping macrophytes with special reference to *Ludwigia peploides* (H.B.K.) Raven. *Aquat. Bot.* 43, 283–299. [https://doi.org/10.1016/0304-3770\(92\)90073-R](https://doi.org/10.1016/0304-3770(92)90073-R)

- Richardson, A.D., Keenan, T.F., Migliavacca, M., Ryu, Y., Sonnentag, O., Toomey, M., 2013. Climate change, phenology, and phenological control of vegetation feedbacks to the climate system. *Agric. For. Meteorol.* 169, 156–173. <https://doi.org/https://doi.org/10.1016/j.agrformet.2012.09.012>
- Rudolf, V.H.W., 2019. The role of seasonal timing and phenological shifts for species coexistence. *Ecol. Lett.* 22, 1324–1338. <https://doi.org/10.1111/ELE.13277>
- Skaer Thomason, M.J., Grewell, B.J., Netherland, M.D., 2018. Dynamics of *Ludwigia hexapetala* invasion at three Spatial Scales in a Regulated River. *Wetlands* 38, 1285–1298. <https://doi.org/10.1007/S13157-018-1053-2/FIGURES/6>
- Sun, C., Li, J., Cao, L., Liu, Y., Jin, S., Zhao, B., 2020. Evaluation of vegetation index-based curve fitting models for accurate classification of salt marsh vegetation using sentinel-2 time-series. *Sensors (Switzerland)* 20, 1–24. <https://doi.org/10.3390/s20195551>
- Sun, C., Li, J., Liu, Yongxue, Liu, Yongchao, Liu, R., 2021. Plant species classification in salt marshes using phenological parameters derived from Sentinel-2 pixel-differential time-series. *Remote Sens. Environ.* 256, 112320. <https://doi.org/10.1016/J.RSE.2021.112320>
- Ta, J., Anderson, L.W.J., Christman, M.A., Khanna, S., Kratville, D., Madsen, J.D., Moran, P.J., Viers, J.H., Ta, J., Anderson, L.W.J., Christman, M.A., Khanna, S., Kratville, D., Madsen, J.D., Moran, P.J., Viers, J.H., 2017. Invasive aquatic vegetation management in the Sacramento-San Joaquin River Delta: Status and recommendations. *San Fr. Estuary Watershed Sci.* 15. <https://doi.org/10.15447/SFEWS.2017V15ISS4ART5>
- Taddeo, S., Dronova, I., 2020. Landscape metrics of post-restoration vegetation dynamics in wetland ecosystems. *Landsc. Ecol.* 35, 275–292. <https://doi.org/10.1007/S10980-019-00946-0/FIGURES/5>
- Thackeray, S.J., Henrys, P.A., Hemming, D., Bell, J.R., Botham, M.S., Burthe, S., Helaouet, P., Johns, D.G., Jones, I.D., Leech, D.I., MacKay, E.B., Massimino, D., Atkinson, S., Bacon, P.J., Brereton, T.M., Carvalho, L., Clutton-Brock, T.H., Duck, C., Edwards, M., Elliott, J.M., Hall, S.J.G., Harrington, R., Pearce-Higgins, J.W., Høye, T.T., Kruuk, L.E.B., Pemberton, J.M., Sparks, T.H., Thompson, P.M., White, I., Winfield, I.J., Wanless, S., 2016. Phenological sensitivity to climate across taxa and trophic levels. *Nat.* 2016 5357611 535, 241–245. <https://doi.org/10.1038/nature18608>
- Thouvenot, L., Haury, J., Thiebaut, G., 2013. A success story: water primroses, aquatic plant pests. *Aquat. Conserv. Mar. Freshw. Ecosyst.* 23, 790–803. <https://doi.org/10.1002/AQC.2387>
- Toomey, M., Friedl, M.A., Froking, S., Hufkens, K., Klosterman, S., Sonnentag, O., Baldocchi, D.D., Bernacchi, C.J., Biraud, S.C., Bohrer, G., Brzostek, E., Burns, S.P., Coursolle, C., Hollinger, D.Y., Margolis, H.A., McCaughey, H., Monson, R.K.,

- Munger, J.W., Pallardy, S., Phillips, R.P., Torn, M.S., Wharton, S., Zeri, M., Richardson, A.D., 2015. Greenness indices from digital cameras predict the timing and seasonal dynamics of canopy-scale photosynthesis. *Ecol. Appl.* 25, 99–115. <https://doi.org/10.1890/14-0005.1>
- Tóth, V.R., Villa, P., Pinardi, M., Bresciani, M., 2019. Aspects of invasiveness of *Ludwigia* and *Nelumbo* in shallow temperate fluvial lakes. *Front. Plant Sci.* 10, 647. <https://doi.org/10.3389/FPLS.2019.00647/BIBTEX>
- Tuxen, K., Schile, L., Stralberg, D., Siegel, S., Parker, T., Vasey, M., Callaway, J., Kelly, M., 2011. Mapping changes in tidal wetland vegetation composition and pattern across a salinity gradient using high spatial resolution imagery. *Wetl. Ecol. Manag.* 19, 141–157. <https://doi.org/10.1007/S11273-010-9207-X>
- Ustin, S.L., Khanna, S., Lay, M., Shapiro, K., Ghajarnia, N., 2017. Enhancement of Delta Smelt (*Hypomesus transpacificus*) habitat through adaptive management of invasive aquatic weeds in the Sacramento-San Joaquin Delta. California Department of Water Resources.
- Vargha, A., Delaney, H.D., 2000. A Critique and Improvement of the CL Common Language Effect Size Statistics of McGraw and Wong. *J. Educ. Behav. Stat.* Summer 25, 101–132.
- Verhoeven, M.R., Glisson, W.J., Larkin, D.J., 2020. Niche Models Differentiate Potential Impacts of Two Aquatic Invasive Plant Species on Native Macrophytes. *Divers.* 2020, Vol. 12, Page 162 12, 162. <https://doi.org/10.3390/D12040162>
- Villa, P., Pinardi, M., Bolpagni, R., Gillier, J.-M., Zinke, P., Nedelcuț, F., Bresciani, M., 2018. Assessing macrophyte seasonal dynamics using dense time series of medium resolution satellite data. *Remote Sens. Environ.* 216, 230–244. <https://doi.org/https://doi.org/10.1016/j.rse.2018.06.048>
- Visser, M.E., Both, C., 2005. Shifts in phenology due to global climate change: the need for a yardstick. *Proc. R. Soc. B Biol. Sci.* 272, 2561–2569. <https://doi.org/10.1098/RSPB.2005.3356>
- Vrieling, A., Meroni, M., Darvishzadeh, R., Skidmore, A.K., Wang, T., Zurita-Milla, R., Oosterbeek, K., O'Connor, B., Paganini, M., 2018. Vegetation phenology from Sentinel-2 and field cameras for a Dutch barrier island. *Remote Sens. Environ.* 215, 517–529. <https://doi.org/10.1016/j.rse.2018.03.014>
- Vroom, J., van der Wegen, M., Martyr-Koller, R.C., Lucas, L. V., 2017. What Determines Water Temperature Dynamics in the San Francisco Bay-Delta System? *Water Resour. Res.* 53, 9901–9921. <https://doi.org/10.1002/2016WR020062>
- Wang, L., Dronova, I., Gong, P., Yang, W., Li, Y., Liu, Q., 2012. A new time series vegetation-water index of phenological-hydrological trait across species and functional types for Poyang Lake wetland ecosystem. *Remote Sens. Environ.* 125, 49–63. <https://doi.org/10.1016/j.rse.2012.07.003>
- Whitley, S.N., Bollens, S.M., 2014. Fish assemblages across a vegetation gradient in a restoring tidal freshwater wetland: Diets and potential for resource competition. *Environ. Biol. Fishes* 97, 659–674. <https://doi.org/10.1007/S10641-013-0168-9/FIGURES/5>
- Wolkovich, E.M., Cleland, E.E., 2014. Editor's choice: Phenological niches and the future of invaded ecosystems with climate change. *AoB Plants* 6.

- <https://doi.org/10.1093/AOBPLA/PLU013>
- Wolkovich, E.M., Cleland, E.E., 2011a. The phenology of plant invasions: a community ecology perspective. *Front. Ecol. Environ.* 9, 287–294.
<https://doi.org/10.1890/100033>
- Wolkovich, E.M., Cleland, E.E., 2011b. The phenology of plant invasions: a community ecology perspective. *Front. Ecol. Environ.* 9, 287–294.
<https://doi.org/10.1890/100033>
- Zhao, B., Yan, Y., Guo, H., He, M., Gu, Y., Li, B., 2009. Monitoring rapid vegetation succession in estuarine wetland using time series MODIS-based indicators: An application in the Yangtze River Delta area. *Ecol. Indic.* 9, 346–356.
<https://doi.org/10.1016/J.ECOLIND.2008.05.009>

5. Conclusions

Satellite remote sensing can be used as a tool to answer fundamental ecology questions, monitor changes, and provide management support in aquatic ecosystems. This dissertation demonstrates the value and need for high temporal and spatial resolution space based observations to map estuarine turbidity (Chapter 1); detect invasive floating aquatic vegetation at the genus level (Chapter 2); and reveal mechanisms of aquatic species invasion related to phenology (Chapter 3).

5.1 Main Findings and future goals

Chapter 1 results from the emergency barrier case study indicate that construction of the barrier impacted turbidity during ebb tides but had little effect during flood tides. This supported previous field measurements and provided additional spatial context. Delta smelt habitat suitability maps revealed that potential refugia were present throughout the drought with little connectivity. We show that the barrier installation may have extended suitable turbidity habitat for Delta Smelt in the San Joaquin river, thereby potentially jeopardizing the fish as they may get stuck in reverse flows caused by water pumping.

Fish habitat suitability is normally determined by models and the methods outlined in this chapter provide the ability to validate these models with observations. The addition of spatially continuous data to in situ monitoring efforts enhances management decisions by providing regional scaling and measurements for areas with limited or no in situ data. Turbidity is one of many water quality variables influencing habitat suitability, thus future work should incorporate actual Sentinel-2 data and other parameters derived from satellite remote sensing (e.g salinity and temperature).

Chapter 2 results demonstrate that Sentinel-2 can be used to distinguish multiple floating vegetation classes and enhance current high-resolution mapping efforts of invasive floating aquatic vegetation in the Delta. Sentinel-2 imagery can be used to fill inter-annual and annual gaps in summer and fall, thereby enabling the tracking of vegetation patch expansion throughout peak growth and in response environmental or anthropogenic disturbance events. This will compliment current imaging spectroscopy flights which are still recommended for detecting smaller patches particularly of water hyacinth. This work documents the first time water primrose has been mapped using satellite data. Future work, should include additional improvements in masking riparian vegetation, classifying patch edges, and evaluation of winter and spring images.

Chapter 3 results revealed that water primrose has a phenological advantage over its competitors explained by ecological theories – priority effects, niche breadth, and environmental plasticity. Our results demonstrate the need to spatially resolve phenology metrics and future work should investigate differences in floating and emergent vegetation sub classes. Future maps should also improve characterization of actual start and end dates and evaluate the relationship between phenology and other environmental variables. Remote sensing derived maps of phenology metrics could be useful to managers, as they not only revealed mechanisms of invasion, but also demonstrate how to track aquatic phenology over multiple years, which can support decisions related herbicide treatment in terms of tracking application success and selection of application window on a site-by-site basis.

All three chapters support management objectives in the Sacramento San Joaquin Delta related to endangered species habitat and invasive species control. However, findings and methods could be extended to other areas of the globe, as deltas worldwide are facing similar pressures due to climate change and invasive species.

This dissertation provides the foundation of a new frontier in remote sensing where researchers are able to better characterize changes and drivers of change in terrestrial aquatic interfaces.